NASA Technical Memorandum 87786

Molecular Clouds in Orion and Monoceros

Ronald J. Maddalena

JUNE 1986

NASA

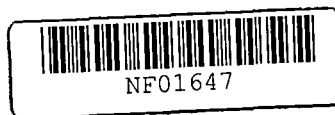# Molecular Clouds in Orion and Monoceros

Ronald J. Maddalena

NASA Goddard Institute for Space Studies
New York, New York

TABLE OF CONTENTS

ACKNOWLEDGMENTS

In some ways a thesis is like a cake which requires only one chef but many ingredients. The success of the cake depends mostly on the quality of the ingredients while its failure lies with the chef, the author of the work. The ingredients that have gone into the baking of this thesis are of the highest quality -- they are all the people who in one way or another have assisted with or inspired this work.

Most of the inspiration for the thesis emanated from the contagious enthusiasm for the Orion project felt by my thesis advisors, Mark Morris and Patrick Thaddeus. The sometimes difficult though never impossible fusion of their comments and criticisms has without a doubt strengthened this work. I also appreciated the help and comments of Tom Dame, Elaine Gottlieb, Isabelle Grenier, Yi-Long Huang, and David Leisawitz, my fellow observers and colleagues, and of Sam Palmer, Dennis Mumma, S. K. Pan, and Tony Kerr, the team which kept the Columbia telescope in working order and provided receivers superior to those of the competition. I am grateful to Joe Montani and Joe Moscowitz who sat many a long night in the telescope control room taking a significant fraction of the observations here described, and to John Bally who provided observations taken with the Bell Labs telescope.

Many sections of this work directly result from the help of others. In particular, Alyssa Goodman helped compile the data base from which Figures IV.11-13 were genereated; Francois Boulanger produced Figures V.14 and V.15 and C. Crezelious graciously provided

iii

CHAPTER I.   INTRODUCTION

"For who would acquire a knowledge of the heavens let him give up
his days and nights to the marvels of Orion," C. E. Barns wrote in
1929:

> Here may be found every conceivable variation of celestial
> phenomena: stars, giants and dwarfs; variables, doubles..
> triples.. multiples; binaries visual and spectroscopic;
> clusters wide and condensed; mysterious rayless rifts and
> nebulae in boundless variety, with the supreme wonder of
> all supernal wonders at its heart--the Great Nebula....
> [an] abundant field for [astronomers], with their super-
> refinements of means and methods, for generations to come....

The wonder expressed by Barns and inspired by the complexity of the

Orion region only intensifies as knowledge of the region expands. At

the time Barns wrote, the true nature of the dark or molecular clouds,

the most massive entities in the region and probably the progenitor of

most of the objects he included in his list of phenomena, remained as

obscured as the clouds are opaque. The pioneering work of Tucker,

Kutner, and Thaddeus (1973); Chin (1978); and Kutner et al. (1977;

hereafter abbreviated to KTCT) revealed the first hints of the true

extent and mass of the molecular clouds in the region. Their

observations conclusively showed that radio emission from carbon

monoxide (CO) acted as an excellent tracer of interstellar molecular

hydrogen $(H_2)^*$ and that previous large-scale surveys of atomic hydrogen

---

* Emission from CO is easier to observe than emission from H_2, the
major constituent of molecular clouds, since H_2 lacks the large dipole
moment of CO and the infrared and ultraviolet (UV) transitions of H_2,
unlike CO observations at millimeter wavelengths, are hindered by the
Earth's atmosphere.

and other tracers of the interstellar medium had been ineffective in identifying the predominent component of the interstellar medium in the Orion region (see Chin 1978 for a review of the previous work). Most molecular line studies of the region (see Goudis 1982 and references therein), excepting KTCT and later surveys of hydroxyl (OH) emission (Baud and Wouterloot 1980) and of formaldehyde (H_2CO) absorption (Cohen et al. 1983), have been confined to radio bright areas immediately surrounding the most prominent regions of star formation (e.g., the Orion Nebula, NGC 2023, 2024, 2063, 2067, 2068, and 2071), because the small beam size of most millimeter-wave telescopes makes a large-scale survey impractical.

The survey by Chin (1978) used the recently built Columbia telescope which, with an 8 arcmin beam, maps large areas of the sky effectively. As this survey showed, the prominent regions of star formation constitute only a small fraction of the volume of the two molecular clouds found. Both clouds have a mass of 10^5 $M_\odot$ and a size of a few tens of parsecs, i.e., a size and mass now known to be typical of most molecular clouds throughout the Galaxy. One cloud is associated with the Orion Nebula and its radio continuum source, Orion A, the other with the radio continuum source Orion B and with the system of reflection nebulae NGC 2064, 2067, 2068, and 2071. (For the rest of this work, these clouds will be labeled the Orion A and B clouds.) These objects are probably the parent clouds from which the young OB association located just in front and slightly west of the clouds formed.

The Orion dark clouds offer an excellent laboratory for studying the formation of stars and the interactions between young stars and the interstellar gas: they are relatively nearby ($\sim$ 500 pc), and the region is well out of the galactic plane and consequently free from confusion created by other objects along the same line of sight. The interplay between clouds and stars may both fashion the appearance of such an active star-forming region and determine its evolution. Without a complete picture of molecular clouds in such a region, and of the star formation process, the largest-scale phenomena, which may ultimately be responsible for the formation of large star clusters and OB associations, are largely overlooked. This study presents a global view of the molecular cloud system in Orion and the neighboring constellation Monoceros, using radio emission from CO as a probe.

The primary goals of the CO survey presented here were to delineate the full extent of molecular material associated with the Orion region and to study the structures found. The new survey includes a reexamination of the Orion A and B molecular clouds with improved sensitivity, better velocity resolution, and increased spatial coverage using the Columbia University radio telescope, an improved version of the instrument used by Chin (1978).

The numerous dark clouds seen on the Palomar Observatory Sky Survey (POSS) prints outside the area surveyed by KTCT suggest that the full extent of the Orion complex of clouds had not been determined. Included in the new CO survey was the region bordered by the Orion molecular complex, the galactic plane, and the Taurus cloud complex, a total surveyed area of 850 deg^2. Figure III.4 indicates the extent of

the survey and shows the location of the objects found in this survey
and previous surveys with the Columbia telescope in the third quadrant
of the Galaxy. The network of molecular features discovered in the
present survey includes two long, thin ($\sim 10°$ x $1/2°$) molecular
filaments, an expanding ring of clouds surrounding the H II region
S 264 (Sharpless 1959) associated with λ Ori, and many small clouds.
The molecular cloud related to the Monoceros R2 association also lies
within the surveyed region and has a linear size and mass indicative of
a typical giant molecular cloud (see Morris, Montani, and Thaddeus
1980; Maddalena et al. 1982; and Thaddeus 1982 for preliminary accounts
of this work). As shown in Chapter V,A and B, all these clouds may
have a common origin and are part of a single cloud system over 300 pc
in diameter and having a total mass of 4×10^5 $M_\odot$. Aside from
locations of the clouds, the data from the survey provides values for
the gross properties of the clouds (e.g., mass, size, luminosity).

Many of the molecular clouds found in this survey have interesting
and unusual or unique properties in some way (Ch. IV,A). Cloud
structures that are discussed at length include the two filamentary
clouds which are cold but have wide spectral lines typical of those
characterizing warmer clouds. The observations from this survey,
combined with the preliminary results from observtions with high
resolution, indicate that magnetic fields may play an important role in
shaping the filaments and dominating their dynamics (Ch. IV,A,4).
Chapter V,C discusses a small, possibly dynamically evolving cloud
which may have internally subsonic motions.

Many of the CO emission peaks show interactions between the clouds

and young stellar objects coincident with the emission peak. These
interactions usually involve only the molecular material local to the
stars, i.e., areas of the clouds less than a few parsecs across. Two
large-scale interactions only hinted at in previous surveys and clearly
seen in this survey are investigated in some detail. The Orion A and B
clouds have temperature and density enhancements along a narrow ridge
located on the sides of the clouds facing the Orion OB association; in
Chapter V,D the ways in which the OB stars could have created such a
ridge is investigated. The λ Ori ring of clouds is a second
large-scale interaction; Chapter V,E provides a scenario for how λ Ori
and its H II region might have produced the expansion and distribution
of gas structures observed in that region of Orion. The size and mass
of the regions affected by each of these interactions are tens of
parsecs and about 5×10^4 $M_\odot$ of interstellar gas.

In the surveyed region along the galactic plane lie distant
molecular clouds not associated with the Orion system, most discovered
during the course of the survey (Chs. IV,B and V,G). A new cloud,
labeled Q in Figure III.4, lies ~ 2.°5 below the galactic plane and
midway between the Rosette and CMa OB 1 cloud complexes (Blitz 1978) on
the plane of the sky. This cloud, if at the most likely distance of
3 kpc, is larger (250 x 100 pc) than all other clouds in Figure III.4
even though it covers less angular area than the closer Orion A, B, and
Monoceros R2 clouds. The complete Orion system of clouds, discussed
above, is the only object in the figure comparable in size and mass
(~ 10^6 $M_\odot$) to cloud Q. Although these smaller, nearby clouds show much
evidence of associated star formation, the distant cloud shows very

little. These unusual properties, as well as the cloud's low temperature and wide spectral lines, are rarely found in combination for other molecular clouds. The observations indicate that Cloud Q may be a young object which has not yet extensively formed massive stars and which, after massive stars form, may in appearance resemble the Orion complex.

Outer galaxy surveys previous to the present one used poorer resolutions, lower sensitivities (Gottlieb, Brock, and Thaddeus 1984; Murphy 1984), or less complete spatial coverage (Sanders, Solomon, and Scoville 1984; Kutner and Mead 1981, 1985) and are inadequate for tracing spiral arms in the outer Galaxy beyond a galactocentric radius of 13 kpc (cf. Grabelsky 1985). Although only a 16° segment of the galactic plane was surveyed (1 ~ 206° to ~ 222°), over a dozen clouds with a total mass of at least 15 x 10^5 $M_\odot$ were mapped, some lying as far as 6 kpc from the Sun, or about 15 kpc from the center of the Galaxy. The sizes of these outer galaxy clouds are similar to what is found locally or in the inner part of the Galaxy, but the luminosity and mass of these clouds are far less than their inner galaxy counterparts, similar to what Kutner and Mead (1981, 1985) have found. Regardless of the low density of molecular material outside the solar circle, the locations and distances of the clouds suggest that they lie in two spiral arms, one possibly a continuation of the Perseus Arm into the third quadrant and the other a more distant spiral arm. These observations give the first indication that CO emission from molecular clouds can be used to trace the spiral arm pattern of our Galaxy out to galactocentric distances of 15 kpc.

CHAPTER II. COLUMBIA TELESCOPE

The survey consists of spectral line observations taken at the
frequencies of the $J = 1 \rightarrow 0$ rotational transition of ^{12}CO (hereafter
CO) and ^{13}CO (115 271 MHz and 110 201 MHz, respectively),
predominately from the Columbia 4 foot millimeter-wave radio
telescope in New York City; further observations of CO and ^{13}CO were
made with the NRAO 36 foot telescope on Kitt Peak; the Bell Telephone
Laboratory's 7 meter telescope at Crawford Hill, New Jersey; and the
2.5 meter Petite Operation Millimetrique (P.O.M) telescope in
Bordeaux, France. This chapter discusses the instrumentation,
pointing accuracy, and calibration of the Columbia telescope, which
provided all of the observations used for the large-scale survey of
Orion. The instrumentation of the three higher-resolution telescopes
used to reinvestigate portions of clouds observed in the Columbia
survey is summarized in Table II.1.

A. Instrumentation

The Columbia telescope, housed in a 12-foot Ash Dome on the roof
of the Pupin Physics Laboratories of Columbia University in northern
Manhattan, commands an unobstructed view of about 80% of the sky.
Operated and maintained jointly by Columbia and the Goddard Space
Flight Center, Institute for Space Studies (GISS), the telescope has
been in use since 1974. Observations for this survey were made from
1978 January through 1985 February, usually from the late fall

through early spring (November through April) when opacity due to
atmospheric water vapor is low. On the average, over 100 days per
year were suitable for observing.

The components of the telescope are: the antenna optics,
receiver, mount and drive, spectrometer, and computer. The optics of
the telescope, a Cassegrain system, consists of a 4 foot parabolic
primary with a focal ratio of f/0.375. When a room-temperature
Schottky diode receiver was replaced by a
superconductor-insulator-superconductor (SIS) tunnel junction
receiver in 1983 May, the effective focal ratio of the system changed
from f/2.8 to f/3.8; the telescope's original hyperbolic secondary
was replaced in order to compensate for the difference in positions
of the two receivers along the optical axis. The accuracy of all
surfaces, $\lambda/75$ at the 2.6 millimeter CO wavelength, is probably
better than that of most telescopes operating at these wavelengths.
In 1979 July, a pyramidal feed horn attached to the Schottky receiver
was replaced by a scalar feed horn, similar to the scalar horn later
used for the SIS receiver.

When a remote 115 GHz transmitter was used as a point source,
the antenna pattern of the telescope was found to be that calculated
from scalar diffraction theory. With the combination of pyramidal
horn, original secondary, and Schottky receiver the measured beam
width of the telescope was 8.'0 at full width at half-maximum (FWHM)
(Cohen 1978), and 8.'7 with the scalar horn, new secondary, and SIS
receiver. Although the antenna pattern for the Schottky receiver
with the scalar horn was not measured, Cohen (1978) calculated that

the beam would be 8.'3. The observed sidelobes in the telescope's diffraction pattern were 20 dB or more below the main lobe of the beam with the scalar horns (15 dB with the pyramidal horn). The beam efficiency of the telescope, altered after the changes in feed horn and receiver, is discussed in Chapter II,C.

The observations before 1983 May, roughly three-quarters of the total, were taken with the Schottky receiver, developed at GISS, which had a single sideband (SSB) receiver noise temperature of 900 K. The rest of the observations were taken with the SIS receiver, also developed at GISS, which had a noise temperature usually below 95 K SSB, the lowest to date for any receiver operating between 100 and 120 GHz. When this SIS receiver was installed, system noise temperatures referred to a point above the Earth's atmosphere (i.e., the combined noise from the telescope, spillover, and from the Earth's atmosphere) decreased from typically 2500 K SSB to 600 K SSB for CO observations (1700 K SSB to 300 K SSB for ^{13}CO), making the SIS receiver about twenty times faster than its predecessor. Unlike the Schottky, the SIS receiver is a true single sideband receiver with 20 dB less sensitivity in its image sideband than in its signal sideband. Complete descriptions of the receivers are given by Cong (1977) and Cong, Kerr, and Mattauch (1979) for the Schottky and by Pan et al. (1983) and Pan (1984) for the SIS.

The antenna and most of the receiver components are pointed by an altitude-azimuth fork mount. Using the output from 16-bit (19."8 resolution) optical shaft encoders and tachometer generators, the computer monitors the pointing and slew rate of the telescope for

each axis of the mount every 0.01 sec and alters the torques supplied by direct-drive motors when necessary. The telescope's relative pointings are maintained to within 2' of the position requested (see Ch. II,B for the absolute pointing accuracy). Similarily, the position of the dome is maintained to within an allowable error of 1°.

After detection and amplification, the incoming signal is passed from the receiver to a filter bank spectrometer, built at GISS following an NRAO design, that has 256 channels, each with a resolution of 0.250 MHz. At the frequencies used for CO and ^{13}CO, the filter bank has resolutions of 0.65 and 0.68 km s^{-1} and bandwidths of 166 and 174 km s^{-1}, respectively, with higher velocity resolution observations possible using the methods described below (Ch. V,C). The outputs from the filter bank are integrated for 48 msec, digitized, and sent to the computer.

The computer (a Nova 1200 replaced in 1984 September by a Nova 4/X, both manufactured by Data General) monitors the telescope's position, updates the various commands to the telescope drives and to the reference frequency source for the receiver's local oscillator, acquires data digitized by the spectrometer, calibrates them (Ch. II,C), and stores them on a cartridge disk. The observer can perform some preliminary data reduction while observing (e.g., to display spectra previously stored on disk or being observed, and revise the parameters used to remove baselines). Available on the same system are various utility programs--for transfer of data from disk to computer tape or automatically searching through a list of

positions for the most suitable reference positions for a position-switched observation (Ch. III,A). After preliminary data reduction and storage of the data at the telescope, the remaining data reduction is performed at GISS with main-frame computers (IBM 4341 and an Amdahl 470/V6).

B. Pointing Accuracy

A comparison between the known optical center of the Sun, obtained from the Nautical Almanac, and the observed radio limb of the Sun is used to test the pointing accuracy because Venus and Jupiter, the sources ordinarily used by millimeter-wave telescopes, subtend an area much smaller than the beam of the Columbia telescope with the result that their emission is severely diluted. The difference between atmospheric refraction at optical and millimeter wavelengths and the size of the telescope beam is assumed to be negligible.

The parameters of the pointing (i.e., the orientation and tilt of the telescope pier and mount) were revised at least annually: first using the radio limb of the Sun to align the radio axis of the telescope on the center of the Sun; second, aligning the axis of an optical telescope, attached to the dish of the radio telescope, on the image of the Sun; and third, measuring with the optical telescope the pointing errors toward roughly 30 stars well distributed in the sky (Cohen 1978). Periodically, the pointing accuracy was checked by observing the radio limb of the Sun, to see if the observed radio

limb remained concentric with the expected optical center and daily

by comparing the intensity toward strong CO sources in Orion and

Monoceros (NGC 1976, NGC 2068, or the core of Mon R2) with

intensities previously obtained. Absolute pointing errors were, at

most, 2' and, typically, 1'.

C. Calibration of Spectra

At 110 and 115 GHz the calibration of spectra must take into

account the attenuation of the Earth's atmosphere, which was assumed

to arise from an unchanging oxygen layer and a variable water vapor

layer. The atmospheric opacities from water vapor were measured by

antenna tipping before each day's observations of the Orion region

(more frequently if the weather changed), and the values of receiver

gain were updated with a chopper wheel calibration before each scan

(Cohen 1978; Kutner 1978). This procedure gave antenna temperatures

consistent to within 5%, regardless of the elevation of the source or

the atmospheric opacity.

The temperatures in the spectra were then converted to radiation

temperatures, T_R (Kutner and Ulich 1981), by correcting for beam

efficiency, η, which, prior to 1979 July, equaled 0.67 but after the

scalar feed horn replaced the pyramidal feed horn became 0.81. After

the SIS receiver was installed η increased to 0.92. (The value of η

for the Schottky receiver with scalar horn and original secondary was

calculated from the theoretical radiation pattern of the scalar horn

and from scalar diffraction theory; the other values of η were obtained by comparing the observed intensities toward strong CO sources, such as Orion A, B 335, and W 51, before and after each modification.) The T_R obtained with the Columbia telescope are 7 to 10% lower than those seen with the Bell Laboratories, NRAO 36-foot, and Five College Radio Astronomy Observatory telescopes.

CHAPTER III. OBSERVATIONS--COLUMBIA TELESCOPE

The Orion survey with the Columbia telescope covers a wide range in galactic latitude ($-25°< \underline{b} < 4°$) so, to make the survey as efficient as possible, different observing techniques were used for different regions. Observations were either position-switched or frequency-switched and taken at either full resolution or lower ($1/4°$ or $1/2°$) in which case the super-beam technique was used. After a description of each technique, the use of the techniques for the particular observations is discussed.

A. Observational Techniques: Position and Frequncy Switching and
    Super-Beam technique

Position-switched observations toward a source position require one or two nearby reference (off) positions found by frequency-switched observations to be devoid of CO emission stronger than typically 0.15 K. Because the spectrometer uses filters with non-linear responses, position-switching occasionally results in non-linear baselines when a large difference in power (DP) exists between the powers emitted by the Earth's atmosphere from the source and off positions. To reduce the baseline problem, two off positions are used, one with an elevation above the source position (negative DP) and one below (positive DP). The total time on the two off

positions equals the total on the source position, but the fraction of time on each off is chosen to produce spectra with a DP as small as possible. Observations with a single off position can give good results if either the sensitivity of the observation is not too high or a flat baseline in only a narrow velocity range is desired. Multiple off positions, which produce spectra requiring at most the removal of a first order baselines across the full bandwith of the spectrometer, give the widest range of usable velocity in the final spectra.

In frequency-switched observations, the reference spectrum is obtained by shifting the frequency of the receiver's local oscillator usually by 10 or 20 MHz for half of the observing time: if CO emission is present along a particular line of sight, the resultant spectrum contains both a signal line and an image of the signal line separated by 10 or 20 MHz. If the CO telluric lines and their images, both lying at predictable velocities, fall at velocities where emission is expected, then observations of the region are either delayed until the telluric lines are no longer a problem (i.e., when the component of the antenna's velocity with respect to the local standard of rest, LSR, along the line of sight changes significantly) or the observations are made by position-switching. Frequency switching is used when narrow spectral lines are expected within a limited velocity range, and when looking for off positions for planned position-switched observations.

After baseline removal--typically by a third-order polynomial

fit to the 20 channels on both sides of the signal and image lines--the frequency-switched spectra were folded, reducing the noise in the spectra so the integration time needed to obtain a certain noise level is $\sqrt{2}$ less than for position-switched observations. Since all observed emission lines were much narrower than the extent of the baseline used in the fit, the high-order fit should not have affected the processed spectra. For a random sample of spectra we checked for differences between this high-order baseline fit and a first-order baseline fit through the half dozen or so channels on either side of the signal and image line and found neither systematic nor significant differences (Fig. III.1); the high-order fit gives more aesthetic plots with a larger useful baseline (~ 40 km s^{-1}) than a first-order fit. Figure III.2 gives examples of both frequency-switched spectra, before and after folding, and position-switched spectra.

The super-beam technique is used when the area to be surveyed is much larger than the area covered by the telescope beam. Since an unmanageable number of observations would be needed to cover that area, the amount of data could have been reduced by averaging or smoothing the high-resolution data after the observations were made. The super-beam technique performs the averaging by moving the telescope through a square grid of full-resolution positions while the data is being collected, thereby synthesizing a larger and essentially square beam; it makes efficient use of the time of the telescope and its computer, since only one observation needs to be taken, proccessed, and stored, but the higher resolution information is no longer available.

B. CO Observations

The large-scale CO survey of Orion and Monoceros covers 850 deg^2 (0.25 steradians) of the celestial sphere, extending roughly from the CMa OB 1 and Rosette (Mon OB 2) cloud complexes along the galactic plane down to a galactic latitude of -25° and from the Taurus dark cloud complex in the north to a declination of -14° (Fig. III.4). Approximately half of the observations were taken by myself or under my supervision; the remaining observations were made either by Mark Morris or Joseph Moscowitz. In total we observed over 12,500 positions within that region at the locations indicated in Figure III.3. With an rms noise level of at most 0.3 K and more typically 0.25 K, each observation, if frequency-switched, took 9 minutes of integration with the Schottky receiver and 1/2 minutes with the SIS, or, if position-switched, 13 minutes and 3/4 minutes, respectively.

The molecular emission from nearby objects at high galactic latitudes was expected to cover a narrower range in velocity than emission from objects along the galactic plane which could have a wide range in distances. For the sake of efficiency, but without compromising the quality of the observations, different observing methods were used for different regions within the survey, and the large survey can be divided into three sub-surveys (Fig. III.4): full-resolution observations at intermediate latitudes, high-latitude observations, and galactic plane observations with 1/4° resolution.

1. Full-Resolution Observations at Intermediate Latitudes

Full-resolution observations at intermediate latitudes constitute about 75% of the Orion survey and concentrated mainly toward the largest molecular clouds either known to exist prior to the start of the survey or found during its course. About a fourth of the observations were position-switched, using either one or two off positions (Table III.1), and the majority frequency-switched. Initially observations were spaced 1/4° or 1/2° apart; when molecular emission from a cloud was found, the full extent of the cloud was covered by observations spaced either 1/4° or 1/8° apart.

2. High-latitude Observations

At high latitudes (b < -20°) in Orion, a great deal of CO emission is not expected first, because stellar winds and strong ultraviolet fluxes from stars in the Orion OB association in this area have probably dispersed or dissociated most molecular material; second, because the region at the 500 pc distance of Orion is four to five times the local scale height of molecular material from the galactic plane; and, third, because galaxy counts of the area indicate little obscuration from dark clouds. The extent of the area required us to space observations 1° apart and to use a super-beam 1/2° on a side; all observations were frequency-switched. When the spectra showed possible emission, full-resolution observations were made to confirm the detection and to map the extent of any cloud found.

3. Galactic Plane, 1/4° Resolution Observations

Observations along the galactic plane, position-switched with two off positions (Table III.1), were taken with the SIS receiver at a resolution of 1/4°, using the super-beam technique, and spaced 1/4° apart. In addition to determining whether there was any molecular emission in the galactic plane associated with the local Orion clouds, the goal of this part of the survey was to find how much molecular material exists outside the solar circle. The sensitivity (rms noise of 0.20 K) and the spatial resolution were sufficient to detect any cloud closer than 5 kpc with a diameter of at least 10 pc and a peak temperature greater than 1 K.

C. ^{13}CO Observation

Since the LTE method of determining cloud masses requires both CO and ^{13}CO observations at the same location within a cloud, we looked for ^{13}CO emission at approximately 135 positions known from the CO survey to have strong emission. All observations were taken at full resolution by frequency-switching to an rms noise level of 0.15 K or better. In addition to full-resolution observations, we similarly surveyed all of the Orion A and B clouds using a super-beam resolution of 1/2° and an rms noise of 0.20 K. The 310 position observed for ^{13}CO emission are shown in Figure III.5.

CHAPTER IV. RESULTS

The observed emission can be separated into emission coming from objects that are part of the local arm of the galaxy and emission from more distant objects that lie in the outer arms of our galaxy. The first section of this chapter concentrates on the results toward clouds with distances of about 1 kpc or less, including clouds associated with the Orion and Monoceros star-forming regions; the rest discusses the outer galaxy clouds. A later chapter discusses some particularly noteworthy cloud structures.

A. Clouds Associated with the Orion and Monoceros Complexes

About 100 deg^2 of the region surveyed show CO emission exceeding a T_R of 0.8 K in the velocity range -10 to 20 km s^{-1}. Most of this molecular material is concentrated into large clouds associated with Orion A, Orion B, Mon R2, and into two filamentary clouds. The remaining clouds can be divided into groups with apparently similar characteristics or a similar origin.

The results are summarized in Figures IV.1-IV.4. Figure IV.1 presents a contour map of velocity-integrated intensity of CO emission, W_{CO}, for the region surveyed. Figure IV.2 identifies the most prominent molecular features and indicates the main peaks in the CO brightness temperature distribution; Table IV.1 lists the position, maximum measured temperature, temperature-weighted mean

velocity, W_{CO}, and associated astronomical objects (e.g., dust clouds or H II regions) for each peak. Figure IV.3 shows the temperature-weighted mean velocity field, ($[\int T_R v\, dv] / \int T_R\, dv$), generally approximating the average velocity of the molecular material in a particular direction. Figure IV.4 displays line widths defined throughout this work, unless otherwise stated, as $W_{CO} / T_R(PEAK)$; since most observed spectral lines are approximately Gaussian in shape, the displayed line widths are equal to 1.064 times FWHM and to 1.253 times twice the rms line widths. For blended lines the velocity displayed in Figure IV.3 is a weighted average of the components; the line width displayed in Figure IV.4, then, lies between those of the individual components and of the whole multiple line. The only large region of double lines with close, overlapping components lies in the Orion B cloud between NGC 2023, 2024 and NGC 2064, 2067, 2068, and 2071. In two regions, near $\alpha = 5h\ 52m$, $\delta = 2°$ and $\alpha = 5h\ 52m$, $\delta = -9°$, the spectra show two widely separated (> 8 km s^{-1}) velocity components that imply overlapping and presumably distinct clouds. Each component is treated separately in these regions, and, for the sake of clarity, the data for one of the velocity components are displaced from their actual positions in Figures IV.1-IV.4.

1. Orion A and B

The molecular clouds associated with Orion A and B, which have a distance of ~ 500 pc, subtend some 29 and 19 deg^2 (see Fig. IV.1 and

the magnified-scale Figs. IV.5 and IV.6), or substantially more than in Chin's (1978) survey which had a detection limit of 2 K, three times that of the present survey. In the present survey, Orion B extends to $\delta = 5°$, well above the $\delta = 2°$ limit of the previous survey. Where Orion B's northern extension narrows at $\delta \sim 1.°5$ and Barnard's loop crosses it in projection, the Orion East cloud (LDN 1621 and 1622) is superposed (Ch. IV,A,6). At the southeastern extreme of the Orion A cloud, where velocities are 3-5 km s^{-1}, a second molecular feature, NGC 2149 (Ch. IV,A,3), with a velocity of 14 km s^{-1}, overlaps the Orion A cloud.

The apparent connection of Orion A and B by low-level emission without a discontinuity in velocity suggests that these clouds may be physically connected. Both Orion A and B have higher CO temperatures on their western edges and a ridge of emission where recent star formation seems preferentially located that falls off more quickly to the west than toward the east; Chapter V,D discusses ways in which the Orion OB I association located just to the west of the molecular clouds may have been responsible for this molecular ridge.

In the region of the Orion B cloud between NGC 2023, 2024 and NGC 2064, 2067, 2068, and 2071 the temperature-weighted mean velocities are systematically lower (7 km s^{-1}) and the line widths are significantly larger than those observed either directly to the north or south (Figs. IV.3 and IV.4). Most of the line profiles in this region are double: the weaker, low velocity component ranges from 3-8 km s^{-1} and the stronger, high velocity component from 8-11 km s^{-1}. The

velocities within this region are summarized in Figure IV.7. The high-velocity component seems continuous from north to south, while the low-velocity appears and disappears. Two explanations of the presence of double spectral lines can be offered: first, two molecular clouds with slightly differing velocities may exist in this region, or, second, strong stellar winds, typical for young stars like those in this region or in the nearby Orion OB I association, may accelerate one part of the molecular cloud relative to another. Except for this region of double lines, the Orion B cloud has no organized or ordered velocity structure.

We confirm for the Orion A cloud the substantial velocity gradient (from 11 km s^{-1} near α = 5h 28m, δ = -3° to 5 km s^{-1} near α = 5h 48m, δ = -10°, Fig. IV.8) noted by Chin (1978) and KTCT, which they suggest may indicate rotation of the cloud about an axis perpendicular to the galactic plane in a direction opposite to galactic rotation. Channel maps for the Orion A and B clouds (Fig. IV.9) illustrate the velocity structure of these two clouds.

A few small clouds (13, 14, 28, 29, 39, and 40, Table IV.1) are located to the west of the Orion A and B clouds 'in the general vicinity of the OB association. The cloud with peaks 39 and 40 (Table IV.1) may be related to Barnard's loop (Ch. IV,A,7). Both cloud 13, associated with the reflection nebula VDB 33 (van den Bergh 1966) with an estimated distance of ~ 420 pc (Racine 1968), and cloud 14, associated with the optical H II region S 278, are located well away from the major clouds. Peak 14 coincides with a position

of excess γ-ray emission that cannot be accounted for by the interaction of cosmic rays with the column density of interstellar gas implied by both 21 cm (Heiles and Habing 1974) and our observations (Bloemen et al. 1984; Bignami and Caraveo 1985). Clouds 13, 14, 28, and 29 may be remnants of the molecular material from which the nearby OB association formed or they may be clouds pushed to their present locations by pressure associated with energetic events (e.g., strong stellar winds, supernova explosions, or H II region expansion) accompanying the evolution of the OB association (Cowie, Songaila, and York 1979; also Ch. V,D).

2. Monoceros R2

The Monoceros R2 complex of reflection nebulae, first studied by van den Bergh (1966) and Racine (1968), is an intense source of molecular emission. Previous studies of CO, CS, HCN, H_2CO, and NH_3 (Loren, Peters, and Vanden Bout 1974; Downes et al. 1975; Kutner and Tucker 1975; Loren 1977; Wilson and Folch-Pi 1981) concentrated on a 4 deg^2 region centered on the reflection nebulae. Mon R2 is also associated with a cluster of embedded infrared sources (Harper 1975; Beckwith et al. 1976; Hudson and Soifer 1976; Thronson et al. 1980), a compact H II region (Shimmins, Clarke, and Ekers 1966; Shimmins et al. 1966; Downes et al. 1975), and both H_2O and OH masers (Downes et al. 1975; Knapp and Brown 1976; Morris and Knapp 1976). The spatial distribution of these indicators of recent star formation suggests that the core of Mon R2 is a less complex, possibly younger version

of the Orion Nebula region (Thronson et al. 1980): a cluster of infrared stars remains embedded and massive stars, inferred from the presence of compact H II regions and reflection nebulae irradiated by B stars, are just beginning to form at the near edge of the cloud.

In the present study, CO emission around Mon R2 is found to subtend 14 deg^2 (Fig. IV.1 and, in more detail, Fig. IV.10), so the Mon R2 cloud, if at a distance of 830 ± 50 pc (Racine 1968; Herbst and Racine 1976), would be comparable in size (110 pc x 40 pc) and in CO luminosity to the Orion A or B clouds: the Mon R2 cloud, then, is a substantial giant molecular cloud.

The outline of the cloud associated with Mon R2, within which $W_{CO} > 6.4$ K km s^{-1}, corresponds remarkably well to the one Lynds (1962) depicted for the dark clouds LDN 1643, 1644, 1645, and 1646. The predominant hot spots (61, 63, and 65, Table IV.1), first identified by Kutner and Tucker (1975), coincide with the greatest concentrations of reflection nebulae on the POSS prints (van den Bergh 1966; Herbst and Racine 1976). Unlike Orion A or B, most of the Mon R2 cloud subtends an area that largely exhibits emission well below 10 K km s^{-1} with a few holes in the CO emission within the cloud boundary. Apparently this cloud is more centrally condensed than either the Orion A or B clouds with most of the emission coming from the cloud's core and little from the envelope. Like Orion A and B, the western edge of Mon R2 (near α ~ 6h 03m, δ ~ -6° 30') has a steeper temperature gradient than the eastern, and the region with the largest temperature gradient has spectral lines significantly

wider ($\sim$ 5 km s^{-1}) than elsewhere in the cloud (Fig. IV.4). In the areas centered on the hot spots coincident with the reflection nebulae (peaks 61, 63, and 65) the lines are similarily wide.

Velocities are higher in the northwest (13 km s^{-1}) than in the southeast (8 km s^{-1}), while the central, active region of Mon R2 has a velocity of 7 km s^{-1}, relatively lower than that of the immediately surrounding areas (Fig. IV.3). Apart from this low velocity region, the overall velocity gradient, although not as smooth, is reminiscent of the gradient found in the Orion A cloud and may also be due to rotation of the cloud about an axis perpendicular to the galactic plane in a direction counter to galactic rotation.

3. NGC 2149 Clouds

Toward the southeastern end of the Orion A molecular cloud, where the velocities are typically 3-5 km s^{-1}, a second component at $\sim$ 14 km s^{-1} indicates a separate object along the line of sight. As the lower inset of Figure IV.1 shows, the emission from this high-velocity feature extends from a point within the boundary of the Orion A cloud (at α = 5h 36m, δ = -9° 00') to the Mon R2 cloud (at α = 6h 04m, δ = -10° 30') and peaks near the reflection nebula NGC 2149 (VDB 66) and further west (peaks 43, 44, and 48, Table IV.1). Three more molecular clouds (peaks 45, 46, and 47) lying immediately to the south of the NGC 2149 cloud have similar velocities and are probably physically related to and at the same distance as peaks 43, 44, and 48.

Both the similarity in velocity between these clouds and the
nearby Mon R2 cloud and the respective distance moduli of 9.6 and 9.5
(Racine 1968) for the irradiating stars of NGC 2149 and the
reflection nebula, VDB 64, associated with peak 47 imply that the
NGC 2149 clouds lie at the same distance as Mon R2 (830 pc,
Ch. IV,A,2). At this distance, the western extreme of the cloud is
~ 300 pc below the galactic plane. Possible relationships between
NGC 2149, Mon R2, and the Southern filament are discussed in the next
section.

4. Northern and Southern Filaments

The Northern filament, a continuous cloud typically 1/2° wide,
extends ~ 10° in right ascension from the eastern edge of the λ Ori
cloud group almost to the Rosette Nebula and its associated molecular
clouds (Blitz 1978). At $\alpha \sim$ 6h 04m, $\delta \sim$ 2° and $\alpha \sim$ 6h 12m, $\delta \sim$ 3°,
the filament widens into features similar to typical molecular
clouds. On the POSS prints the Northern filament appears as
unconnected, opaque patches. There is no evidence of T Tauri stars
or reflection nebulae, nor of other signs of recent star formation
within this filament, so its distance is hard to estimate. Following
the method of Herbst and Sawyer (1981), star counts imply that the
distance is 801 ± 91 pc to the Northern filament (details presented
in Table IV.2). This method is crude, and, given the almost
identical 11 km s^{-1} velocities of the filament and the nearby Orion B

cloud, the filament is likely to be at the Orion B distance of 500 pc, which is the distance adopted. The Northern filament has smooth velocity gradients along spans of a few degrees and, where velocities shift abruptly by 2-3 km s^{-1}, both optical obscuration on the POSS prints and W_{CO} tend to increase. If the smooth velocity gradients indicate that material accelerates along the filament, presumably from the pull of gravity toward the galactic plane, then those places of abrupt velocity changes, higher obscuration, and increased W_{CO} might be where the filament is bent along the line of sight.

The Southern filament, another long, thin (10° x < 1/2°), and almost continuous feature, extends eastward from the southeastern edge of Mon R2 to the galactic plane near CMa OB I. Like the Northern filament, it makes an average angle of 50° with the galactic plane and has much wider spectral lines than are expected in an apparently quiescent cloud without young stars. A smooth velocity gradient exists along its length, from 8 km s^{-1} at α = 6h 20m, δ = -10° 30' to 18 km s^{-1} at α = 6h 52m, δ = -11° 30', which, like gradients seen in the Northern filament, may be due to the accelerated flow of material toward the galactic plane. East of 6h 52m, the velocity field in the Southern filament undergoes abrupt and apparently unsystematic shifts that may indicate line of sight confusion between the filament and the molecular clouds associated with CMa OB I (Blitz 1978).

A second linear feature, ~ 3° long, intersects the Southern

filament near the position α = 6h 30m, δ = -9° 30' and creates an object we call the Crossbones. It appears to be a single cloud, not a chance superposition of two clouds; the velocity gradients along both its arms are in the same sense and merge smoothly at the intersection.

The velocities of the western portion of the Southern filament being roughly the same as those of the nearby Mon R2 cloud, the distance to that portion of the filament may be the same as to Mon R2 (830 pc). Of several CO emission peaks discernible in the Crossbones, one (67, Table IV.1) coincides with three reflection nebulae, VDB 80a, b, and c which have associated stars at about 912 pc (Racine 1968), close to the distance of 1009 ± 77 pc estimated from star counts (Table IV.2). Six reflection nebulae (VDB 88, 89, 90, 92a, b, and c), with an average distance of 1060 ± 130 pc (Racine 1968; Eggen 1978), lie just beyond the eastern end of the Southern filament (α = 7h 04m, δ = -12°), but whether they are physically associated with this filament or with the nearby CMa OB 1 clouds, which have a distance of 1200 pc (Eggen 1978), is unclear. The Southern filament is less discernible on the POSS prints than the Northern filament, implying more foreground stars for the Southern filament and corroborating the greater distance. These distance estimates indicate that the Southern filament may extend some 230 pc along the line of sight, which is similar to its projected length on the sky. It is possible that the Southern filament is a physical bridge between the Mon R2 and CMa OB 1 clouds. The continuity in velocity from the NGC 2149 cloud to the southern end of the Mon R2

cloud and from the Mon R2 cloud to the Southern filament suggests that the southern part of the Mon R2 cloud connects the NGC 2149 clouds and the Southern filament; if so, a single, continuous, and linear structure would then extend 300 pc in the plane of the sky, from 5h 36m to 7h 04m.

One naturally wonders how molecular gas is confined to such long, slender filamentary structures. The ρ Oph clouds, also filamentary but smaller, possess interstellar magnetic fields aligned along the long axis (Vrba, Strom, and Strom 1976); Vrba (1977) suggests that the shape of the ρ Oph clouds come from the confinement of molecular material by the magnetic field. The polarization of light from stars behind the Orion filaments may provide a clue as to the field orientation near these clouds and whether the shape of the clouds result from magnetic fields. Although some stars in the direction of the filament have measured polarizations (see Fig. IV.11 and references in the caption), too few lie behind or near the filaments (Figs. IV.12 and IV.13) to conclusively indicate the direction of the magnetic field. If the gas presuure implied by the observation ($\propto \rho \, [\Delta V_{FWHM}]^2$, where ρ is the density derived from the estimated volume and mass of the filaments [Table V.1] and ΔV_{FWHM} is the observed line width) is comparable to the magnetic field pressure ($B^2 / 8 \pi$) then a crude estimate to the field strength is 30 μG, a value ten times higher than is typical for diffuse H I clouds and 3 times higher than that measures by Heiles and Troland (1982) in the envelope of the Orion A cloud.

The relationship between the filaments and the other objects in the region is unclear. If the molecular clouds formed at about their present displacement from the galactic plane, then the material in the filaments may represent gas which was originally part of the Orion A, B or Mon R2 clouds but now is falling toward the galactic plane probably along paths dictated by magnetic fields. If the clouds formed in or close to the plane and then moved out of the plane, possibly because of their own velocities or that imparted by explosive events such as supernovae, then the filaments may represent material left behind as the clouds moved. The filaments may also have formed through a method proposed by Chiang (1984) and Chiang and Prendergast (1985). In their numerical simulation of the interaction between young stars and the interstellar medium, filamentary structures, with properties very similar to those observed in Orion, frequently formed alongside larger gas condensations.

High resolution observations were made toward both filaments using the NRAO 36 foot telescope, the Bell Telephone Laboratory's 7 meter telescope, and the Petite Operation Millimetrique (P.O.M) 4 meter telescope (see Table II.1 for the instrumentation and observing methods for each telescope) in the hope of learning more about the internal structure of these enigmatic clouds. As shown in Figures IV.14, the observations consist of strips of positions oriented parallel or perpendicular to the long axis of the filaments; Figure IV.15, contour maps of the velocity structure within strips, presents representative results from the telescope at Bell Laboratory.

Although the analysis of the high resolution data is not yet complete, the observations indicate the same wide lines as seen by the Columbia telescope and reveal multiple emission peaks and velocity structures within the clouds that abruptly change form one strip to the next ~ 1.3 pc away (e.g., Fig. IV.15b and c). The filaments probably consist of an envelope of low density molecular material in which is embedded numerous denser clumps moving at speeds of a few km s^{-1} relative to each other; the magnetic fields proposed above, and as discussed in Chapter V,A, may tie the clumps together and prevent the expansion of the clouds. The observations show some evidence of a general velocity gradient across the width of the Southern filament that may be due to rotation of the cloud about its long axis (Fig. IV.15e, f, and g), but each of the clumps within the Northern filament have different and opposing velocity gradients. Other systematic trends in the velocity structure were looked for but none has yet been found. A more detailed study of the filaments is in preparation.

5. λ Orionis

Several molecular clouds (peaks 1-12) are located along the border of S 264, the large, conspicuous H II region centered on a complex of OB stars including the O8 star λ Ori. Although no large-scale molecular surveys have been done, several observations have been made toward some of the dark clouds lying along the border

of the H II region (Lada and Black 1976; Kutner et al. 1980; Baran
1983).

Murdin and Penston (1977) and Duerr, Imhoff, and Lada (1982), who
investigated the ages and distribution of the OB stars and Hα emission
objects in the region, suggest that soon after the OB stars in the λ
Ori complex formed, the expansion of the resultant H II region
disrupted the parent molecular cloud. Resembling a classical
Stromgren sphere which is ionization bounded and in a late stage of
development, the H II region now is surrounded by dark clouds (Barnard
1927; Coulson et al. 1978) and possibly an expanding H I shell (Wade
1957, 1958; Crezelius 1984), all either remnants of the disrupted
parent cloud or material swept up during the expansion of the H II
region.

The molecular clouds revealed by our survey are arranged on a
ring that has the same radius as both the 100μm ring seen by IRAS and
the radius of the H II region found by Reich (1978) in the radio
continuum and by Isobe (1973) in Hα emission. The large, systematic
velocity shifts, similar to those found for H I (Wade 1957, 1958;
Crezelius 1984), suggest that the dark clouds, rather than being
spherically distributed, lie on a ring expanding away from a center
located close to λ Ori; see Chapter V,E for a discussion of the
shape, orientation, and dynamics of the ring, and proof that λ Ori is
responsible for the ring of clouds.

Three of the molecular clouds forming the λ Ori ring which were
originally cataloged by Barnard (1927) as dust clouds (B 30, B 35,

and B 223) have bright optical rims toward λ Ori where CO temperatures tend to be higher than elsewhere in the clouds. According to Lada and Wilking (1980), the temperature enhancement for B 35 seen by Lada and Black (1976) and in our data may result from heating or compression of the molecular gas by the stellar wind from λ Ori; from the shock front associated with the expansion of S 264; or from magnetic viscous heating (Ch. V,D,2). No luminous, embedded infrared source, which might otherwise account for the heating of this cloud, seems to be present (Lada and Black 1976; Lada and Wilking 1980; Lada et al. 1981). Heating processes like those conjectured for B 35 may be occurring in the other clouds of the λ Ori ring.

Other individual clouds in the ring are noteworthy. In particular, one cloud (peaks 2 and 3), which has strong CO emission but has not been cataloged as a dark nebula and is invisible on the POSS prints, is associated with the two reflection nebulae VDB 35 and 37. The star associated with VDB 35 has a distance of about 460 pc (Racine 1968), close to the 400 pc of the λ Ori association. Duerr et al. (1982) suggest that the B 30 cloud (9, Table IV.1) may have been the parent molecular cloud for a group of Hα emission objects clustered around a center southeast of the cloud; for these young stars to be currently visible, the originally obscuring cloud material must have been dissipated by the H II region or pushed aside by its expansion (Ch. V,E,2).

The molecular cloud B 223 associated with the H II regions S 263

and S 265 contains the dark clouds LDN 1588, 1589, and 1590 which

have bright rims both on their northeast edge facing λ Ori and toward

the south; Hα and UV maps of the Orion region (O'Dell, York, and

Henize 1967; Isobe 1973; Reynolds and Ogden 1979) show a faint

extension of Barnard's loop superposed on the B 223 cloud

(Fig. IV.2). The average distance of 307 ± 50 pc for three

reflection nebulae associated with this cloud, VDB 38, 40, and 43

(Racine 1968), is comparable to the 400 pc to λ Ori and Barnard's

loop (Reynolds and Ogden 1979), suggesting that the loop may be

responsible for the bright southern rims.

6. Orion East (LDN 1621 and 1622)

The bright-rimmed cloud called Orion East by Herbig and Rao

(1972), at an estimated distance of 500 ± 140 pc (Herbst 1982;

Table IV.2), is associated with LDN 1621 and 1622, at least five

T Tauri stars (Herbig and Rao 1972; Cohen and Kuhi 1979) and the two

reflection nebulae VDB 62 and VDB 63 (Fig. IV.16); it is very well

defined on the POSS prints 1° northeast of Barnard's loop. CO

emission from Orion East covers ∼ 1 deg^2 at a v_{LSR} ∼ 1 km s^{-1}

(Fig. IV.16), 9 km s^{-1} less than that of the Orion B cloud in this

direction. An interaction of this cloud with Barnard's loop is

suggested by the strong CO emission along the edge of the cloud

closest to the loop and, noticeable on the POSS prints, the bright

rim on the side of the cloud facing the loop. In addition to the

possible heating oт the gas arising from this interaction, heating by
T Tauri stars and reflection nebulae within 1/2° of the strongest CO
emission peak may be significant. Embedded infrared sources, if
present, would also contribute to the heating of the cloud. The
cloud's line widths are small, generally less than 1.5 km s^{-1};
usually, wider lines are found for clouds which have similarly
intense CO lines and are interacting with young stars and objects
similar to Barnard's loop. Even with the low spectral resolution of
the filter bank (0.65 km s^{-1}), velocity shifts between different
positions within the cloud suggest that the cloud may not be
gravitationally bound. In an attempt to see if the cloud is bound,
and also to determine whether the narrow lines indicate subsonic
motions, CO and ^{13}CO observations with high velocity resolution
(0.22 km s^{-1}) were made at three positions within the cloud
(Fig. IV.16). See Chapter V,C for the observational techniques, data
reduction, and the implication of the observations.

7. Barnard's Loop

At least three clouds other than Orion East may be related to
Barnard's loop. Two (41 and 42, Table IV.1) located directly on the
loop are possibly the northern and southern sections of LDN 1638 (see
Fig. 1, KTCT). Whether these clouds, with velocities and positions
intermediate between the western side of Mon R2 and the eastern side
of the Orion A and B clouds, are associated with the loop or Mon R2
or Orion A and B remains unclear.

The third cloud (39 and 40, Table IV.1) lies between the Orion B and B 223 clouds near where Barnard's loop fades away on the POSS prints. The cloud has no bright rims and, unlike most clouds with such strong CO emission, is barely discernible on the prints. Peak 39, probably associated with the reflection nebula VDB 49 and its illuminating star ω Ori, may be at an approximate distance of 320 pc (Racine 1968), similar to the distances of 400 pc to Barnard's loop (Reynolds and Ogden 1979) and 307 pc to B 223. Since neither of these distances is well known, this cloud could be physically related to Barnard's loop, to B 223, or both. The western portion near peak 39 has a velocity of approximately 3 km s^{-1} and shows some evidence for a north-south velocity gradient, while the velocity of its eastern portion near peak 40 is approximately 9 km s^{-1} (Fig. IV.3). In the region between peaks 39 and 40, double spectral lines with velocities of 6 and 10 km s^{-1} indicate that the cloud may actually consist of two unrelated components seen in projection.

8. LDN 1653, 1654, 1655, and 1656

North of the Southern filament CO emission matches the dark nebula LDN 1653, 1654, 1655, and 1656 on the western border of the CMa OB I complex (Fig. IV.2) observed by Blitz (1978). Emission from CO intensifies at 74 (Table IV.1) toward the H II region 220-01/1 in Marsalkova's (1974) catalog and its associated bright nebula

NGC 2316. The velocity one beam (7.'5) to the east of this peak is 7 km s^{-1}, versus 12 km s^{-1} found toward the rest of the cloud, a discontinuity suggestive of an interaction between the H II region and the cloud. Peak 72 (Table IV.1) lies near the reflection nebula VDB 86, which has an associated star with a distance of 500 pc (Eggen 1978). The proximity of clouds 72-74 to CMa OB 1, and the modest difference in the velocity of these clouds (12 km s^{-1}) compared to that of CMa OB 1 (18 km s^{-1}, Blitz 1978), lead us tentatively to adopt for the LDN 1653, 1654, 1655, and 1656 clouds the same 1200 pc distance as that of CMa OB 1 (Eggen 1978). Alternatively, these may be associated with the neighboring section of the Southern filament at a distance of approximately 1060 pc (Ch. IV,A,4).

B. Outer Galaxy

Observations along the galactic plane revealed emission which in part probably arises from clouds at distances greater than 1 kpc from the Sun. The results of the 1/4° super-beam observation (Ch. III,B,3) are summarized in Figures IV.17-IV.20, maps of W_{CO} integrated over various velocity ranges, and in Figure IV.21, a galactic longitude-velocity (l-v) diagram integrated over galactic latitude. A section of the Rosette cloud complex (B, Figs. IV.17 and IV.18) previously observed by Blitz (1978), is included in the figures as well as a section of the Northern filament and the LDN 1653, 1654, 1655, and 1656 clouds (A and T, Figs. IV.17 and

IV.18), discussed above. Table IV.3 lists the observed parameters, estimated distances, displacements from the galactic plane, and masses (Chs. V,A; V,F; and V,G) for the clouds labelled in Figures IV.17-IV.21.

A cloud located at $l \sim 216°$, $b \sim -2.5°$ (Q, Table IV.3) covers the largest angular area of any cloud along the galactic plane in the observed range of galactic longitude. Figure IV.22 gives the spatial distribution of T_R and the positions of observation. Other than the newly discovered cloud located at $l = 216°$, $b = -2.5°$, Figure IV.22 shows a small cloud (P, Table IV.2) with low intensity CO emission and a significant molecular cloud located at $l = 218°$, $b = 0°$ (S, Table IV.3), associated with the optical H II region S 287.

The properties of the large cloud differ from those of the smaller clouds and of other typical molecular clouds found throughout the Galaxy. Its T_R rarely exceeds 2 K (significantly less than the 5 K typical for envelopes of large molecular clouds; Fig. IV.22b), yet its spectral line widths (~ 7 km s^{-1} FWHM) are as wide as those found toward the small emission peaks in the Orion molecular clouds where temperatures are far higher. Figure IV.23 gives both the averaged spectrum and a typical observed spectrum for this cloud. The temperatures obtained from ^{13}CO observations at a few positions within the cloud were typically 1/4 or 1/5 as intense as the CO emission at the same position, as is normally found toward molecular clouds. Spot checks of CO and ^{13}CO with the 4.9 meter radio telescope at McDonald Observatory, University of Texas (Leisawitz

1984; Morris 1984) and the 14 m telescope of Five College Radio Astronomy Observatory (Solomon 1985) yielded temperatures that agree with ours, indicating that the observed T_R reflects a low kinetic temperature for the cloud rather than effects of clumping or of optically thin CO. The cloud covers nearly 6 deg^2 of sky and its velocity with respect to the local standard of rest is 27 km s^{-1}. Figure IV.24, a velocity-longitude diagram for the cloud, shows a velocity gradient from 25 km s^{-1} at l = 215° to 32 km s^{-1} at l = 219°, close to that expected from differential galactic rotation. (An extended discussion of this object is given in Chapter V,F and by Maddalena and Thaddeus 1985)

Some features at low velocity (< 18 km s^{-1}) located between $l \sim$ 206° and 211° (C, D, E, G, I, and J, Table IV.3) are probably related to the Mon OB 2 cloud complexes previously surveyed by Blitz (1978). One object (L, Table IV.2) with a velocity of 7 km s^{-1} and an unknown distance may be a local cloud. At higher velocities (> 35 km s^{-1}), the linear arrangement of the observed clouds (F, H, K, M, N, O, and R, Table IV.2) on the l-v diagram (Fig. IV.21) indicates that these clouds may be part of a large galactic structure such as an outer arm to our Galaxy. (Further details as to distances, masses, associated objects, and a comparison of the outer galaxy clouds with local or inner galaxy clouds are presented in Chapter V,G.)

CHAPTER V. DISCUSSION

A. Cloud Masses

For each of the local clouds in Table V.1 we estimated virial masses M_{vir}, LTE masses M_{LTE}, and CO masses M_{CO}. (For a detailed discussion of the methods, see Appendix A.) Both M_{vir} and M_{LTE}, as explained in Appendix A, are upper limits, and for M_{LTE} and M_{CO} we assumed that all hydrogen within the clouds is molecular in form. Each method is based on an independent set of assumptions and each gives values roughly within a factor of 2 of the others (Table V.1), an agreement supportive of the validity of the estimates. Only CO masses were calculated for the outer galaxy clouds (Table IV.3) since M_{CO} is easier to derive than M_{vir} and M_{LTE}, and appears to be equally reliable.

Taking into account that the extent of emission in our survey greatly exceeds that of previous surveys, we find that the masses for Orion A ($\sim 1.0 \times 10^5 \, M_\odot$) and Orion B ($\sim 0.8 \times 10^5 \, M_\odot$) are consistent with those previously found using CO ($1.0 \times 10^5 \, M_\odot$ and $0.6 \times 10^5 \, M_\odot$, KTCT), OH (Baud and Wouterlout 1980) and formaldehyde (Cohen et al. 1983). Similarly, previous estimates of mass for the Mon R2 cloud derived from the spatially limited CO surveys of Kutner and Tucker ($M > 0.32 \times 10^5 \, M_\odot$; 1975) and Loren ($M = 0.23 \times 10^5 \, M_\odot$; 1977) are consistent with our results ($M \sim 0.9 \times 10^5 \, M_\odot$).

Although virial masses are sensitive to the assumed shape and internal structure of the cloud, M_{vir} agrees fairly well with M_{LTE} and

M_{CO}. For the Northern and Southern filaments, M_{vir} are about five times higher than M_{CO} and M_{LTE} suggesting that the clouds may not be graviationally bound and could be rapidly evolving. If these clouds are not short-lived structures, a force acting to confine the clouds is needed. The pressure from the magnetic fields proposed in Chapter IV,A,4 may act as the confining force if the fields outside of the clouds are substantially tied to the intercloud gas so that they cannot move. The discrepency in the mass estimates is resolved when the effects of such a magnetic field is included in the virial mass calculation. Alternatively, the discrepancy might be explained if the filaments were sheets seen edge-on, a geometry inconsistent with the form of the virial theorem selected; this second possibility, however, is unlikely, because two sheets seen edge-on probably would not be parallel to each other, have such large apparent length-to-width ratios, or remain planar over the large scale observed.

B. Relationships Between the Orion and Monoceros R2 Cloud Complexes

It is worth asking whether most of the molecular clouds observed between 400 and 1200 pc are related and form a single large-scale system with, perhaps, a common origin. The Orion A and B clouds are probably related since they lie at the same distance, have similar velocities, and are connected in emission. Relationships between the Orion B and both the λ Ori clouds and the Northern filament are also plausible, since these clouds are close to each other and have similar

velocities, and are connected in emission. Relationships between the Orion B and both the λ Ori clouds and the Northern filament are also plausible, since these clouds are close to each other and have similar velocities or distances. There is little doubt that, due to similarities in their distances and velocities, the Southern filament, the Mon R2 cloud, and the NGC 2149 clouds are related. The question remains, however, whether the Orion complex (Orion A, B, Northern filament, and λ Ori clouds) is associated with the Mon R2 complex (Southern filament, Mon R2, and NGC 2149 clouds).

From the observed mass spectrum of molecular clouds (Dame 1983) and the density of molecular material within 1 kpc of the Sun (Dame and Thaddeus 1985) we find it unlikely on an a priori basis that two such complexes would lie so close together. On the other hand, the boundary of the survey were chosen to include both the Orion and Mon R2 complexes so statistical arguments are inconclusive. Were the Orion and Mon R2 complexes part of a single, gravitationally-bound unit, then the virial mass for the entire surveyed region would be approximately the sum of masses given in Table V.1 plus the mass of atomic gas between the clouds. The FWHM for a composite spectral line for all clouds with distances of 1 kpc or less is 6 km s^{-1}, a velocity dispersion due probably to either random motions of the clouds or the expansion of the cloud system from galactic tidal forces, and taking a radius of 8° for the region surveyed and an average cloud distance of 700 pc gives a virial mass of 7 x 10^5 M$_\odot$, which is comparable to the sum of the molecular masses ($\sim$ 4 x 105 M$_\odot$; Table V.1) and the atomic gas (2 x 10^5 M$_\odot$) implied by 21 cm observations (Heiles and Habing 1974).

A demonstration of clouds located along the line of sight between the Orion and Mon R2 complexes would provide the strongest argument for a relationship between the two complexes. The NGC 2149 clouds, extending in projection from Mon R2 to Orion A (Fig. IV.2), may span the difference in line-of-sight distance (300 pc). A bridge of this kind between the Orion and Mon R2 complexes would appear even more plausible if the velocities between Orion A and the Mon R2 clouds were continuous, which they are not, and were either the distance to the southwestern section of Mon R2 less than 830 pc or the distance to the southeastern section of Orion A more than 500 pc. If it can be shown that the Orion and Mon R2 complexes are physically connected, a common origin for the whole system would be worth consideration.

C. High Velocity Resolution Observations of the Orion East Cloud

The line widths toward the major fraction of the Orion East cloud (LDN 1621 and 1622) which are mostly at the resolution of the telescope's spectrometer (0.65 km s^{-1}) are comparable to differences in velocities between locations within the cloud. If the line width observed at any point in a cloud reflects the velocity dispersion of the gas through the cloud averaged over the beam of the telescope, then the mass within that beam as well as the local escape velocity of the cloud at that point can be calculated using the virial theorem. If the difference in velocity between points within a cloud is larger than the typical line widths, then the relative velocities between points in the

cloud exceed the escape velocity and the cloud cannot be in gravitational equilibrium: the cloud may be expanding or contracting, or possibly not gravitationally bound. Narrow line widths may indicate subsonic motion within the cloud, usually seen only in small, Bok globule-like clouds (see, e.g., Dickman and Clemens 1983).

To obtain high velocity resolution with our low-resolution spectrometer, a position in the cloud was observed three times, the velocity of the center of the spectrometer shifted by one-third of a channel width (0.22 km s^{-1}) between observations. Since the response of the filters in the spectrometer are known to a high accuracy, the response of the filters was easily deconvolved from the three observations to produce a high resolution (0.22 km s^{-1}) spectrum. This procedure was performed for CO and ^{13}CO at three positions within the cloud: at the position of the strongest CO emission, at the geometric center of the cloud, and near one edge of the cloud (Fig. IV.16). Figures V.1 and V.2 show the deconvolved spectra and Table V.2 presents the parameters for the spectra.

Although observations of CO cannot be used to investigate subsonic motion because the emission lines are probably saturated, they can be used to measure velocity shifts from one point to another. The largest difference in velocity (1.4 ± 0.2 km s^{-1}) occurs between points 2 and 3 (Table V.2). All three ^{13}CO observations, which are less apt to be saturated and so should better represent the actual velocity dispersion through the cloud, have line widths of 0.9 km s^{-1} FWHM. The differences in velocity between positions in the cloud exceed the line widths indicating that the cloud is evolving dynamically; possibly,

having been stable at one time, the cloud is now being disturbed by the star formation occurring within it or by an interaction with nearby Barnard's loop.

The maximum turbulent velocity dispersion (σ) within the cloud (see, e.g., Dickman and Clemens 1983), is given by:

$$\sigma = [\; 3 \left(\frac{\Delta v^2}{8 \ln 2} - \frac{kT}{m_{CO}} \right]^{1/2} . \qquad (V.1)$$

We get $\sigma = 0.65$ km s^{-1} after taking Δv equal to the observed ^{13}CO FWHM line width (0.9 km s^{-1}), T the kinetic temperature of the cloud ($\sim$ 14 K as implied by the CO observations), and m_{CO} the ^{13}CO molecular mass. The adiabatic sound speed (C = $[5kT/3\mu]^{1/2}$ $\sim$ 0.3 km s^{-1} where μ is 1.26, the mean mass per particle) is less than half σ_0 implying supersonic motion.

However, the actual value of σ is probably smaller than that calculated: the observed Δv may be contaminated by either the proposed expansion or contraction of the cloud, or by saturation effects. Observations of rarer isotopes or a less saturated transition (e.g., ^{12}C^{18}O J = 1 $\rightarrow$ 0 or CO J = 2 $\rightarrow$ 1) may confirm the prescence of subsonic turbulence.

D. The Molecular Ridge in the Orion A and B Molecular Clouds

The western halves of the Orion A and B clouds, as mentioned in Chapter IV,A,1, have higher T_R and W_{CO} than the eastern halves. Figures V.3-V.6 imply that the western halves are twice as warm as the eastern halves and, if $N(H_2)$ is proportional to W_{CO} (Appendix A) have twice the column density. This ridge of emission where most of the

present star formation apparently occurs in these clouds has kinetic temperatures of about 15 K and $n(H_2) \sim 300$ cm^{-3}, if the star forming regions are ignored and if the clouds can be assumed to extend ~ 30 pc along the line of sight. In contrast, the eastern, non-ridge regions have kinetic temperatures and densities of about 8 K and 150 cm^{-3}. Figures IV.5-IV.6 and Figure V.3-V.6, show a much sharper falling off in CO emission west of the ridge than toward the east. A similar but less steep falling off is seen in H I and, not surprisingly, galaxy counts increase just west of the ridge.

The location of most of the stars in the Orion OB Association west of the clouds suggests that the density and temperature enhancements along the ridge may have been created by interactions between the clouds and the starlight, stellar winds, or the occasional supernovae remnant produced by the association over the course of its lifetime.

1. Density Enhancement

The density enhancement may reflect the dissociation of the molecular material preferentially along the western edges of the clouds by the UV photons emanating from the OB association; if the clouds were originally symmetric with a dense core, the increased dissociation on one side of the cloud would leave them noticeably asymmetric after a long enough time. The flux of photons, however, is probably not high enough to have dissociated a significant fraction of the cloud over the lifetime of the association (Jura 1974; Hill and Hollenbach 1978), nor, as would

be expected, are the highest column densities of H I or H II found just west of the clouds. Instead the density enhancement was probably created by the compression of the gas by a region of high pressure abutting the edge of the cloud. The star formation in the clouds, located almost exclusively along the full length of the ridge, may have been stimulated by the compression of the gas. Possible sources of pressure include radiation pressure from optical photons and stellar winds from the nearby OB stars, the most likely candidate being the pressure source which creates the highest pressure.

The radiation pressure from the stars is 1×10^{-12} ergs cm^{-3} if we assume that $P_{rad} = L* \, Q \, / \, (16 \, \pi \, r^2 \, c)$ where $L*$ is the total luminosity of the stars in the association ($\sim 2 \times 10^5 \, L_\odot$), Q equals 2 if the incident photons are absorbed by the dust in the cloud and re-radiated isotropically, and r is an assumed distance of 30 pc between the source of the photons and the edge of the cloud. If the mass loss rate by stellar winds for each of the stars in Orion is given by $dM/dt = 6.8 \times 10^{-13} \, (L*/L_\odot)^{1.10} \, M_\odot \, yr^{-1}$ (Barlow and Cohen 1977), and if the wind velocity (V_{SW}) is approximately three times the escape velocity for the stars (Abbott 1978) or ~ 3000 km s^{-1}, then the pressure from stellar winds ($P_{SW} = dM_T/dt \, [V_{SW} \, / \, 4 \, \pi \, r^2]$ where dM_T/dt is the sum of the mass loss rates for the OB stars [$\sim 4 \times 10^{-6} \, M_\odot \, yr^{-1}$]) is 2×10^{-12} ergs cm^{-3}.

According to the models of Cowie et al. (1979), with the confirming results of Reynolds and Ogden (1979), a pressure of magnitude $P* \sim 10^{-10}$ ergs cm^{-3}, probably created by the cumulative effects of the

roughly ten supernovae which occurred in the association over its lifetime, extends for 45 pc around the center of the OB association (Fig. V.7). According to this model, derived from UV absorption line measurements toward stars in the region, Barnard's Loop, an ionization shock, delineates the eastern edge of the high pressure region which expands with a velocity of 10 km s^{-1}. A lower pressure region ($\sim$ 10^{-12} ergs cm^{-3}) outside the high pressure region extends as far as a radiative shock, with a radius of 100 pc and expansion velocity of 100 km s^{-1}, that most likely was created by the last supernova that occurred in Orion probably less than 1 Myrs ago. Outside the radiative shell the pressure is that of the ambient interstellar medium ($\sim$ 10^{-13} ergs cm^{-3}). The Loop and the OB stars, as seen on the POSS prints, lie in front of the molecular clouds, so it can be conjectured that the clouds lie partially on the back surface of the high pressure region (Fig. V.7). When the high pressure region first hit the cloud, most likely along its western side, a shock wave would propagate through the cloud with a velocity of $\sim (P^*/\rho)^{1/2}$, assuming that the pre-shock pressure is much lower than P^*. The width of the ridge, using the density (ρ) implied by the observations, would then be the propagation velocity ($\sim$ 5 km s^{-1}) times the length of time during which P^* has abutted the cloud ($\sim$ 2 Myrs; Cowie et al. 1979), or about 10 pc. This width is roughly the same as the observed 5 pc so, if the model and its geometry are correct, the density enhancement may reflect the compression of the molecular gas by the high pressure region.

2. Temperature Enhancement

The higher temperatures in the ridge may come from heating by starlight from stars embedded within the clouds or stars external to the clouds; by shocks within the clouds produced by stellar winds, supernovae, ionization fronts or dissociation fronts; or by the relaxation of magnetic fields within the clouds. Optical photons, when absorbed by the dust grains in the cloud, heat the grains which can then heat the gas if enough collisions between the gas molecules and the grains occur before the grains have a chance to radiate away their heat in the infrared. Densities in excess of $n(H_2) = 10^4$ cm^{-3} are needed for this mechanism to be efficient (Leung 1975; Goldsmith and Langer 1978), and the heating would only affect a thin section of the cloud since optical photons do not penetrate deeply into a cloud. A very large number of embedded stars located along the full length of the ridge, each surrounded by a dense molecular region, would be needed to produce the observed temperature enhancement.

The maximum depth to which a shock wave, generated by any mechanism, can heat a cloud is given by: $\lambda < (\rho \Delta v^2 u / 8 \Lambda)$ (Elmegreen, Dickinson, and Lada 1978) where ρ and Δv are the density and velocity dispersion in the shocked layer, u the shock velocity, and Λ the cooling rate for the shocked material. Using the observed densities and line widths of the ridge, and taking u = 10 km s^{-1} and Λ suggested by Goldsmith and Langer (1978) for these densities and temperature, λ is many orders of magnitude less than the observed 5 pc

width of the ridge, indicating that shocks, like starlight, will not heat a large fraction of the cloud.

Along with the compression of the cloud gas by the high pressure region found by Cowie et al. (1979), the magnetic field within the cloud would be compressed and accelerate the relaxation of the field within the cloud. Viscous processes between the ions, moving with the quickly diffusing field, and the stationary neutral particles provide an additional heat source for the cloud. In this heating mechanism the compression of the gas acts only as a catalyst which allows the energy stored in the magnetic field to enter the cloud as heat.

If this mechanism is at work, then the total heating rate (Γ_T), assumed to be the sum of the heating by cosmic rays (Γ_{CR}), the most likely heat source for cold molecular clouds, and the relaxation of the magnetic field (Γ_B), should balance the molecular cooling rate (Λ), or, $\Gamma_T = \Gamma_{CR} + \Gamma_B = \Lambda$. The rate of cosmic-ray heating is $\Gamma_{CR} \sim 6 \times 10^{-28}$ $n(H_2)$ (Goldsmith and Langer 1978) while, at the density of either the ridge or non-ridge region in the Orion A and B clouds, $\Lambda \sim 5 \times 10^{-27}$ $T^{1.6}$ (Goldsmith and Langer 1978). The magnetic heating rate is simply the energy density of the field ($B^2 / 8 \pi$) divided by the magnetic diffusion time, τ_B, which, if the diffusion of the ions through the neutral gas is supersonic, is given by:

$$\tau_B = \lambda^{3/2} (4 \pi m_{H_2} n(H_2) n_i <\sigma C> / C)^{1/2} / B \qquad (V.2)$$

(Elmegreen 1981). The quantity λ is the distance over which the the field is diffusing, (assumed to be the width of the ridge), m_{H_2} is the mass of a hydrogen molecule, n_i is the ion density assumed to be

5×10^{-8} n(H$_2$) (Wootten, Snell, and Glassgold 1979), C the sound speed in the region, and $<\sigma$ C$> = 2 \times 10^{-9}$ ergs (Spitzer 1978) where σ is the cross section for ion-neutral collisions. Given that $\Gamma_B \propto B^3$, the total heating rate depends crucially on the little known magnetic field strengths within the clouds. If clouds are supported from compression by the magnetic field pressure, the field strength in the ridge and non-ridge regions can be estimated by $B^2 = 8 \pi$ P where P is the external pressure impinging upon the clouds on their western ($\sim 10^{-10}$ ergs cm^{-3}) and eastern ($\sim 10^{-12}$ ergs cm^{-3}) faces. Table V.3 lists the parameters used in estimating Γ_T and Λ for the ridge and non-ridge regions of the Orion A and B clouds. As expected, τ_B for the ridge is longer than the lifetime of the pressure source (2 Myrs) if heating still occurs and is much less than that for the non-ridge regions. The predicted heating rates are close to the predicted cooling rates indicating that the 10^{-10} ergs cm^{-3} pressure region surrounding the Orion OB association could cause the observed temperature enhancement, as well as the density enhancement.

E. The λ Orionis Ring of Clouds

1. Expansion and Mass of Ring

The λ Ori ring of molecular clouds displays another kind of interaction between a young, massive star and its environment. In addition to strong CO emission usually present on the sides of the

clouds facing λ Ori (see below), the velocity structure of the overall system of clouds indicates a large-scale, dynamic interaction between the clouds and the H II region formed by λ Ori. The nearly circularly arranged clouds coincide with the edge of the H II region, as defined by the distribution of radio continuum (Reich 1978; Crezelius 1984) and by Hα (Isobe 1973), and, proceeding counterclockwise from the B 30 cloud, the smooth, systematic increase and then decrease in velocities suggests that the clouds are distributed on an expanding or contracting ring with an axis tilted slightly to the line of sight. Although peaks 1, 2, and 3 (Table IV.1) lie well outside the edge of the ionized region, and may not be part of the ring but only accidentally nearby, their velocities fall nicely into the systematic pattern found for the rest of the clouds. Since the ring is associated with an expanding H II region and the total mass inside it is small (shown below), a contracting or rotating ring is unlikely.

Figures V.9-V.11 show a least-square fit to the positions and velocities of the peaks within the λ Ori clouds, assuming the clouds lie on an expanding ring with central coordinates α_0, δ_0, radial velocity V_0, radius R, and an expansion velocity V_X, tilted at an angle ϕ with respect to the plane of the sky along an axis with position angle θ (Fig. V.8). The fitted values for α_0, δ_0, V_0, V_X, R, ϕ, and θ are given in Table V.4. Note the good agreement beween the coordinates of λ Ori (α = 5h 34.1m, δ = 9° 55') and the center of the ring (Figure V.9) and between the age of the star (2-4 Myrs; Murdin and Penston 1977) and the expansion age of the ring (T_X ~ 2.4 Myrs). The

deviations of the clouds from the fitted ring is best illustrated in Figure V.11 where, as seen from the center of the ring, the angle between the plane of the sky and each cloud is plotted against the position angle of each cloud; the sine curve is derived from the model ring.

The combined results of the CO, 21 cm (Wade 1957, 1958; Heiles and Habing 1974; Crezelius 1984), radio continuum (Reich 1978; Crezelius 1984), and infrared (Boulanger 1985) surveys indicate the following morphology for the region. The H II region which has a radius of $\sim 4°$ in the radio continuum (Fig V.12) contains approximately 5×10^3 $M_\odot$ of ionized material at a temperature of 7500 K and electron density of 2.2 cm^{-3}. The excitation parameter for the H II region (47.3 pc cm^{-2}) is consistent with λ Ori being responsible for the ionization (Crezelius 1984). Concentric with the center of the H II region and the position of λ Ori, molecular clouds with a total mass of about 3×10^4 $M_\odot$ lie just outside the H II region on an expanding ring with a 5° radius (Fig. V.13).

Figure V.14 shows that the column density of atomic gas is low toward the center of the H II region, as expected if either the UV photons from λ Ori ionized the gas or the leading edge of the expanding H II region had swept up the gas. The H I column density rises where the H II region ends and the molecular ring begins (Figures V.13-V.14). Analyzing the H I emission in more detail, Wade (1957,1958) and Crezelius (1984) find a similar velocity structure to what is observed in CO but less clearly seen; they disagree between themselves on the amount of atomic gas in the ring by an order of magnitude (7×10^4 vs

7×10^3 $M_\odot$). Coulson et al. (1978), measuring the column density of dust within a small section of the ring, suggest a total mass of 7×10^4 $M_\odot$ in the ring; this dust is apparently associated with H I gas since there is little CO emission in the region they surveyed. However, the H I column density over a wide range in longitude outside the borders of the H II region is fairly constant (Fig. V.14); an enhancement of as little as 10^4 $M_\odot$ of atomic gas lying in a ring with dimensions similar to the molecular ring would be noticeable, if it were present, in Figure V.14. (The change in column density with latitude is almost exclusively due to the gradient in atomic gas perpendicular to the galactic plane.) Approximately 10^4 Mg of atomic gas would be swept up by the H II region if it expanded into an intercloud medium with a density of 1 cm^{-3}. Thus, the maximum amount of atomic gas in the shell is closer to 10^4 $M_\odot$ than to 7×10^4 $M_\odot$.

In contrast to the molecular emission which occupies less than one-half the perimeter of the ring, infrared emission from warm dust, seen by IRAS at 100μ (Fig. V.15), makes an almost perfect ring coincident with all of the molecular clouds except peaks 1, 2, and 3 (Table IV.1). If the dissociating UV flux from λ Ori is typical of stars of its type, the amount of molecular material dissociated over the lifetime of the star is likely to be only a few percent of the present molecular mass (Jura 1974; Hill and Hollenbach 1978). The infrared emission observed along the full perimeter of the ring, and between the molecular clouds, must primarily be associated with warm dust accompanying swept-up atomic gas rather than dissociated molecular

gas. Because of the difficulty in separating the emission from foreground and background emission at 21 cm from that associated with the H II region, it is impossible to determine whether the atomic gas and the infrared ring are tilted with respect to the line of sight in the same way as the molecular clouds.

Most of the mass associated with the λ Ori H II region is concentrated in the molecular clouds. The total mass in the ring, including a maximum contribution of 10^4 M_0 from atomic gas, is ~ 4 x 10^4 $M_\odot$, implying a kinetic energy of 8 x 10^{49} ergs and a momentum (P_{cloud}) of 1 x 10^{44} g cm s^{-1} for all the gas within the ring, if it is expanding at the 14 km s^{-1} determined by the least-square fit.

2. Evolution of the λ Orionis Cloud System

From the optical, radio continuum, H I, infrared, and CO observations of the ring, an evolutionary scenario can be devised. The small deviations of the molecular clouds from the fitted ring and the orientation of the molecular ring with respect to the Sun suggest that λ Ori, along with the few B stars in the region with similar ages, formed at the center of a flattened molecular cloud with an axis tilted at an angle of ~ 36° with respect to the line of sight. After the formation of λ Ori and its H II region, momentum might have been transferred to the clouds by the stellar winds from λ Ori, by radiation pressure from stellar photons, or by the gas pressure in the H II region.

The maximum momentum imparted to the clouds by stellar winds over the lifetime of λ Ori is given by

$$P_{SW} = \tau \ V_{SW} \ (dM/dt) \ (\Omega/4\pi), \qquad (V.4)$$

where Ω is the solid angle subtended by the clouds as seen by λ Ori, averaged over τ the age of the star (2-4 Myrs), and V_{SW} and dM/dt the measured wind velocity (3050 km s^{-1}) and mass loss rate (3.8 x 10^{-7} $M_{\odot}$ yr^{-1}) (Barlow and Cohen 1977); P_{SW} [$\sim$ 5 x 10^{41} ($\Omega/4\pi$) g cm s^{-1}] is then at least two orders of magnitude less than P_{cloud} (1 x 10^{44} g cm s^{-1}).

Using the measured luminosity of λ Ori (L$_*$ $\sim$ 1.7 x 10^5 L$_{\odot}$), and assuming dust reradiates an absorbed photon isotropically (i.e., $Q = 2$),

$$P_{rad} = \tau \ L_* \ Q \ (\Omega/4\pi)/ \ 4 \ c \quad \sim \quad 7 \ x \ 10^{41} \ (\Omega/4\pi) \ g \ cm \ s^{-1}, \qquad (V.5)$$

a value much lower than P_{cloud}. These mechanisms for transferring momentum may have been more important in the past than now had dM/dt, V_{SW}, or L$_*$ then been much higher; it is unlikely, however, that any of these parameters were two orders of magnitude higher in the past.

Were the clouds situated at the edge of or just outside the H II region, the gas pressure within the H II region would accelerate them. If the clouds were always just at the edge of the H II region, and ignoring negligible gas pressure within the clouds,

$$P_{gas} = 4 \ \pi \ r^2 \ \mu \ n_e \ k \ T \ \tau, \qquad (V.6)$$

where μ is the mean mass per electron in the H II region (2.09), r, n_e,

and T are the radius, electron density, and temperature of the H II
region, respectively, and k the Boltzmann constant. With values of
$r = 35$ pc, $n_e = 2.2$ cm^{-3}, and $T = 7500$ K, (Crezelius 1984),
$P_{gas} \sim 6 \times 10^{43}$ g cm s^{-1}, or roughly the same as P_{cloud}. Mazurek
(1980) solved the equation of motion for the momentum transfer between
an expanding H II region and a massive cloud in which the H II region
was originally embedded; applying his results to the λ Ori system,
yields a predicted expansion velocity (~ 12 km s^{-1}) similar to V_x.
(Using parameters for the λ Ori system that subsequently were updated,
Mazurek has independently derived a similar expansion velocity for the
ring.)

The gas pressure from the H II region would then have accelerated
the cloud material preferentially along the long dimension of the cloud
almost perpendicular to the present-day line of sight (Fig. V.16a). At
some point the size of the H II region would become comparable to the
small dimension of the cloud and the edge of the H II region would
break through the surface of the cloud (Fig. V.16b), possibly tearing
the cloud into the fragments constituting the molecular ring. At this
time the H II region would rapidly expand along the line of sight into
the low density gas outside of the cloud. The molecular clouds,
however, would still confine the H II region from rapidly expanding
perpendicular to the line of sight. Thus, the extent of the H II
region along the line of sight would exceed that observed perpendicular
to the line of sight (Fig. V.16c).

The rocket effect may also contribute to the acceleration of the

clouds. When an H II region originally embedded within a molecular cloud expands so its edge bursts through the nearest surface of the cloud, the H II region would grow rapidly where the rupture occurred since it would no longer be confined by the high density molecular material (Fig. V.16b). Starting at the location of the rupture, a rarification wave would propagate back through the H II region, lowering the column density of gas between the ionizing star and the remaining molecular clouds. The UV photons from the ionizing star, originally absorbed by the intervening gas, then could reach the clouds and increase the dissociation and ionization of cloud material on the sides facing the star. Each dissociated or ionized gas particle would move away from the clouds preferentially toward the H II region at the sound speed of the H II region ($\sim$ 10 km s^{-1}) and give an impulse to the cloud in the opposite direction, ultimately accelerating the clouds radially outward from the H II region. If a molecular cloud were to be engulfed by the H II region, the dissociation and ionization of the gas in the cloud, though still preferentially occuring on the side of the cloud facing the ionizing star, would also occur on all sides of the cloud and, thereby, would reduce the magnitude of the rocket effect. Bally and Scoville (1980) investigated the effect of this mechanism on a similar H II region associated with the Pelican nebula and, although the parameters in their models differ slightly from those for the λ Ori system, predicted a 10 km s^{-1} expansion velocity after 4 Myrs. The momentum of the clouds, therefore, may have been produced over all or part of the lifetime of the H II region either by the gas pressure within it, or by the pressure produced by the rocket effect. As shown

in Appendix B, a more rigorous and detailed theoretical model for the disruption of a spherical molecular cloud, a combination of gas pressure and the rocket effect could produce the gas and velocity structures found in the vicinity of λ Ori.

The acceleration of the clouds would have compressed the gas on the sides of the clouds facing the H II region and, probably through the ion-viscous processes previously described (Chapter V,D,2), heated the edges of the clouds as observed in CO. The compression of the gas may have triggered the formation in the clouds of the observed low mass stars which were left behind as the clouds subsequently were further accelerated (Fig. V.16c,d; also Duerr et al. 1982). As the H II region and the molecular ring expanded, H I gas and its associated dust would have been swept up into a shell- or ring-like structure (Fig. V.16c,d). Unlike the formation of massive stars in other molecular clouds in the Galaxy (e.g., the Orion A and B clouds) which occurs mostly at the edges of the parent clouds, this scenario of the evolution of the λ Ori system may depict the disruptive effects of a massive star which formed at the center of a molecular cloud.

This scenario, however, cannot easily explain the proper motion and radial velocity of λ Ori nor UV absorption line measurements toward the star. The proper motion of λ Ori (Boss 1937) would imply that if the star had not recently aquired this velocity then 2 Myrs ago the star was not at the center of the ring but close to one side (Fig. V.9); the errors in the measured proper motion are comparable to the values themselves and should be measured again. If the H II region

centered on λ Ori created the velocity structure in the ring, then the radial velocity of λ Ori (33.4 ± 0.5 km s-1 heliocentric or 18 ± 0.5 km s^{-1} with respect to LSR; Wilson 1963) should fall within the ring structure seen in Figure V.10; but it does not. The UV absorption by interstellar gas between the star and the Sun occurs at velocities (10.6 and 1.6 km s-1 v_{LSR}; Hobbs 1969) that correspond to both the near and far sides of the ring, indicating that the star may be behind the ring rather than in it.

For an evolutionary scenario for λ Ori to be consistent with these observations, the UV absorption features would have to arise from unassociated atomic clouds coincidentally having the same velocities as the ring, and the present day velocity of λ Ori would have to reflect a recent acceleration of the star by, for example, either a close encounter with another star or the expulsion of a stellar companion from the multiple star system of which λ Ori is or was a member. Alternatively, if the original molecular clouds and λ Ori had a relative drift velocity of ~ 12 km s^{-1} along the line of sight when the H II region started to form, then the ring of clouds would remain centered where λ Ori was located 2 Myrs ago, but the star would drift and eventually pass through the rear side of the more slowly expanding ring. (In 2 Myrs, the star would travel ~ 24 pc along the line of sight relative to the center of the ring.) Since the H II region would have been centered on the star as it drifted, this scenario would imply that the projected radii of both the H II region and molecular ring are coincidentally the same. The proposed mechanisms for accelerating the

clouds, however, would also have to be modified, because the clouds would have to have been accelerated to their present velocities soon after the H II region formed.

Another possibility is that the expanding ring is unrelated to λ Ori and was formed either by the action of another star that subsequently became a supernova, or perhaps by the remnant of such a supernova. If the progenitor of the supernova and λ Ori wer part of the same multiple star system, then λ Ori might now be a runaway star; the discordant velocity of λ Ori could have resulted in this way. The kinetic energy in the expanding ring of cloud ($\sim 10^{50}$ ergs) is a few percent of what are typical for supernovae. The supernova would have occured $\sim$ 2 Myrs ago, the expansion age of the ring, so the remnant probably is today impossible to detect. In this case, λ Ori has usurped the pre-eminece of the former star.

F. Large and Unusual Cloud in the Galactic Plane

1. Distance and Size

The large and cold outer galaxy cloud labeled Q in Figures IV.17 and IV.19, and whose observational charactersistics are summarized in Figures IV.22-IV.24, has a kinematic distance of 2.7 kpc as determined from the flat rotation curve of Blitz (1979). Because the rotation curve is based on few observations inside the region $205° < l < 225°$ with distances greater than 1.5 kpc, the uncertainty

in the distance is probably as large as 1 kpc. Further evidence for this distance comes from S 287, the H II region located nearby at l = 218.°1, b = -0.°4, which has a photometric distance of 3.2 kpc (Moffat, Fitzgerald, and Jackson 1979). The radial velocity of cloud Q and that of the molecular cloud associated with S 287 (S, Table IV.3) are similar (27 km s^{-1}; also Blitz, Fich, and Stark 1982). The proximity between the S 287 cloud and the large cloud Q in Figure IV.22 and the similarity in cloud velocities suggest that these clouds are part of the same complex. Since no emission appears to connect them, they may be unrelated.

The open cluster NGC 2286, at 1.28 kpc (Becker and Fenkart 1971), is within the cloud boundary at l = 215.°3, b = -2.°3. The low color excess (0.41 mag) for the stars in the cluster and the age of the cluster (10^8 years), determined from the earliest spectral type found within the cluster, indicate that the cluster is a foreground object unrelated to cloud Q.

In Figure III.4 the fairly small angular separation between cloud Q and the sets of clouds associated with the Rosette Nebula (distance = 1.6 kpc, Turner 1976; velocity = 15 km s^{-1}, Blitz 1978) and CMa OB 1 (distance = 1.2 kpc, Eggen 1978; velocity = 18 km s^{-1} Blitz 1978), suggest that cloud Q might be related physically to either set, but the velocity discrepancy of about 11 km s^{-1} probably rules out any association. Although the size and mass of cloud Q would be significantly smaller than those derived below if the distance were 1.2 kpc instead of 3 kpc, the cloud would remain an unusual object.

At 3 kpc, cloud Q is one of the largest molecular clouds known, with a major axis of 250 pc and a minor axis of 100 pc. The outer Galaxy is not warped at the location of the cloud (Henderson, Jackson, and Kerr 1982), so its galactic latitude probably corresponds to a true displacement from the galactic midplane. The displacement is similar to that of the nearby Orion cloud and, likewise, is unusually large: 145 pc or about two times the half-thickness at half-maximum of molecular material at the solar circle (Dame and Thaddeus 1985; see Ch. V,G for more details).

2. Associated Objects

The POSS prints for the location of cloud Q show a slight trace of optical obscuration, consistent with the cloud's large distance and with most observable stars being in the foreground. Khavtassi (1955) notes a dark cloud subtending about 3 deg^2 in the same general region. The object coincides with a region of H I enhancement (Weaver and Williams 1973) and an excess of γ-ray emission not entirely accounted for by the interaction of cosmic rays and the gas implied by 21 cm observations (Bloemen et al. 1984). The cloud is not a source of infrared emission; all cataloged point infrared sources in its direction have been attributed to nearby stars (Neugebauer and Leighton 1969; Walker and Price 1975; Longmore, Hyland, and Allen 1976; Price and Walker 1976) and the cloud does not show up in the 100μm IRAS survey (Boulanger 1985).

Low mass stars, T Tauri stars, or Herbig-Haro objects would be

difficult to detect because of this cloud's large distance. Any H II regions or OB stars on the near side of the cloud should be visible; the cloud itself is optically visible, and S 287, lying in the galactic plane where foreground obscuration presumably is the same or higher, is easily seen. There are no H II regions or OB stars toward this cloud in the standard catalogs (Sharpless 1959; Goy 1973; Cruz-Gonzalez et al. 1974; Marsalkova 1974; Humphreys 1978).

Radio continuum surveys toward the general area of the molecular cloud (see Table V.5) were used to see if any obscured H II regions were present. First, it was determined which of the continuum sources in the direction of the cloud have the thermal spectrum indicative of an H II region. Second, excitation parameters, $u(pc\ cm^{-2})$ = $K(\nu,T)\ [D(kpc)^2\ S_\nu(Jy)]^{1/3}$, were found for the possible H II regions; D is the distance to the H II region (assumed 3 kpc), S_ν is the observed flux density at frequency ν, and $K(\nu,T)$, which depends on the temperature assumed for the HII region ($\sim 10^4$ K) and only slightly on the frequency of observation, equals 13.5 for ν = 1415 MHz (Hjellming 1968). It is assumed that the H II region is unresolved, ionization bounded, and optically thin at the frequency of the observations used to find u. Last, from u one can ascertain the number and type of O or B zero-age main sequence (ZAMS) stars responsible for the H II region (Panagia 1973).

A proper analysis depends on whether the possible H II region is optically thin at the frequency used to calculate u. The radio surveys completed toward this cloud remain inadequate to determine optical

thickness, and the sensitivities of these surveys are low; at 3 kpc, only H II regions excited by stars earlier than a B0 star could have been detected. Table V.5 presents preliminary estimates of u and stellar spectral types; all need to be checked by surveys of higher sensitivity.

Of the five continuum sources detected toward the molecular cloud, only 4C-02.28 appears to be an H II region which, if at a distance of 3 kpc, may be excited by an O6 ZAMS star. Recombination line studies toward 4C-02.28 could test whether a relation exists between the cloud and the H II region. If the H II region is unrelated to the molecular cloud, recombination line observations may determine whether the radial velocity of the H II region differs from the cloud's velocity.

3. Evolutionary State of Cloud Q

There is little evidence that cloud Q is currently forming stars. Although S 287, at the same distance as this cloud, has at least three associated early-type stars (Moffat et al 1979), no stars of this type were found in the direction of cloud Q. Were young stars embedded in the cloud and interacting with it, its far-infrared emission would be expected to be more intense than was observed by IRAS (Boulanger 1985); strong temperature peaks, a common sign of newly formed stars that interact with the parent molecular cloud, are absent. Since M_{CO} is comparable to M_{vir} (Table IV.3), the internal

pressure sources created, for example, by strong stellar winds from young stars or gas heated by recently formed stars, may be absent. Radio continuum data suggest that 4C-02.28 may be an H II region, but it cannot be said whether the H II region is associated with the cloud.

Most molecular objects of the size and mass of cloud Q are cloud complexes consisting of a collection of individual clouds whose ragged internal structure is usually attributed to the violent activity that accompanies massive star formation (e.g., H II region expansion, strong stellar winds, supernovae). Unlike cloud complexes, cloud Q is a single, continuous object, and these violent events are not likely to have occurred near it.

The unusual spectra, as well as the absence of star formation, suggest three interpretations for the cloud. First, it may possibly be a member of a small population of objects that never form massive stars, although clouds of such size and mass should gravitationally contract and form stars in a fairly short time. Second, even though the cloud may have formed stars in the past, it is now quiescent; but previous star formation should have left some evidence in the cloud's vicinity (e.g., a cluster of stars) and the cloud should be more fragmented than it appears. The third, and most plausible possibility is that the cloud is young and in a stage of evolution prior to the onset of star formation. A molecular cloud recently formed out of a diffuse H I cloud, for which line widths are typically 10 km s^{-1}, may have line widths as large as those found for

the new cloud. The short free-fall time for molecular clouds implies that cloud Q will soon begin to form stars and that, given enough time, it may mature into a typical cloud complex, similar in size, mass, and structure to the nearby Orion complex.

4. Clouds with Similar Properties

To estimate the number of clouds in the Galaxy with properties similar to those of the new cloud, the extensive Columbia CO surveys of the first, second, and third quadrants were examined for clouds with masses greater than 10^5 $M_\odot$, with lines weaker than 2 K and wider than 6 km s^{-1}, and having no indications of star formation.

Within 1 kpc of the sun, large molecular clouds, with spectra that showed typically higher T_R and narrower line widths than those found toward the cloud Q, are invariably associated with extensive star formation. Although the Orion molecular filaments (Ch. IV,A,4) have wide lines but no star formation, their masses are an order of magnitude less than that of the new cloud (Table IV.3 and V.1). There is no evidence for similar clouds in the Perseus arm (Gottlieb, Brock, and Thaddeus 1984) or elsewhere in the second and third quadrants (Blitz 1978; Baran 1983; Huang 1985).

The analysis of large cloud complexes in the first quadrant by Dame et al. (1985) was generally limited to clouds with a total CO luminosity ($S_{CO} = \int W_{CO} \, d\Omega$) of 8 K km s^{-1} deg^2 or greater, so an object with S_{CO} equal to that of cloud Q (42.6 K km s^{-1} deg^2 at

3 kpc) would have been designated a cloud if it were closer than 7 kpc from the Sun. Unfortunately, the diffuse CO background emission in the inner Galaxy, and the methods used by Dame et al. (1985) to separate clouds from the background emission would make it difficult to pick out clouds with temperatures as low as those found for cloud Q.

Nevertheless, two clouds, which Dame et al. (1985) designated (39,32) and (41,37), have $T_R < 2.5$ K and large spectral line widths (6 km s^{-1} FWHM). Located near each other, between $l = 38°$ and $42°$ at $b \sim 0.°5$, with a $v_{LSR} \sim 35$ km s^{-1} and at a distance of 2.2-2.6 kpc, and possibly associated with the W50 molecular cloud (Huang, Dame, and Thaddeus 1983), these clouds may be a single object with a mass of 10^6 $M_\odot$ and a linear size about half that of the new cloud. Both are apparently devoid of the usual signs of associated star formation (e.g., H II regions or far-infrared sources, Myers et al. 1985).

In conclusion, such clouds in the outer Galaxy are probably rare and do not make up a significant fraction of the molecular gas in the Milky Way. They might be more common in the inner Galaxy where they might be confused with the CO emission from numerous very small clouds. It is not clear that observations with higher angular resolution will be of much help in distinguishing such clouds.

G. Outer Galaxy Clouds

1. Distances and Locations Within Spiral Arms in the Outer Galaxy

The distances to most of the outer galaxy clouds were estimated using the rotation curve of Blitz (1979), but this rotation curve does not extend to the galactocentric distance (R^G) of clouds K, M, N, O, and R (Table IV.3) for which a flat rotation curve (R_Θ = 10 kpc, Θ_Θ = 250 km s^{-1} kpc^{-1}) was adopted. For a few objects with velocities and positions close to that of the Rosette complex, the distance to that complex, 1.6 kpc (Turner 1976), was assumed. Clouds I, J, M, and S may be associated with H II regions and reflection nebulae with estimated photometric distances; in these cases the photometric distances agree remarkably well with the cloud distances estimated from the rotation curves, suggesting that the distances assumed for clouds without associated objects are not seriously in error. The large distances (3-5 kpc) attributed to the optical objects associated with the clouds illustrate the unusually low obscuration from foreground material in this region of the galactic plane. Very little of the molecular emission in the region comes from local clouds. Either the local material usually found in the galactic plane is absent from these directions, or, more likely, the nearby Orion clouds represent local material which should be in the plane but which has been displaced by some unknown cause (Ch. IV,A,4).

All clouds, except those associated with the Rosette complex, lie either at distances of ~ 3 kpc (P, Q, and S, Table IV.3) or

~ 5.5 kpc (F, K, M, N, O, and R, Table IV.3). The 3 kpc distance of the Gem OB 1 cloud complex at l ~ 190° (Fig. III.4), approximately the same distance as clouds located within the Perseus Arm near l = 170° (Gottlieb et al., 1984), suggests that the clouds with distance close to 3 kpc form part of an extension of the Perseus arm of the Galaxy in the third quadrant. Other authors (e.g., Verschuur 1973; Moffat et al. 1979; Henderson et al. 1982) looking at the distribution of young objects and the atomic gas in which the molecular clouds are apparently embedded, have suggested this extension of the Perseus arm. The more distant clouds (at ~ 5.5 kpc) lie within a major and extensive H I feature in the Galaxy (Minn and Greenburg 1973; Weaver and Williams 1973; Henderson et al. 1982) which apparently delineates an outer arm to our Galaxy; the observed molecular clouds are probably the first examples of molecular clouds tracing out a spiral arm at such a large galactocentric distance as 15 kpc. (Kutner and Mead (1985) have observed clouds out to 18 kpc; the spatial coverage of their observations is inadequate to trace the pattern of spiral arms.) Though only 15° of the galactic plane was sampled, these observations, with the coinciding H I structure, suggest that other molecular clouds probably exist within that outer arm of the Galaxy and that molecular clouds can be used as a tracer of outer-galaxy spiral structure even though, as shown by Sanders, Solomon, and Scoville (1984) and as will be shown here, the density of molecular clouds in the outer galaxy is low.

2. Comparison Between Outer and Inner Galaxy Clouds

A comparison of the properties of clouds in the outer galaxy with those in the inner galaxy may be useful even though the sample of outer galaxy clouds in the present survey is not extensive, does not cover a significant fraction of the outer galaxy, and because small, cold clouds, which may be an important part of the molecular content of the outer Galaxy, would have been overlooked because of beam dilution from the low resolution of the observations.

The sizes of the clouds in Table IV.3 were defined by counting the number of observed positions where emission exceeded 0.6 K at velocities within a few km s^{-1} to that of the rest of the cloud. (The areas which the clouds cover are usually twice that shown in Figures V.17-V.20). The cloud sizes are similar to what is seen in the inner parts of the galaxy although, due to the resolution of the survey, the smaller clouds have been missed. If the Orion complex was at a distance of 3 or 5 kpc, and was observed with the same resolution as that used for the outer galaxy survey, its observed peak temperature and S_{CO} would be, respectively, about two and four times higher than those seen for the outer galaxy clouds (Fig. V.17); the emission from the Mon R2 cloud at those distances would still be stronger but not as impressive as the Orion clouds. If the Orion and Monoceros clouds are typical of local clouds, the outer galaxy clouds, even though they have similar sizes, are apparently a little colder and have lower W_{CO} than inner galaxy clouds. Kutner and Mead (1981, 1985), observing a similar

dependence of cloud emissivity as a function of R^G, suggest that the difference in emission may be due to a metallicity or cosmic-ray gradient in the galaxy, either of which could change the cooling and heating rates for clouds at different R^G.

The CO masses derived for the outer galaxy clouds are lower than those found for objects of similar size in the inner galaxy. However, these masses must be taken with some caution: the value of $N(H_2)/W_{CO}$ used, similar to what is found throughout the inner galaxy (Bloemen et al. 1985), may be inappropriate for clouds beyond the solar circle. The mass within the observed section of the galactic plane, if typical of the rest of the galaxy, implies a total mass of 4×10^7 $M_\odot$ for molecular clouds with masses greater than a few times 10^4 $M_\odot$ lying between $R^G = 10$ and 15 kpc. The surface density of molecular material projected onto the plane of the galaxy, including the contribution from He, would be 0.10 $M_\odot$ pc^{-2}, 100 times less than that within the molecular ring (Sanders et al. 1984). This value, possibly low by a factor of two or so because some molecular material may have been missed in the survey, is about twenty times lower than the local value (Dame and Thaddeus 1985) and about five times lower than that found by Sanders et al. (1984) for the same range in R^G if their analysis had used the same $N(H_2)/W_{CO}$ as used here. The Sanders et al. survey covered a smaller total area than the present survey but looked at a wider range in galactic longitudes so it may have been contaminated by occasional, but uncorrelated, areas rich in molecular material while the results of the present survey may reflect an unusually rare and large area with little molecular gas.

The z-distribution of molecular material outside of the solar circle, as well as surface density, is summarized in Table V.6. In determing the centroid of molecular material [$Z_c = (\sum M_i Z_i) / (\sum M_i)$ where the M_i and Z_i are the mass and z-displacements of the individual clouds, Table IV.3] and the rms dispersion [$Z_{rms}^2 = (\sum M_i (Z_i - Z_c)^2) / (\sum M_i)$], the distribution of the large molecular clouds (Table IV.3) is assumed to follow the distribution of all molecular clouds, including those low mass clouds not detected. The rms dispersion, similar to the local value (Dame and Thaddeus 1985), is fairly constant from $R^G = 10$ to 15 kpc (about 65 pc corresponding to a half width at half density of 78 pc), although Z_c shows a significant deviation of -98 pc from the galactic plane between $R^G = 10$ and 13 kpc which is solely due to the large z-displacement of cloud Q (Table IV.3). If that cloud is dropped from the calculation of Z_c, then Z_c is reduced to -32 pc. The value of Z_c for all ranges in R^G are consistent with the distribution of atomic gas (Henderson et al. 1982).

CHAPTER VI. SUMMARY

Approximately one-eighth of the 850 deg^2 region surveyed in

Orion and Monoceros showed CO emission, either from 1) clouds at

distances upto 1 kpc and having locations well out of the galactic

plane or 2) emission from more distant clouds lying within a few

degrees of the plane.

Masses for many of the clouds were calculated by three different

methods; the results show that masses derived from the CO

luminosity of the cloud are consistent with more complicated

approximations. About 4.3 x 10^5 M$_\odot$ lies within 1 kpc of the Sun

between $\underline{l}$ = 206° and 222°; however, only 15.6 x 10^5 M$_\odot$ was found

between 1 and 6 kpc in the same sector indicating that the Orion

region is either rich in molecular clouds or that the part of the

outer galaxy surveyed has little molecular material.

Most of the local emission comes from the large molecular clouds

associated with Orion A and B, previously mapped with lower

sensitivity and velocity resolution (KTCT) than in the present

survey, and from a large cloud associated with the Monoceros R2

system of reflection nebulae. Two thin filamentary clouds were

discovered as well as clouds distributed symmetrically in a ring

surrounding the H II region S 264 ionized by λ Ori. Clouds that may

be associated with Barnard's loop and the CMa OB 1 association were

also found.

The filaments, which may represent a new type of object, are

extremely narrow (~ 10 pc), one possibly longer than 300 pc, and have

large line widths indicative of strong turbulence, low temperatures, and no apparent associated star formation. Preliminary analysis of high resolution observations indicate that the filaments can be modelled in terms of a number of small clumps moving at speeds of a few km s^{-1} relative to each other. The filamentary shapes, similar to those of the ρ Oph clouds, may be dictated by oriented magnetic fields which may also help tie the clumps together preventing the filaments from expanding. The few polarization measurements made toward background stars are not sufficient to determine field directions; more polarization measurements and a determination of field strengths may provide clues to the causes of the enigmatic properties of the clouds.

Other clouds in the survey showed unusual properties. For example, Orion East, apparently interacting with Barnard's loop, has high temperatures ($\sim$ 10 K) but line widths at or below the velocity resolution of the telescope's spectrometer. Observations with high velocity resolution (Chap. V,C) hint that this cloud may have subsonic line widths and may be contracting, expanding, or unbound; future observation of optically thin transitions are needed.

A few large-scale interactions between the events accompanying massive star formation and the parent molecular clouds are evident in the data for the local (< 1 kpc) clouds. The double-line region in the Orion B cloud may be due to the acceleration of one part of the cloud relative to another by the pressures from the winds of nearby young stars. A ridge of high temperature and high density extends almost the full length of the Orion A and B clouds just inside their

western borders. Neither stellar radiation, stellar winds,
ionization or dissociation fronts, nor shock fronts from supernovae
could have created the large-scale temperature and density
enhancement along the ridge. A high pressure (10^{-10} ergs cm^{-3})
region created by the cumulative effects of about ten supernovae, may
exist inside Barnard's loop; if such a pressure was abutting the
clouds on one side, a geometry which is very plausible, then the
density and temperature enhancements could be explained by
compression of the gas and the increase in heating from ion-neutral
viscous processes as a compressed magnetic field rapidly diffuses out
of the cloud.

The λ Ori ring of clouds is another example of an interaction
between a young star and its parent cloud. The observed velocity
structure of the system of clouds in the ring suggest that the clouds
are confined to an expanding ring with an axis roughly perpendicular
to the line of sight. A detailed evolutionary sequence to explain
the CO, H I, infrared, and radio continuum structures associated with
λ Ori, is given in Chapter V,E. High resolution surveys toward more
distant complexes may reveal that structures like the ridge in the
Orion A and B clouds and the λ Ori ring are common throughout the
Galaxy.

The distances and distributions of the local clouds suggest
that, at most, two molecular complexes are present; the Orion complex
at 500 pc and the Mon R2 complex at 830 pc or more. The low
probability that two such complexes would accidently lie so close to
each other suggests that these complexes may actually be components

of a single system. Better determinations of the distances to objects associated with clouds are needed to confirm this suggested relationship.

Beyond 1 kpc and along the galactic plane, clouds with distances of up to 6 kpc or more were observed; one of them (Q, Table IV.3) is large with the unusual property of both being cold but quite massive, and with wide CO lines across its entire face. If at 3 kpc, the cloud is one of the largest known, its size, 250 pc by 100 pc, and mass, $7-11 \times 10^5$ M_Θ, comparable to those of a typical molecular cloud complex. Unlike a typical cloud complex, cloud Q is apparently a single, continuous object with, except for a possible H II region, no associated star formation. This is consistent with the idea that star formation and the disruptive activity associated with it has not yet occurred. Similar objects are apparently rare in the Galaxy. It is reasonable to imagine that this is a young cloud not yet forming stars that may evolve into a typical cloud complex when star formation occurs.

Only a small fraction of the galactic plane was surveyed for outer galaxy clouds, and small, cold clouds which may be widespread in the outer galaxy, may have been missed because of the coarse resolution of the observation. The distances and placement of the outer galaxy clouds is suggestive of two outer arms to the galaxy, one of which may be an extension of the Perseus arm of the galaxy into the third quadrant. Molecular clouds apparently can be used to trace spiral structure out to galactocentric radii of 15 kpc, even though the density of molecular material beyond the solar circle is

low. The outer galaxy clouds are colder and have much lower CO
luminosities (S_{CO}) than inner galaxy clouds, even though they have
similar sizes. The scale height of molecular material outside the
solar circle is consistently the same as the local value (65 pc rms)
but the surface density may be twenty times lower.

APPENDIX A. CLOUD MASSES

1. Virial Masses

The virial theorem for a homogeneous sphere with no density gradient implies that $M_{vir} = 5 R (\Delta V_{FWHM})^2 / [8 G \ln(2)]$, or

$$M_{vir}(M_\odot) = 209.6 \ D(pc) \ [\Delta V_{FWHM}(km \ s^{-1})]^2 \ \tan(\Theta), \quad \text{(App.1)}$$

where G is the gravitational constant, R the radius of the cloud, D its distance, and Θ its angular radius. This is an upper limit to the mass of a cloud, since the effects of density gradients, magnetic fields, sources of pressure, and cloud contractions have been omitted. Intensity gradients close to the edges of the clouds indicate little CO below the sensitivity limit of the lowest contour level (~ 1.3 K km s^{-1}) so Θ was taken to be $(A / \pi)^{1/2}$, where A is the area in square degrees subtended by CO emission.

Since the actual FWHM velocity dispersion of gas in the cloud is unknown, it is assumed that it can be represented by the composite CO line width. Composite spectra for each region in Table V.1 were determined by interpolating T_R(PEAK), V(PEAK), and W_{CO} for each unmeasured grid point and then summing Gaussian line profiles with height T_R(PEAK), Gaussian equivalent FWHM width of $0.94 \ W_{CO} / T_R$(PEAK), and centers on V(PEAK) over all grid points within the region (not including the effects of double spectral lines). As a check, composite spectra for the Orion A cloud and the

large galactic plane cloud (Q, Table IV.2) were constructed by adding
the actual spectra for those fully sampled clouds. A comparison of
these composite spectra and the previous results showed no significant
differences (Figs. APPENDIX.1-APPENDIX.2).

Since the above form of the virial theorem may be inappropriate
to the geometry of the filamentary clouds, a form appropriate to a
cylinder with a radius much smaller than its length was used for the
Northern and Southern filaments. Then $M_{vir} = L (\Delta V_{FWHM})^2 / [4 G \ln(2)]$
or

$$M_{vir}(M_\odot) = 83.8 \ D(pc) \ [\Delta V_{FWHM}(km \ s^{-1})]^2 \tan(1) \qquad (App.2)$$

was used where L is the linear length of the filament and l its
angular length in degrees.

2. LTE Masses

For Orion A and B, CO spectra were synthesized with a resolution
of 1/2° from the single-beam data, and, using the LTE method of Blitz
(1978) and a value of 2×10^{-6} for $N(^{13}CO)/N(H_2)$ (Dickman 1978), these
spectra were combined with observations of ^{13}CO which have the same
resolution (Ch. III,C) to obtain average hydrogen molecule column
densities, $N_{LTE}(H_2)$. If the areas covered by ^{13}CO emission (11.3 deg^2
for Orion A and 4.8 deg^2 for Orion B) were used, the masses derived
from column densities would be lower limits, because the CO survey
shows that the clouds are actually much larger. Assuming that 1.36 is
the mean atomic weight per H atom for the interstellar medium and that

all hydrogen is molecular, the lower limits are 0.38×10^5 $M_\odot$ for Orion A and 0.19 x 10^5 $M_\odot$ for Orion B. To obtain upper limits to the masses (Table V.1), the average column density in the cloud periphery where ^{13}CO was not detected is assumed to be equal to the mean value of the derived column densities in the small, denser, central areas detected in ^{13}CO.

For all regions in Table IV.1, including the Orion A and B clouds, between three and twelve full-resolution ^{13}CO spectra near and away from CO temperature peaks were combined with the CO spectra for the same positions to give column densities. By assuming that the derived column densities are representive of the area covered by CO emission, upper limits to the LTE masses (Table V.1) could be obtained for all clouds. The masses calculated in this fashion for Orion A and B were consistent with the upper limits derived above. Since ^{13}CO observations were not made toward the galactic plane clouds, M_{LTE} were not calculated for them.

3. W_{CO} Masses

Empirically, W_{CO} traces the molecular column density, although CO is generally believed to be so abundant that most of its emission lines should be saturated; for example, optically thick CO line profiles generally mimic thin ^{13}CO line profiles observed at the same positions. To convert from W_{CO} to $N(H_2)$ the results of Bloemen et al. (1984) were used. They assume that the γ-ray flux observed by the COS-B satellite toward a large subsection of the region covered in the Columbia CO survey of Orion is proportional to the number of nucleons,

N(H I) and N(H$_2$), along the line of sight. If W$_{CO}$ is proportional to N(H$_2$), the predicted γ-ray flux will be F$_\gamma$ = A N(H I) + B W$_{CO}$ + C, where the observations determine A, the emissivity per nucleon, B, which equals 2 A N(H$_2$) / W$_{CO}$, and C, the contribution from background sources. In a maximum likelihood analysis of predicted versus observed γ-ray flux which combined the CO observations and the Berkeley 21 cm surveys, Bloemen et al. (1984) found N(H$_2$)/W$_{CO}$ = (2.6 $\pm$ 1.3) x 10^{20} cm^{-2} (K km s^{-1})$^{-1}$. Similarly, Lebrun et al. (1983), investigating the inner galaxy, used the W$_{CO}$ measurements from the Columbia first quadrant survey and found a ratio of (1 - 3) x 10^{20}. These are approximately the same values Kutner and Leung (1985) found by applying radiative transfer theory to theoretical radiative transfer models of the type of cloud envelopes that make up the major portion of our survey. Using visual extinction and W$_{CO}$ measurements toward Taurus, Frerking, Langer, and Wilson (1982) obtained a ratio of 1.8 x 10^{20}. However, Sanders, Solomon, and Scoville (1984), who used the same extinction measurements as Frerking et al. but instead used ^{13}CO integrated intensities to infer CO intensities, obtained 3.6 x 10^{20}. All these ratios are somewhat smaller than the value proposed by Liszt (1982): 5 x 10^{20}.

Using various beam sizes (i.e., full-resolution and 1/2° resolution observations corresponding to 1.25 and 5 pc at a distance of 500 pc), N$_{LTE}$(H$_2$) appears to be proportional to W$_{CO}$ over a wide range in densities (Fig. APPENDIX.3). The somewhat low value for the W$_{CO}$-to-N(H$_2$) ratio (0.91 x 10^{20} cm^{-2} (K km s^{-1})$^{-1}$) implied by

Figure APPENDIX.3 suggests that either the proposed $N(H_2)/W_{CO}$ values are systematically too high or, more likely, the low values for N_{LTE} resulted from using a value for $N(^{13}CO)/N(H_2)$ which was high by a factor of 2 or so.

Assuming that the correct value for $N(H_2)/W_{CO}$ is 2.6×10^{20} cm^{-2} (K km s^{-1})$^{-1}$, that the mean atomic weight per H atom for the interstellar medium is 1.36, and that all hydrogen is molecular

$$M_{CO}(M_\odot) = 1.73 \times 10^{-3} \, D(pc)^2 \, S_{CO}(K \text{ km s}^{-1} \text{ deg}^2) \quad \text{(App.3)}$$

where D is the distance to a region and S_{CO} is the integrated CO emission summed over that region.

Appendix B. MODEL FOR THE DISRUPTION OF A MOLECULAR CLOUD BY AN
            EMBEDDED H II REGION

As shown in Chapter V,E, the structures in the interstellar medium now surrounding λ Ori may have been caused by expansion of the H II region excited by the star. The symmetric distribution of the molecular, atomic, and ionized gases indicate that after the star formed, probably near the center of a molecular cloud, the disruption of the interstellar gases proceeded symmetrically around the star; the half-dozen molecular clouds detected by the present CO survey are probably fragments of the original cloud.

This appendix presents a theoretical model to show how an H II region created by a star similar to λ Ori might disrupt the molecular cloud in which it formed. The model entails the transfer of momentum from the H II region to the surrounding medium and predicts the distribution of molecular, atomic, and ionized gases and the expansion velocities of the gas structures at different stages in the region's evolution. The predictions are then compared to the observed distributions and velocities of the λ Ori system. Although the model can be applied to a wide range of cloud sizes and types of stars, I will concentrate on initial parameters suitable for the λ Ori system.

A newly-formed star, taken to be of spectral type O8, and its associated H II region are centered within a molecular cloud at the initial stage of the model. Although the observed clouds in the λ Ori system lie in a single plane, suggesting that the original cloud was shaped more like a pancake than a sphere (Fig. V.16a), I will consider

only the case of a spherical cloud. Were the original dimensions of the λ Ori molecular cloud known, a more detailed model could be constructed.

It is assumed that the cloud has a uniform density, $n(H_2)$, of 150 cm^{-3} (the average density of the molecular clouds found in the Orion survey), and is surrounded by an intercloud medium of uniform atomic gas at a density, $n(H)$, of 1.5 cm^{-3}. Both the molecular and atomic gases are taken to be dust-free and composed only of hydrogen. Throughout all stages of the model, the ionization, dissociation, and shock fronts associated with the expansion of the H II region are considered a single discontinuity; since the model never approaches the stage where the pressure in the H II region equals that of the surrounding gas, the difference between the velocities of the shock-fronts and ionization-fronts remains small (Spitzer 1978), so the fronts stay close together. The initial radius of the cloud, assumed to be 10 pc, is the only parameter in the model for which observations do not suggest a value. The model predicts, as a function of radius for the H II region, the expansion velocity of the H II region, the elapsed time since the start of the expansion, the atomic and molecular mass associated with the shell surrounding the H II region, and the density and mass of ionized gas within the H II region.

The model evolves through four stages:

A. Initial Expansion

The expansion of the H II region to its Stromgren radius, r_0,

occurs rapidly (for a detailed description see Spitzer 1978). If the molecular cloud has a proton density, n_c = 2 $n(H_2)$, then r_o^3 = 3 Q / 4 π α n_c^2, Q being the number of ionizing photons per second produced by the star and α the hydrogen recombination coefficient. For $n(H_2)$ = 150 cm^{-3}, Q appropriate for an 08 star (3.9 x 10^{48} s^{-1}), and α = 3.1 x 10^{-13} cm^{-3} s^{-1} (Spitzer 1978), the Stromgren radius is 1 pc, much smaller than the 10 pc radius of the molecular cloud. At the end of this stage, the expansion velocity, U_s, of the H II region will be (4 C^2 / 3)$^{1/2}$, where C is the isothermal velocity within the H II region and equals (2 R T_{ii})$^{1/2}$ for gas constant R. If the gas temperature within the H II region has remained constant over the lifetime of the system (7500 K; Crezelius 1984), then C = 11.2 km s^{-1} and U_s = 12.9 km s^{-1}. The initial mass within the H II region (M_{ii}^0) is then 35 $M_\odot$.

B. Expansion and Growth of the Molecular Shell

The gas pressure within the H II region, exceeding the typical pressure in the molecular cloud by 3 orders of magnitude, drives the expansion of the H II region into the molecular cloud. A shell of high density molecular gas forms just outside the H II region and accumulates mass as the H II region grows in size. The results of Mazurek (1980) are summarized here.

If r is the radius of the shell, U_s its expansion velocity (dr/dt), n_{ii} the particle density within the H II region (= 2 n_c [r_o / r]$^{3/2}$; Spitzer 1978), and P the gas pressure within the

H II region (n_{ii} k T_{ii}), then the change in momentum per unit time for the shell satisfies

$$\frac{d}{dt}(M_s U_s) = 4 \pi r^2 P - \frac{G M_s (M_s + 2M_{ii})}{2 r^2} - U_s \frac{d}{dt} M_{ii} \quad . \quad \text{(App. 4)}$$

The insignificant forces from the pressure external to the H II region, from stellar winds, and from radiation pressure are ignored. The next to last term represents the sum of the approximate self-gravity force on a shell of mass M_s plus the force on the shell from the mass of ionized gas (M_{ii}) within the H II region. The rate of momentum transfer to the H II region is given by the last term. Defining $x = r / r_0$, $y = U_s^2 / C^2$, and $\beta = G M_{ii}^0 / r_0 C^2$, then M_{ii} and M_s equal $M_{ii}^0 x^{3/2}$ and $M_{ii}^0 x^3 (1 - x^{-3/2})$, respectively, and the equation of motion can be rewritten as:

$$\frac{dy}{dx} = \frac{6 x^{1/2}}{x^3 - x^{3/2}} - \beta x (1 + x^{-3/2}) - \frac{6 x^2 - 1.5 x^{1/2}}{x^3 - x^{3/2}} y \quad . \quad \text{(App. 5)}$$

The equation being of the form $dy/dx = P(x) y + Q(x)$, it can be solved analytically, though with some difficulty. Instead of approximately solving the equation, as Mazurek has done, I solved it numerically using the third-order predictor-corrector method of Adams-Moulton. Figure APPENDIX.4 illustrates the results obtained with the parameters of the λ Ori system using as initial values the radius and expansion velocities of the H II region at the end of the first stage in evolution. The numerical results agree with the results of

Mazurek: as the mass in the shell grows with the expansion of the H II region, U_S decreases.

The third evolutionary stage begins when the outer radius of the shell reaches the radius of the cloud. For the cloud and star under consideration, this process takes 2.5 Myrs, at which point $U_S = 2.0$ km s^{-1}. Were the cloud 14 pc or larger in radius, instead of 10 pc, expansion would halt before all molecular material is enveloped by the shell, and the third evolutionary stage would not occur. For a nonspherical cloud, the third stage begins when the radius of the shell approaches half the short diameter of the cloud. The evolution of spherical and nonspherical clouds is identical up to this point.

C. Expansion of the Shell into the Intercloud Medium

When the shell reaches the edge of the cloud, the expansion accelerates because, during expansion into the low density intercloud medium, the shell accumulates mass at a low rate. A growing H I shell precedes the molecular shell, which continues to lose mass to the expanding H II region, and the surface density of molecular and atomic gas in the shell decreases as the shell radius expands. Equation App. 4 remains appropriate for this stage of evolution, but now $M_S = M_c (1 - f - \delta z^{3/2} + f z^3)$ and $M_{ii} = M_c \delta z^{3/2}$, where the original mass of the molecular cloud, M_c, equals 3.1×10^4 M_0, $f = n(H) / n(H_2) = 0.005$, $\delta = (r_0 / r_c)^{3/2} = 0.034$, and $z = r / r_c$. Similar to the way Equation App. 5 was obtained, the new equation of motion can be written as:

$$\frac{dy}{dz} = \frac{6 \ z^{1/2} \ \delta}{1 - f - f \ z^3 - \delta \ z^3} + (\delta \ \beta \ z^{1/2} - 3 \ f \ z^2) \ (1 - f - f \ z^3 + \delta \ z^3)$$

$$+ \ \frac{1.5 \ \delta \ z^{1/2} - 3 \ f \ z^2}{1 - f - f \ z^3 - \delta \ z^3} \ y \quad . \qquad\qquad (App. \ 6)$$

The results of the numerical differentiation, which uses the final velocity of the second stage as the initial velocity, are shown in Figure APPENDIX.4. In calculating the masses in the figure, I have assumed that atomic gas is not converted into molecular gas, and vice versa, and that only molecular gas enters the H II region.

If the shell does not enter the fourth stage of evolution, expansion stops when enough mass accumulates in the shell, when the pressure within the H II region approaches the external pressure, or when the star evolves off the main sequence. Because Mazurek did not include the intercloud medium, the shell in his model accelerates at a higher rate during this stage of evolution and stops expanding only when the pressure inside the H II region approaches the external pressure or when the star evolves.

If the cloud were shaped like a pancake instead of a sphere, some sections of it would continue to go through the second stage of evolution while other sections would already be in the third (Fig. V.16b). Depending on the exact dimensions of the cloud, the shell may stop expanding along the major axis of the cloud and expand rapidly along the minor axis. In this case, the velocity structure of the system would be difficult to predict.

Accelerated by the low-density gas in the H II region, the shell

eventually develops a Rayleigh-Taylor instability. The once-uniform molecular material forms clumps and eventually a break in the shell occurs. No longer confined at the location of the break, the gas in the H II region flows rapidly through the hole in the shell. If the molecular clumps in the shell have a turbulent velocity dispersion, V_t, typical of molecular clouds (~ 2 km s^{-1}), and if the acceleration of the shell is g, then the thickness of the shell, λ, is $\sim V_t^2 / 2$ g and the growth time, τ, for the development of the instability is $\sim (2 \pi \lambda / g)^{1/2}$ or $2^{1/2} V_t / g$. The instability does not have a chance to grow significantly during the second stage of the model since g is low then. However, with the high acceleration during the third stage, τ becomes shorter than 1 Myrs. Since the depressurization of the H II region takes $\sim r / C$, or an additional 1 Myrs after the shell is punctured, the model progresses to the fourth stage approximately 2 Myrs after the start of the third stage. At the close of the third stage, the radius and expansion velocity of the shell are 18.6 pc and 6.6 km s^{-1}.

D. Expansion After the Shell is Punctured.

Many studies (e.g., Tenorio-Tagle 1978; Bodenheimer et al. 1979; Bally and Scoville 1980) investigated the evolution of an H II region after its border breaks through a confining shell into the intercloud medium. The H II region wants to expand approximately to the size it might have had if it had formed in the intercloud medium (~ 40 pc). The border of the expanded H II region is not spherical; the remnant of the shell delineates some fraction of the border of the H II region. If the

puncture of the shell occurred over a small region of the shell, most of the atomic gas exterior to the molecular shell should be unaffected.

Since the shell remnant lies within the new Stromgren radius of the H II region, ionization of shell material increases on the side of the shell facing the star. The ionized gases stream away from the shell remnant at about the sound speed in the H II region and, rather like a rocket engine, give an impulse back to the remnant. The rate of ionization is self-regulating; an excess flux of UV photons increases ionization, but newly ionized gases subsequently absorb the excess. The flux of ionized gases away from the remnant, therefore, is $\sim n_{ii}$ C, and the force on the remnant from the rocket effect is approximately the same as the force of the gas pressure. If the shell retains most of its original spherical geometry, the equation of motion can be derived from Equations App. 4 and App. 6 simply by doubling the pressure term. The shell, still accumulating atomic mass, continues to expand, but will finally come to rest. In the meantime, the pressure forces die out as the central star evolves.

At a comparable radius of 34 pc, the observed parameters of the λ Ori system and those predicted by the model, agree rather well (Table App.1), even though the geometry of the λ Ori molecular cloud was probably nonspherical. The radius of the molecular cloud being the only parameter in the model for which observations do not suggest a value, the agreement between predictions and observations is probably more than fortuitous.

Table II.1

Comparison Among Telescopes

===

Parameter	Telescope		
	NRAO	Bell Telephone	P.O.M.
Aperature	11 m	7 m	2.5 m
Molecule	CO	^{13}CO	^{13}CO
Beam Width	1.'0	1.'5	4.'4
Spacing Between Observations	1.'0	1.'0	4.'4
Velocity Resolution	0.65 km s^{-1}	0.65 km s^{-1}	0.26 km s^{-1}
rms Noise	0.2 K	0.1 K	0.15 k

Note: All observations were position-switched with first-order baselines removed. The rms noise values given are approximate or average.

Table III.1

Off Positions

===

α(1950)	δ(1950)	α(1950)	δ(1950)	α(1950)	δ(1950)

$5^h20^m27^s$	$20°57'26''$*	$6^h06^m52^s$	$9°08'24''$*	$6^h37^m14^s$	$18°43'14''$*
5 41 00	8 40 00	6 10 50	-11 22 30	6 39 27	-6 17 12*
5 44 50	-11 15 00	6 11 00	2 47 30	6 42 55	13 49 53*
5 46 29	17 47 11*	6 11 41	6 57 13*	6 44 01	-8 30 18*
5 48 00	5 10 00	6 12 16	21 16 08*	6 47 33	11 36 44*
5 48 00	-3 35 00	6 14 50	-7 15 00	6 52 09	9 23 33*
5 50 20	-7 00 00*	6 14 52	24 46 34*	6 52 20	-7 30 00*
5 51 47	15 38 32*	6 16 30	-8 52 30	7 01 17	4 57 23*
5 53 07	21 02 02*	6 17 33	10 34 32*	7 05 51	2 44 29*
5 54 20	-14 07 30	6 18 36	24 53 22*	7 13 43	-15 59 25*
5 56 20	-6 00 00*	6 18 39	16 24 00*	7 15 03	-1 40 41*
5 56 50	0 47 30	6 21 06	2 33 35*	7 19 42	-3 52 50*
5 56 56	13 29 07*	6 23 40	22 41 11*	7 24 25	-6 04 37*
5 59 00	-3 05 00	6 26 44	20 14 49*	7 29 12	-8 15 59*
5 59 20	-8 15 00*	6 28 38	20 28 40*	7 35 04	-10 52 58*
6 01 57	11 19 03*	6 30 19	-1 51 22*	7 45 46	-17 26 16*
6 06 00	4 02 30				

Note: All off positions were observed to an rms noise level of 0.20 K
or, if marked with an asterisk, to 0.15 K or less.

Table IV.1

CO Emission Peaks - Local Clouds

===

No.	α(1950) (h m)	δ(1950) (° ')	T_R (K)	<V> (km s^{-1})	W_{CO} (K km s^{-1})	Associated Objects[a]

λ Orionis Clouds

No.	α(1950) (h m)	δ(1950) (° ')	T_R (K)	<V> (km s^{-1})	W_{CO} (K km s^{-1})	Associated Objects
1	5 8.0	10 38	5.7	1.4	9.3	LDN 1571,72
2	5 14.0	15 0	5.2	0.8	15.7	
3	5 16.0	13 0	5.4	0.8	17.6	VDB 37
4	5 18.1	7 30	6.6	1.9	29.4	B 223; LDN 1588,89,90; S 263,65; VDB 38; Mel 1
5	5 22.5	7 8	3.7	3.4	14.7	LDN 1595*; VDB 40
6	5 25.5	6 8	3.3	0.6	6.1	LDN 1595; VDB 40*
7	5 26.5	14 23	3.8	8.3	11.2	
8	5 28.5	16 0	2.8	8.7	9.0	
9	5 28.5	12 30	9.8	10.2	18.9	B 30,31,32,225; LDN 1573,77,81,82,83,84
10	5 42.4	9 3	6.6	11.5	14.0	B 35; LDN 1594,96

Table IV.1 (Continued)

===

No.	α(1950)	δ(1950)	T_R	<V>	W_{CO}	Associated Objects

No.	α(1950)	δ(1950)	T_R	<V>	W_{CO}	Associated Objects
11	5 42.4	6 3	3.7	13.2	8.8	LDN 1602,03
12	5 50.0	8 25	6.6	11.7	15.1	B 36*; LDN 1598; LDN 1597,99*

Orion A Cloud

No.	α(1950)	δ(1950)	T_R	<V>	W_{CO}	Associated Objects
13	5 04.0	-3 23	5.8	7.7	15.2	LDN 1615,16; NGC 1788; VDB 33
14	5 17.0	-5 53	6.1	7.9	14.5	LDN 1634; S 278
15	5 26.5	-2 30	5.3	11.9	15.0	
16	5 28.0	-3 0	8.5	10.6	19.2	
17	5 28.5	-4 23	8.0	10.7	29.4	VDB 44; IC 420
18	5 29.5	-5 30	5.7	9.6	17.6	VDB 42
19	5 31.0	-3 53	7.1	11.0	23.7	
20	5 32.8	-5 25	30.8	9.3	161.9	Orion Nebula; NGC 1976,82;
21	5 33.5	-6 15	16.1	8.4	55.6	NGC 1999*; IC 427,28*; VDB 46*;
						HH 33,34,40; HH 1,2,3,35,36*
22	5 36.5	-7 8	9.2	5.4	42.9	IC 429,30; LDN 1641; HH 38,43
23[b]	5 36.5	-8 30	6.0	5.9	22.7	LDN 1641
			2.8	11.8	6.4	

Table IV.1 (Continued)

No.	α(1950)	δ(1950)	T_R	<V>	W_{CO}	Associated Objects
24[b]	5 38.5	-9 23	7.3	2.8	20.0	LDN 1647; VDB 53
			2.8	11.0	5.9	
25[c]	5 40.0	-8 15	12.5	2.8	28.7	VDB 55
			7.4	6.9	14.8	
26	5 43.0	-5 30	8.0	9.2	20.1	
27	6 0.2	-10 45	5.5	4.9	8.1	

Orion B Cloud

No.	α(1950)	δ(1950)	T_R	<V>	W_{CO}	Associated Objects
28	5 29.0	-0 53	3.9	12.3	11.8	Delta Ori[*]; IC 423,24[*]
29	5 31.5	0 0	2.3	12.0	6.7	Delta Ori[*]; IC 424
30[c]	5 39.0	-1 45	3.4	3.9	11.7	NGC 2024; S 277; IC 432; IC 431[*]; VDB 51;
			20.5	9.9	95.1	VDB 50[*]
31	5 39.0	-2 15	17.6	10.1	73.6	Horsehead Nebula; B 33; NGC 2023;
						IC 434,35; VDB 52; VDB 57[*]
32[c]	5 41.0	-1 30	5.8	3.0	26.0	LDN 1630
33	5 42.5	-3 30	7.3	9.2	26.9	

Table IV.1 (Continued)

===

No.	α(1950)	δ(1950)	T_R	<V>	W_{CO}	Associated Objects

No.	α(1950)	δ(1950)	T_R	<V>	W_{CO}	Associated Objects
34	5 44.0	0 0	16.2	10.3	54.4	LDN 1627; NGC 2064,67,68,71; VDB 59,60; HH 19 - HH 27
35[c]	5 45.0	-0 53	3.2	4.8	16.3	LDN 1630
			7.0	10.3	17.3	
36	5 48.5	4 40	4.8	8.3	10.7	LDN 1617; VDB 61*
37[c]	5 50.5	2 25	5.5	8.6	12.1	LDN 1617
			3.5	10.9	11.4	

Orion East Cloud

No.	α(1950)	δ(1950)	T_R	<V>	W_{CO}	Associated Objects
38[d]	5 52.0	1 48	9.3	0.7	20.2	LDN 1621,22; VDB 62,63
			4.1	10.4	9.6	

Barnard's Loop Clouds

No.	α(1950)	δ(1950)	T_R	<V>	W_{CO}	Associated Objects
39	5 39.0	3 23	3.4	2.6	9.9	VDB 49*
40	5 40.5	3 15	3.9	9.1	12.2	
41	5 54.3	-6 45	3.0	9.1	3.7	LDN 1638*
42	5 55.5	-3 5	4.1	9.0	9.6	LDN 1638

Table IV.1 (Continued)

==

No.	α(1950)	δ(1950)	T_R	<V>	W_{CO}	Associated Objects

NGC 2149 Clouds

No.	α(1950)	δ(1950)	T_R	<V>	W_{CO}	Associated Objects
43[e]	5 43.0	-9 23	1.0	4.0	3.7	LDN 1647*
			3.3	10.3	4.0	
44	5 48.6	-9 0	4.1	11.1	7.7	LDN 1648
45[e]	5 51.6	-10 30	1.6	5.8	4.4	
			5.5	10.3	12.5	
46	5 54.6	-12 0	2.3	11.4	5.9	
47	5 55.6	-13 38	3.8	9.5	9.6	VDB 64
48	5 58.2	-9 53	4.7	12.3	19.5	
49	6 0.8	-9 45	7.9	12.3	23.9	NGC 2149; VDB 66

Northern Filament

No.	α(1950)	δ(1950)	T_R	<V>	W_{CO}	Associated Objects
50	5 49.0	6 3	4.2	12.5	8.0	
51	5 53.0	5 40	3.5	9.1	9.9	
52[c]	5 57.5	5 10	3.5	8.8	5.1	LDN 1611; LDN 1612*
			3.8	11.4	8.8	
53	6 3.0	4 10	4.4	9.9	11.0	LDN 1618,19

Table IV.1 (Continued)

No.	α(1950)	δ(1950)	T_R	\<V\>	W_{CO}	Associated Objects
54	6 7.0	2 48	3.4	9.3	13.6	LDN 1628,29
55[c]	6 7.5	2 40	1.7	6.2	4.8	LDN 1628,29
			4.4	9.8	10.7	
56	6 8.5	1 55	3.6	7.8	14.0	
57	6 16.6	3 55	4.0	9.4	13.6	
58	6 20.5	0 25	2.4	15.6	4.0	
59[c]	6 21.6	3 40	3.5	7.0	10.7	LDN 1633
			3.4	10.0	10.3	

Monoceros R2 Cloud

No.	α(1950)	δ(1950)	T_R	\<V\>	W_{CO}	Associated Objects
60	6 2.0	-4 20	3.5	13.7	15.1	LDN 1643*
61	6 5.3	-6 23	13.9	10.7	62.9	LDN 1646; NGC 2170; VDB 67,68,69
62	6 5.3	-6 53	5.9	10.0	25.0	
63[c]	6 6.3	-6 0	4.4	10.3	7.7	LDN 1646; NGC 2182*; VDB 68,69,72*
			5.8	12.4	13.6	
64	6 7.4	-8 45	3.0	11.0	13.2	
65	6 8.4	-6 15	6.9	10.7	28.3	LDN 1646*; NGC 2182,83,85; VDB 72,73,74

Table IV.1 (Continued)

==

No.	$\alpha(1950)$	$\delta(1950)$	T_R	$<V>$	W_{CO}	Associated Objects

----

Southern Filament

66	6 24.6	-10 8	3.0	12.2	12.9	LDN 1652
67	6 28.7	-9 30	4.7	11.8	13.2	'CROSSBONES'[f]; VDB 80
68	6 32.7	-9 8	4.1	12.0	9.6	'CROSSBONES'[f]
69	6 34.3	-10 38	3.0	12.7	11.0	
70	6 36.4	-10 30	2.8	14.4	9.6	
71	6 54.8	-11 30	4.0	11.9	7.7	

LDN 1653,54,55,56 Clouds

72	6 54.1	-10 8	3.4	12.8	11.4	VDB 86
73	6 54.4	-8 23	3.5	13.1	8.1	LDN 1655,56; S 291[*]
74	6 57.3	-7 45	5.6	13.3	16.2	LDN 1654; NGC 2316; MRSL 220-01/1

----

[a] LDN, Dark clouds (Lynds 1962); VDB, Reflection nebulae (van den Bergh 1966); B, Dark clouds (Barnard 1927); S, HII regions (Sharpless 1959); Mel, Bright nebulae (Melotte

Table IV.1 (Continued)

1926); NGC, Nonstellar objects (Sulentic and Tift 1973); IC, Nonstellar objects (Dreyer 1908); HH, Herbig-Haro objects (Herbig 1974); MRSL, HII regions (Marsalkova 1974). Asterisks indicate an object or objects not coincident with and perhaps not associated with CO peak.

[b] Second spectral line due to overlapping NGC 2149 Cloud.

[c] Double CO lines.

[d] Second spectral line due to overlapping Orion B Cloud.

[e] First spectral line due to overlapping Orion A Cloud.

[f] Refers to molecular feature crossing the Southern Filament.

Table IV.2

Star Counts

===

Cloud	Position[a]		A[b]	n⋆[c]	N_{CT}[d]	Distance[e]
	α(1950)	δ(1950)				(pc)
Northern Filament	5h 58m	5° 15'	98.	25	5.0 ± 1.0	801 ± 91
	6 03	4 15				
	6 07	2 45				
Southern Filament	6 25	-10 00	157.	60	7.5 ± 1.0	1009 ± 77
	6 28	-9 30				
Orion East[f]	5 52	1 45	216.	22	2.0 ± 0.4	475 ± 54
Orion A[g]	5 38	-9 00	137.	14	2.0 ± 0.5	475 ± 68
	5 40	-10 15				
Monoceros R2[g]	6 05	-5 15	196.	58	5.8 ± 0.8	872 ± 69
	6 03	-6 30				

Notes: [a] Position given to within nearest 1/4°; chosen near locations
of high W_{CO} to reduce number of background stars.

[b] The total area (square arcmin) in which stars were counted; a
5' diaphragm was used at a number of locations roughly
centered on the indicated positions.

[c] Total number of stars found on POSS blue prints within A.

Table IV.2 (Continued)

d Average number of stars found within a 5' diaphragm.

e Distance from empirical relation of Herbst and Sawyer (1981).

f Included as a test of the method; distance agrees with that found by Herbst (1982) using the same method.

g Included as a test of the method; distances agree with previously determined photometric distances of associated stars.

Table IV.3

Molecular Clouds -- Outer Galaxy

Cloud	l	b	$\langle v \rangle^a$	$AREA^b$	T_R^c	S_{CO}^d	D^e	z^f	M_{CO}^g	Notes
	(°)	(°)	(km s-1)	(deg^2)	(K)		(kpc)	(pc)		
A	204.3	-8.2	10.	9.1	4.4	52.3	0.5	-71.	0.2	*
B	207.3	-1.8	15.	2.5	21.0	...	1.6^h	-50.	~3.	*
C	207.6	2.4	14.	$>0.8^i$	2.1	$>2.4^i$	1.6^h	67.	$>0.1^i$	
D	207.6	1.1	18.	$>0.2^i$	1.7	$>0.8^i$	1.6^h	31.	$>0.04^i$	
E	208.9	2.1	11.	2.1	4.0	9.5	1.6^h	59.	0.4	*
F	209.6	0.6	30.	0.3	1.6	0.6	4.7^j	49.	0.2	
G	209.6	-0.1	15.	$>0.4^i$	1.0	$>0.8^i$	1.6^h	0.	$>0.04^i$	
H	210.4	-0.1	37.	0.1	3.3	0.7	6.0^j	-10.	0.4	
I	210.9	-3.3	21.	0.8	1.8	2.8	1.6^h	-92.	0.1	*
J	211.4	-0.4	22.	0.4	2.1	0.6	2.3^j	-16.	0.05	*
K	211.6	1.1	45.	0.3	1.1	0.7	5.8^k	111.	0.4	
L	211.9	1.9	7.	$>0.5^i$	2.7	$>1.7^i$	~1.	33.	$>0.03^i$	*
M	212.1	-0.9	44.	0.5	2.0	1.3	5.5^k	-86.	0.7	*
N	212.9	1.1	44.	0.8	1.4	1.4	5.5^k	106.	0.7	
O	215.1	0.9	48.	0.5	2.1	1.6	5.7^k	90.	0.9	
P	215.4	-0.4	28.	1.1	1.6	1.5	2.9^j	-20.	0.2	
Q	216.6	-2.8	27.	5.8	3.8	42.6	3.0^l	-145.	6.6	*

Table IV.3 (Continued)

===

Cloud	l	b	\<v\>	AREA	T_R	S_{CO}	D	z	M_{CO}	Notes
R	217.4	0.1	49.	0.8	1.8	1.9	5.5^k	10.	1.0	*
S	218.1	-0.4	27.	1.3	3.3	5.1	3.0^l	-21	0.8	*
T	221.8	-2.6	13.	1.9	5.6	15.4	1.2	-54.	0.3	*

Notes to Individual Clouds:

A) Section of the Northern filament (Chap. IV,A,4).

B) Section of the Rosette cloud complex; data for the complex is from Blitz (1978).

E) Associated with LDN 1639.

I) May be associated with S 280 and S 282 (photometric distances of 1.5 ± 0.5 kpc; Georgelin 1975).

J) May be associated with NGC 2282, IC 2172, MRSL 211-00/1, and VDB 85 (photometric distance of 1.7 ± 0.4 kpc; Racine 1968).

L) Associated with cloud 184 in Khavtassi (1955). No reliable distance estimate; assumed 1 kpc.

M) Associated with the H II regions Bo2 and S 284 with photometric distances of 4.8 ± 0.7 and 5.2 ± 0.8 kpc (Moffat and Vogt 1975; Moffat, Fitzgerald, and Jackson 1979).

Q) Cloud described in Chap. V,F. Associated with cloud 181 in Khavtassi (1955). $M_{vir} = 10.8 \times 10^5 \ M_\Theta$ using 8.5 km s^{-1} line width from Fig. IV.23.

Table IV.3 (Continued)

R) Possibly associated with S 286.

S) Associated with S 287 with a photometric distance of 3.2 ± 0.8 kpc

(Moffat et al. 1979) and with LDN 1649 and 1650.

T) Section of the LDN 1652, 1653, 1654, and 1655 clouds (Chap. IV,A,8).

Notes:

[a] Mean velocity of the cloud.

[b] Area subtended by the cloud (Chap. V,G).

[c] Maximum radiation temperature observed within the cloud.

[d] Intensity of CO emission integrated over the extent of the cloud

$(K \ km \ s^{-1} \ deg^2)$.

[e] Distance from the Sun.

[f] Displacement of the cloud from the galactic plane.

[g] Mass from the CO luminosity (App. A,3) in units of $10^5 \ M_\odot$.

[h] Assumed distance the same as the Rosette Complex (1.6 kpc; Turner

1976).

[i] Not fully covered in this survey; Area, S_{CO}, and M_{CO} are minimum

values.

[j] Distance estimated from the rotation curve of Blitz (1979).

[k] Distance estimated from a flat rotation curve ($\theta_\odot = 250 \ km \ s^{-1} \ kpc^{-1}$,

$R_\odot = 10$ kpc).

[l] Distance determination described in Ch. V,F,1.

Table V.1

Masses - Local Clouds

==

Object	D	ΔV[a]	A	S_{CO}	M_{vir}	M_{LTE}	M_{CO}
	(pc)	(km s^{-1})	(deg^2)	(K km s^{-1} deg^2)		(10^5 M$_\odot$)	
λ Orionis	400	...	11.7	100.6	...	0.14	0.28
Orion A	500	5.1	28.6	309.6	1.44	0.98	1.04
Orion B	500	4.0	19.0	246.9	0.72	0.74	0.83
Orion East	500	1.6	0.8	5.0	0.02	0.04	0.02
Barnard's Loop	320	...	1.8	6.2	...	0.01	0.01
NGC 2149	830	2.9	7.9	47.4	0.41	0.44	0.44
Northern Filament	500	3.6	9.1	52.3	1.01[b]	0.13	0.18
Monoceros R2	830	3.9	13.6	93.8	0.96	1.22	0.86
Southern Filament	900	3.0	6.1	28.9	1.26[b]	0.41	0.32
LDN 1653,4,5,6	1200	3.4	1.9	15.4	0.40	0.25	0.30
Total:			100.5	906.1	6.51	4.36	4.28

Notes: [a] FWHM of composite spectral line.

[b] Assuming cylindrical geometry.

Table V.2

High Velocity Resolution Observations of Orion East

==

	Position		Molecule	T_R[b]	W_{CO}	V[c]	ΔV[d]
No.[a]	a(1950)	δ(1950)		(K)	(K km s^{-1})	(km s^{-1})	(km s^{-1})

1	5h 52m	1° 40'	CO	8.2	11.2	0.99	1.58
			^{13}CO	2.2	2.4	1.14	0.97
2	5 52	2 17.5	CO	3.1	4.5	0.26	1.37
			^{13}CO	0.5	0.5	-0.18	0.85
3	5 53.5	2 10	CO	6.6	8.6	1.61	1.24
			^{13}CO	1.9	1.9	1.69	0.92

----

[a] Number refers to the positions circled in Fig. IV.16.

[b] The rms noise levels are 0.15 and 0.10 for CO and ^{13}CO. Second velocity component from the Orion B cloud is ignored.

[c] Velocity of Gaussian fitted to deconvolved spectra; the high signal-to-noise for CO observations implies that the CO velocities are more accurate than ^{13}CO. The 1σ errors in the fitted Gaussians are typically 0.1 and 0.2 km s^{-1} for CO and ^{13}CO observations, respectively.

[d] FWHM width of deconvolved spectra; 1σ errors are about the same as for V.

Table V.3

Orion A and B Ridge Heating and Cooling

===

Parameter	Ridge	Non-Ridge
λ	5 pc	10 pc
P_{ext}	10^{-10} ergs cm^{-3}	10^{-12} ergs cm^{-3}
n(H2)	300 cm^{-3}	150 cm^{-3}
T_K	15 K	8 K
n_e	1.5×10^{-5} cm^{-3}	7.5×10^{-5} cm^{-3}
C	0.27 km s-1	0.20 km s-1
B	50 μG	5 μG
τ_B	5 Myrs	75 Myrs
Γ_{CR}	2×10^{-25} ergs cm^{-3} s^{-1}	1×10^{-25} ergs cm^{-3} s^{-1}
Γ_B	7×10^{-25} ergs cm^{-3} s^{-1}	4×10^{-28} ergs cm^{-3} s^{-1}
Γ_T	9×10^{-25} ergs cm^{-3} s^{-1}	1×10^{-25} ergs cm^{-3} s^{-1}
Λ	4×10^{-25} ergs cm^{-3} s^{-1}	1×10^{-25} ergs cm^{-3} s^{-1}

Note: See Chapter V,D for description of paramaters.

Table V.4

Fitted Parameters of Lambda Orionis Ring

===

Paramater	Value
α_0	5h 29.8m ± 1.6m
δ_0	9° 54' ± 24'
V_0	6.0 ± 0.9 km s^{-1}
θ	156.°1 ± 7.°6
ϕ	-36.4 ± 5.°1
V_X	14.3 ± 2.5 km s^{-1}
R_X	34.5 ± 2.0 pc
	(5.°0 ± 0.°1)
T_X (= R_X / V_X)	2.4 ± 0.4 Myrs

Note: Errors correspond to the σ of the fitted model. See Fig. V.8 for explanation of parameters.

Table V.5

Radio Continuum Observations Toward Large and Unusual Cloud

Source	l	b	ν(MHz)	S(Jy)[a]	Ref.	α	Spectrum	u(pc cm^{-2})[b]	Star[c]
4C-02.28	214.°7	-1.°7	178	6.1	1	~ 0.3[d]	thermal	~ 60.[d,e]	~ 06[d,e]
			408	~ 9.[d]	2				
			820	~ 10.[d]	3				
			1415[e]	...	4				
OH 066	214.9	-3.8	178	< 2.	1	> -0.6	nonthermal?	23.9	09.5
			1415	0.62	4				
4C-03.24	215.4	-2.9	86	< 20.	5	-2.6 to -1.4	nonthermal	< 15.2	
			178	2.9	1				
			1415	< 0.16	4				
4C-03.25	215.8	-1.5	178	2.5	1	-0.7	nonthermal	22.7	
			1415	0.53	4				
4C-05.24	217.6	-3.2	86	25.	5	-1.4	nonthermal	22.0	
			178	5.2	1				
			1415	0.48	4				

Table V.5 (Continued)

NOTES: [a] Upper limits in flux densities are from the catalogs.

[b] Excitation parameter using the flux density at the highest observed frequency and assuming a distance of 3 kpc.

[c] Spectral type of ZAMS star which, if the source were thermal, would give the derived u. Used Table 2 of Panagia (1973).

[d] Flux densities are not accurate and were derived, after subtracting an approximate galactic background flux, from published contour plots. The α, u, and derived spectral type are approximations.

[e] Source only partially covered by survey at 1415 MHz (Ehman, Dixon, and Kraus 1970) with no accurate flux density ascertainable at this frequency. Used observations at 820 MHZ to derive u and stellar spectral type.

REFERENCES: (1) Gower, Scott, and Wills (1967); (2) Haslam, Quigley, and Salter (1970); Haslam et al. (1982); (3) Berkhuijsen (1972); (4) Ehman, Dixon, and Kraus (1970); (5) Mills, Slee, and Hill (1958).

Table V.6

Outer Galaxy Molecular Gas

Range in R^G	$\sigma_0{}^a$	$M_{CO}{}^a$	Z_c	ΔZ_{rms}
$10 < R^G < 13$ kpc	0.13 $M_\odot$ pc^{-2}	34×10^6 $M_\odot$	-98 pc	61 pc
$13 < R^G < 15$	0.06	13×10^6	+36	69
$10 < R^G < 15$	0.10	47×10^6	-61	87

[a] Surface density and mass of molecular clouds, including the contribution from He and metals, implied for the whole of the outer galaxy from the observations between $l = 206°$ and $l = 222°$.

Table App. 1

Comparison Between Predictions and Observations of the λ Ori System

===

Quantity	Predictions	Observations
U_S	14.0 km s^{-1}	14.3 ± 2.5 km s^{-1}
T_{exp}	5.9 Myrs	2-6 Myrs
$M(H_2) = M_c$	2.4×10^4 M$_\odot$	2.8×10^4 M$_\odot$
$M(H\ I) = M_s - M_c$	6.0×10^3 M$_\odot$	$< 1 \times 10^4$ M$_\odot$
$M(H\ II)$	6.5×10^3 M$_\odot$	$5 \pm 2 \times 10^3$ M$_\odot$
n_{ii}	3.5 cm^{-3}	4.4 ± 1.0 cm^{-3}

Predictions when r in the model equals 34 pc, the observed radius of the λ Ori ring (Chap. V,E). Observed U_S and $M(H_2)$ from the CO observations. T_{exp} should correspond to age of λ Ori which Murdin and Penston (1977) estimate as 2-4 Myrs; Stothers (1985) estimates 6 Myrs. All other observed quantities from Crezelius (1984)

REFERENCES

Abbott, D. C. 1978, Ap. J., 225, 893.

Appenzeller, I. 1966, Z. Astr., 64, 269.

_____ 1968, Ap. J., 151, 907.

_____ 1974, Astr. Ap., 36, 99.

Axon, D. J., and Ellis, R. S. 1976, M.N.R.A.S, 177, 499.

Baran, G. P. 1983, Ph. D. thesis, Columbia University.

Bally, J., and Scoville, N. Z. 1980, Ap. J., 239, 121.

Barlow, M. J., and Cohen, M. 1977, Ap. J., 213, 737.

Barnard, E. E. 1927, in A Photographic Atlas of Selected Regions of
     the Milky Way, ed. E. B. Frost, and M. R. Calvert (Washington,
     D.C.: Carnegie Institution of Washington).

Barns, C.E. 1929, 1001 Celestial Wonders (California: Pacific Science
     Press).

Baud, B., and Wouterloot, J. G. A. 1980, Astr. Ap., 90, 297.

Becker, W., and Fenkart, R. 1971, Astr. Ap. Suppl., 4, 241.

Beckwith, S., Evans, N. J. II, Becklin, E. E., and Neugebauer, G. 1976,
     Ap. J., 208, 390.

Berkhuijsen, E. M. 1972, Astr. Ap. Suppl., 5, 263.

Bignami, G. F., and Caraveo, P. A. 1985, private communication.

Blitz, L. 1978, Ph. D. thesis, Columbia University.

Blitz, L. 1979, Ap. J. (Letters), 231, L115.

Blitz, L., Fich, M., and Stark, A. A. 1982, Ap. J. Suppl., 49, 183.

Bloemen, J. B. G. M. et al. 1985, Astr. Ap., submitted.

Bloemen, J. B. G. M., Caraveo, P. A., Hermsen, W., Lebrun, F., Maddalena, R. J., Strong, A. W., and Thaddeus, P. 1984, Astr. Ap., 139, 37.

Boss, B. 1937, General Catalogue of 33342 Stars for the Epoch 1950 (Washington D.C.: Carnegie Institution of Washington).

Bodenheimer, P., Tenorio-TAgle, G., and Yorke, H. W. 1979, Ap. J., 233, 85.

Boulanger, F. 1985, private communication.

Chiang, W.-H. 1984, Ph. D thesis, Columbia University.

Chiang, W.-H., and Prendergast, K. H. 1985, Ap. J., 297, 507.

Chin, G. 1978, Ph. D. thesis, Columbia University.

Cohen, M., and Kuhi, L. V. 1979, Ap. J. Suppl., 41, 743.

Cohen, R. J., Matthews, N., Few, R. W., and Booth, R. S. 1982, M.N.R.A.S., 203, 1123.

Cohen, R. S. 1978, Ph. D. thesis, Columbia University.

Cong, H.-I. 1977, Ph. D. thesis, Columbia University.

Cong, H.-I., Kerr, A. R., and Mattauch, R. J. 1979, IEEE Trans. MTT-27, No. 3, p. 245.

Coulson, I. M., Murdin, P. G., MacGillivray, H. T., and Zealey, W. J. 1978, M.N.R.A.S., 184, 171.

Cowie, L. L., Songaila, A., and York, D. G. 1979, Ap. J., 230, 469.

Crezelius, C. 1984, private communication.

Cruz-Gonzalez, C., Recillas-Cruz, E., Costero, R., Peimbert, M., and Torres-Peimbert, S. 1974, Rev. Mexicana Astr. Ap., 1, 211.

Dame, T. M. 1983, Ph. D. thesis, Columbia University.

Dame, T. M., Elmegreen, B. G., Cohen, R. S., and Thaddeus, P. 1985, Ap. J., submitted.

Dame, T. M., and Thaddeus, P. 1985, Ap. J., 297, 751.

Dickman, R. L. 1978, Ap. J. Suppl., 37, 407.

Dickman, R. L., and Clemens, D. P. 1983, Ap. J., 271, 143.

Downes, D., Winnberg, A., Goss, W. M., and Johansson, L. E. B. 1975, Astr. Ap., 44, 243.

Dreyer, J. L. E. 1910, Second Index Catalogue of Nebulae and Clusters of Stars, Mem. R.A.S., 59, 105.

Duerr, R., Imhoff, C. L., and Lada, C. J. 1982, Ap. J., 261, 135.

Eggen, O. J. 1978, Pub. A.S.P., 90, 436.

Ehman, J. R., Dixon, R. S., and Kraus, J. D. 1970, A. J., 75, 351.

Elmegreen, B. G. 1981 in The Formation of Planetary Systems, ed. A. Brahic (Touleuse: Cepadues Editions), p. 61.

Elmegreen, B. G., Dickinson, D. F., and Lada, C. J. 1978, Ap. J., 220, 853.

Frerking, M. A., Langer, W. D., and Wilson, R. W. 1982, Ap. J., 262, 590.

Georgelin, Y. M. 1975, thesis, University of Marseille.

Goldsmith, P. F., and Langer, W. D. 1978, Ap. J., 222, 881.

Gottlieb, E. W., Brock, J., and Thaddeus, P. 1984, private communication.

Goudis, C. 1982, The Orion Complex: A Case Study of Interstellar Matter (Dordecht: D. Reidel), p. 156.

Gower, J. F. R., Scott, P. F., and Wills, D. 1967, Mem. R.A.S., 71, 49.

Goy, G. 1973, Astr. Ap. Suppl., 12, 277.

Grabelsky, D. A. 1985, Ph. D. thesis, Columbia University.

Hall, J. S., 1958, Publ. U.S. Naval Obs., 2nd Ser, Vol. 17, Part 14.

Harper, D. A. 1975, in H II Regions and Related Topics, ed. T. L. Wilson, and D. Downes (New York: Springer-Verlag), p. 343.

Haslam, C. G. T., Quigley, M. J. S., and Salter, C. J. 1970, M.N.R.A.S., 147, 405.

Haslam, C. G. T., Salter, C. J., Stoffel, H., and Wilson, W. E. 1982, Astr. Ap. Suppl., 47, 1.

Heiles, C., and Habing, H. J. 1974, Astr. Ap. Suppl., 14, 1.

Heiles, C., and Troland, T. H. 1982, Ap. J. (Letters), 260, L23.

Henderson, A. P., Jackson, P. D., and Kerr, F. J. 1982, Ap. J., 263, 116.

Herbig, G. H. 1974, Lick Obs. Bull., 658, 5.

Herbig, G. H., and Rao, N. K. 1972, Ap. J., 174, 401.

Herbst, W. 1982, private communication.

Herbst, W., and Racine, R. 1976, A. J., 81, 840.

Herbst, W., and Sawyer, D. L. 1981, Ap. J., 243, 935.

Hill, J. K., and Hollenbach, D. J. 1978, Ap. J., 225, 390.

Hiltner, W. A. 1951, Ap. J., 114, 241.

_____ 1954a, Ap. J., 120, 41.

_____ 1954b, Ap. J., 120, 454.

Hjellming, R. M. 1968, Ap. J., 154, 533.

Hobbs, L. M. 1969, Ap. J., 157, 135.

Huang, Y.-L. 1985, Ph. D. thesis, Columbia University.

Huang, Y.-L., Dame, T. M., and Thaddeus, P. 1983, Ap. J., 272, 609.

Hudson, H. S., and Soifer, B. T. 1976, Ap. J., 206, 100.

Humphreys, R. M. 1978, Ap. J. Suppl., 38, 309.

Isobe, S. 1973, in IAU Symposium 52, Interstellar Dust and Related
    Topics, ed. J. M. Greenberg, and H. C. Van de Hulst (Dordrecht:
    D. Reidel), p. 433.

Jura, M. 1974, Ap. J., 191, 375.

Khavtassi, D. Sh. 1955, Bull. Abastumanskoy Ap. Obs., No. 18, p. 29.

Knapp, G. R., and Brown, R. L. 1976, Ap. J., 204, 21.

Kutner, M. L. 1978, Ap. Letters, 19, 81.

Kutner, M. L., and Leung, C. M. 1985, Ap. J., 291, 188.

Kutner, M. L., Machnik, D. E., Tucker, K. D., and Dickman, R. L. 1980,
    Ap. J., 237, 734.

Kutner, M. L., and Mead, K. 1981, Ap. J. (Letters), 249, L15

_____ 1985, private communication.

Kutner, M. L., and Tucker, K. D. 1975, Ap. J., 199, 79.

Kutner, M. L., Tucker, K. D., Chin, G., and Thaddeus, P. 1977, Ap. J.,
    215, 521 (KTCT).

Kutner, M. L., and Ulich, B. L. 1981, Ap. J., 250, 341.

Lada, C. J., and Black, J. H. 1976, Ap. J. (Letters), 203, L75.

Lada, C. J., Thronson, H. A. Jr., Smith, H. A., Harper, D. A., Keene,
    J., Loewenstein, R. F., and Smith, J. 1981, Ap. J. (Letters),
    251, L91.

Lada, C. J., and Wilking, B. A. 1980, Ap. J., 242, 1056.

Lebrun, F. et al. 1983, Ap. J., 274, 231.

Leisawitz, D. 1984, private communication.

Leung, C. M. 1975, Ap. J., 199, 340.

Liszt, H. S. 1982, Ap. J., 262, 198.

Longmore, A. J., Hyland, A. R., and Allen, D. A. 1976, Proc. Astr. Soc. Australia., 3, 47.

Loren, R. B. 1977, Ap. J., 215, 129.

Loren, R. B. Peters, W. L., and Vanden Bout, P. A. 1974, Ap. J. (Letters). 194, L103.

Lynds, B. T. 1962, Ap. J. Suppl., 7, 1.

Maddalena, R. J., Moscowitz, J., Morris, M., and Thaddeus, P. 1982, Bul. A.A.S., 14, 615.

Maddalena, R. J., and Thaddeus, P. 1985, Ap. J., 294, 231.

Marsalkova, P. 1974, Ap. Space Sci., 27, 3.

Mathewson, D. S., and Ford, V. L. 1970, Mem. R.A.S., 74, 139.

Mazurek, T. J. 1980, Astr. Ap., 90, 65.

Melotte, P. J. 1926, M.N.R.A.S., 86, 636.

Mills, B. Y., Slee, O. B., and Hill, E. R. 1958, Australian J. Phys., 11, 360.

Minn, Y. K., and Greenburg, J. M. 1973, Astr. Ap., 24, 393.

Moffat, A. F. J., Fitzgerald, M. P., and Jackson, P. D. 1979, Astron. Ap. Suppl., 38, 197.

Moffat, A. F. J., and Vogt, N. 1975, Astr. Ap. Suppl., 20, 85.

Morris, M. 1984, private communiction.

Morris, M., and Knapp, G. R. 1976, Ap. J., 204, 415.

Morris, M., Montani, J., and Thaddeus, P. 1980, in IAU Symposium 87, Interstellar Molecules, ed. B. H. Andrew (Dordecht: D. Reidel), p. 197.

Murdin, P., and Penston, M. V. 1977, M.N.R.A.S., 181, 657.

Murphy, D. 1984, private communication.

Myers P. C., Dame, T. M., Thaddeus, P., Cohen, R. S., Silverberg, R. F., Dwek, E., Hauser, M. G. 1985, Ap. J., submitted.

Neugebauer, G., and Leighton, R. B. 1969, Two Micron Sky Survey: A Preliminary Catalog, (Pasadena: California Institute of Technology).

O'Dell C. R., York, D. G., and Henize, K. G. 1967, A. J., 72, 820.

Pan, S.-K. 1984, Ph. D. thesis, Columbia University.

Pan, S.-K., Feldman, M. J., Kerr, A. R., and Timbie, P. 1983, Appl. Phys. Letters, 43, 786.

Panagia, N. 1973, A. J., 78, 929.

Price, S. D., and Walker, R. G. 1976, The AFGL Four Color Infrared Sky Survey: Catalog of Obsevations at 4.2, 11.0, 19.8, and 27.4 μm (AFGL-TR-76-0208).

Racine, R. 1968, A. J. 73, 233.

Reich, W. 1978, Astr. Ap., 64, 407.

Reynolds, R. J., and Ogden, P. M. 1979, Ap. J., 229, 942.

Sanders, D. B., Solomon, P. M., and Scoville, N. Z. 1984, Ap. J., 276, 182.

Sharpless, S. 1959, Ap. J. Suppl., 4, 257.

Shimmins, A. J., Clarke, M. E., and Ekers, R. D. 1966, Australian
    J. Phys., 19, 649.

Shimmins, A. J., Day, G. A., Ekers, R. D., and Cole, D. J. 1966,
    Australian J. Phys., 19, 837.

Smith, E. van P. 1956, Ap. J., 124, 43.

Solomon, P. M. 1985, private communication.

Spitzer, L. Jr. 1978, Physical Processes in the Interstellar Medium,
    (New York: John Wiley and Sons).

Stothers, R. 1985, private communication.

Sulentic, J. W., and Tifft, W. G. 1973, The Revised New General
    Catalogue of Nonstellar Astronomical Objects (Tuscon: University
    of Arizonia Press).

Tenorio-Tagle, G. 1979, Astr. Ap., 71, 59.

Thaddeus, P. 1982 in Symposium on the Orion Nebula to Honor Henry
    Draper, ed. A. E. Glassgold, P. J. Huggins, and E. L. Schucking
    (Ann. NY Acad. Sci., No. 395), p. 9.

Thronson, H. A. Jr., Gatley, I., Harvey, P. M., Sellgren, K., and
    Werner, M. W. 1980, Ap. J., 237, 66.

Tucker, K. D., Kutner, M. L., and Thaddeus, P. 1973, Ap. J. (Letters),
    186, L13.

Turner, D. G. 1976, Ap. J., 210, 65.

van den Bergh, S. 1966, A. J., 71, 990.

Verschuur, G. L. 1973, Astr. Ap., 27, 73.

Vrba, F. J. 1977, A. J., 82, 198.

Vrba, F. J., Strom, S. E., and Strom, K. M., 1976, A. J., 81, 958.

Wade, C. M. 1957, A. J., 62, 148.

_____, 1958, Rev. Modern Phys., 30, 946.

Walker, R. G., and Price, S. D. 1975, AFCRL Infrared Sky Survey:
Volume 1. Catalog of Observations at 4, 11, and 20 Microns
(AFCRL-TR-75-0373).

Weaver, H., and Williams, D. R. W. 1973, Astr. Ap. Suppl., 8, 1.

Wilson, R. E. 1953, General Catalogue of Stellar Radial Velocities
(Washington, D. C.: Carnegie Institution of Washington).

Willson, R. F., and Folch-Pi, F. J. 1981, A. J., 86, 1084.

Wootten, T. A., Snell, R., and Glassgold, A. E. 1979, Ap. J., 234,
876.

FIGURE CAPTIONS

Figure III.1. Comparison of total integrated intensity (W_{CO}) obtained after a third-order baseline fit (x-axis) and a first-order fit (y-axis) for a random sample of 65 position observed by frequency switching. The solid line has a slope of one and the dashed line is the line of best-fit through the data (slope = 1.07) through the origin.

Figure III.2. The top row shows two typical frequency-switched spectra taken with the SIS receiver and the next row shows the same spectra after third-order baseline removal and folding. The bottom row shows two typical position-switched spectra after a constant term was taken out of each channel. The y-axis in all cases is in units of antenna temperature and the x-axis is in units of channel number, except the middle row, which is in units of v_{LSR}.

Figure III.3. The 12,520 positions observed for CO. Small circles indicate the positions of full resolution (8.'7) observations and large circles indicate the positions of 1/4° and 1/2° resolution observations. The equivalent beam shape for low resolution observations (1/4° and 1/2°) is roughly square, not circular as shown (see Ch. III,A).

Figure III.4. The distribution of the larger molecular clouds found by the Columbia millimeter-wave telescope in the third galactic quadrant

(Blitz 1978; Baran 1983; Huang 1984; and this work). All molecular clouds larger than 0.5 deg^2 in area and with $W_{CO} > 2.5$ K km s^{-1} and located within the region outlined by the dashed line have probably been found. The region surveyed for this work is outlined by the thick solid line. The areas labeled 1, 2, and 3 correspond to the subsurveys discussed in Ch. III,B.

Figure III.5. The 310 positions observed for ^{13}CO emission. As in Fig. III.3, the small circles indicate the positions of full resolution observations and the large circles indicate the positions of 1/2° resolution observations.

Figure IV.1. Contour map of integrated intensity of CO emission (W_{CO}) in the velocity range of -10 to 20 km s^{-1}. (Along the galactic plane, CO emission was found at higher velocities, presumably from unrelated clouds, shown in Figs. IV.17-IV.24, more distant than the Orion clouds.) The lowest contour level is at 1.28 K km s^{-1} with subsequent levels at 3, 5, 7, ... times this value. The peaks of emission from the Orion Nebula and from NGC 2023 and 2024 (see Fig. IV.2) are designated by crosses. Two clouds, shown here in insets (see Ch. IV,A and also Figs. IV.2-IV.5), that overlap other clouds in the survey lie at the positions indicated by arrows.

Figure IV.2. Schematic diagram of the molecular clouds using the lowest contour from Fig. IV.1. Dots with numbers corresponding to those in Table IV.1 indicate locations of CO emission peaks. Some NGC

numbers indicate optically prominent objects coincident with CO peaks. The extent of UV emission from Barnard's Loop is indicated by the shaded arc (from O'Dell, York, and Henize 1967; Isobe 1973). The dashed line roughly indicates the extent of the λ Ori ring of clouds (Ch. IV,A,6).

Figure IV.3. False-color map of temperature-weighted mean velocity for the clouds in Fig. IV.1 and for some molecular clouds in the Taurus complex of dark nebulae previously observed by Baran (1983) and not discussed here.

Figure IV.4. False-color diagram of line width (defined in Ch. IV.A) for the clouds in Fig. IV.3.

Figure IV.5. Contour map of CO emission (W_{CO}) for the Orion A cloud. Contour levels are more widely spaced here (the lowest is at 1.28 K km s^{-1}, with subsequent levels at 5, 9, 11, ... times this value) than in Fig. IV.1 to emphasize the high intensity, central region of the cloud.

Figure IV.6. Orion B; contours of W_{CO}, as in Fig. IV.5.

Figure IV.7. Position-velocity diagrams for the region between NGC 2023 and 2024 and NGC 2064-71. Each diagram has contour values of 1., 3., 5., ... K and consists of slices through the Orion B cloud along lines of constant declination from δ = -2.°5 to 0.°0 and spaced by 0.°25.

Figure IV.8. Position-velocity diagram through the Orion A cloud parallel to the galactic plane at a latitude of -19.°4; initial contour level and increment are 1.5 K.

Figure IV.9. Series of channel maps of the Orion A and B clouds; velocity range for each map indicated in lower right corner. Initial contour level is 1.5 K km s^{-1}, with subsequent levels at 3, 5, 7,... times this value.

Figure IV.10. Monoceros R2; contours of W_{CO}, as in Fig. IV.5.

Figure IV.11. Dots indicate all stars within the surveyed region (Fig. III.4) for which polarization measurements are available (Hiltner 1951, 1954a, 1954b; Smith 1956; Hall 1958; Appenzeller 1966, 1968, 1974; Mathewson and Ford 1970; Axon and Ellis 1976); lengths of the vectors are proportional to the measured polarization (1° equals 2% polarization).

Figure 1V.12. Same as in Fig. IV.11 but for stars with known distances in excess of 400 pc.

Figure IV.13. Same as in Fig. IV.12 but for stars with known distances in excess of 800 pc.

Figure IV.14. (a) The locations of the high resolution strips observed

at NRAO (thick dashed lines), Bell Telephone Laboratories (thick solid lines), and P.O.M (thin dashed lines) superimposed on the outline of the Northern Filament.

(b) Same as (a) for the Southern Filament.

Figure IV.15. (a) Velocity-position diagram for a strip of positions observed in ^{13}CO with the Bell Telephone Labs telescope across the Northern Filament; the x-axis is labeled in offsets in arcmin of declination from α = 6h 22m 57s, δ = 3° 20' 12" and the strip is oriented as in Fig. IV.14. Initial contour level and increment are 0.1 K in units of antenna temperature.

(b) Same as (a) except offsets are from α = 6h 22m 28s, δ = 3° 25' 49".

(c) Same as (a) except offsets are from α = 6h 21m 53s, δ = 3° 32' 52" and contour levels are at 0.2 K.

(d) Same as (a) except offsets are from α = 6h 21m 39s, δ = 3° 35' 50".

(e) Same as (a) for the Southern Filament except offsets are from α = 6h 35m 50s, δ = -10° 15'.

(f) Same as (e) except offsets are from α = 6h 36m 30s, δ = -10° 15'.

(g) Same as (e) except offsets are from α = 6h 36m 50s, δ = -10° 15'.

(h) Same as (e) except offsets are from α = 6h 36m 30s, δ = -10° 15'.

Figure IV.16. Contour diagram of W_{CO} for the Orion East cloud with initial contour level and increment of 1.3 K km s^{-1}; the positions of T Tauri stars and reflection nebulae are indicated. The positions observed with high velocity resolution (Ch. V,C) are numbered as in Table V.2.

Figure IV.17. W_{CO} for clouds found along the galactic plane within the velocity range of -10 to 60 km s^{-1}; initial contour level and increment are 1.5 K km s^{-1}. All channels with $T_R < 0.6$ K were set to zero to increase the contrast between emission from clouds and noise. The area within the dashed line was surveyed fully at 1/4° resolution while outside that area full-resolution (8.'7) observations were made at the positions indicated by dots. The letters next to the clouds correspond to those in Table IV.3; clouds A and T are illustrated in Figs. IV.1-IV.4.

Figure IV.18. Same as Fig. IV.17, only for a velocity range (-10 to 17 km s^{-1}) that should include most clouds with distances less than 1.7 kpc.

Figure IV.19. Same as Fig. IV.17, only for a velocity range (17 to 35 km s^{-1}) that should include most clouds with distances between 1.7-4. kpc.

Figure IV.20. Same as Fig. IV.17 only for a velocity range (35 to 60 km s^{-1}) that should include most clouds with distances between 4.-8. kpc.

Figure IV.21. Longitude-velocity diagram for galactic plane clouds integrated from $\underline{b}$ = -1° to $\underline{b}$ = 4°, the letters corresponding to those in the figures above and in Table IV.3. All channels with T_R < 0.6 K were set to zero and the initial contour level and increment are 0.25 K deg.

Figure IV.22. (a) A map of cloud Q (Table IV.3) and its vicinity that shows T_R in the velocity range of 15 to 40 km s^{-1}. The lowest contour level and the increment between levels are 1 K. Dots indicate the positions of observations at full angular resolution (8.'7). North of the dotted line the resolution of the telescope was reduced to 1/4°.

Figure IV.23. (a) Sum of all spectra for cloud Q (Table IV.3) with -5° < $\underline{b}$ < -1°. Includes interpolated spectra for unobserved positions within the surveyed region (see Fig. APPENDIX.2).

(b) The spectrum observed toward $\underline{1}$ = 216.375°, $\underline{b}$ = -2.75°, typical of those found toward the cloud.

Figure IV.24. Velocity-longitude diagram for cloud Q (Table IV.3) constructed by integrating over the galactic latitude extent of the cloud (-5 < $\underline{b}$ < -1°). The contour level and increment are 0.24 K deg.

Figure V.1. The three high velocity resolution observations of CO toward Orion East. In the first three panels *'s indicate observed spectral values and the curves represent Gaussians fitted to the

deconvolved spectra.; the deconvolved spectra are superimposed in the fourth panel. Numbers accompanying the spectra refer to those in Fig. IV.16 and Table V.2.

Figure V.2. Same as Fig. V.1 but for ^{13}CO observations.

Figure V.3. The variation of T_R in strips across the Orion A cloud separated in declination by 0.°5; the scale was chosen so one degree in declination equals 31 K.

Figure V.4. The variation of W_{CO} in strips across the Orion A cloud separated in declination by 0.°5; the scale was chosen so one degree in declination equals 62 K km s^{-1}.

Figure V.5. Same as Fig. V.4 but for the Orion B cloud.

Figure V.6. Same as Fig. V.4 but for the Orion B cloud.

Figure V.7. The large-scale model of the Orion region proposed by Cowie et al. (1978). The *'s indicate the general locations of the subassociations within the Orion OB association and the thick lines represent molecular clouds. An expanding high-pressure and high-temperature H II region, probably created by cumulative effects of supernovae ($\sim$ 10) which occurred in the association, is enclosed by an

ionization shock, its eastern border being seen in Hα as Barnard's Loop; the western side of the shock, owing to inhomogeneities in the interstellar medium, is not well defined. Molecular clouds, probably located just within the back side of the shock, first felt effects of the high pressure region on the western faces. The latest supernova probably produced a second, possibly radiative shock lying outside the first.

Figure V.8. Paramaters of the ring fitted to the λ Ori cloud system. Initial guesses were made for the center (α_0, δ_0, and V_0), radius (R_X), and expansion velocity (V_X) of the ring. A circle of radius R_X was centered at α_0, δ_0, $D = 0$ where D is distance relative to the center of the ring. The circle was then tilted at an angle ϕ along an axis with a position angle of θ. Each cloud in the ring would have coordinates α_i, δ_i, and D_i [$= (V_i - V_0) R_X / V_X$, where V_i is the radial velocity of each cloud]. Paramaters α_0, δ_0, V_0, R_X, V_X, ϕ, and θ were then modfified to minimize the sum of the square of distances between the circle and the clouds.

Figure V.9. Contour diagram of W_{CO} (same levels as in Fig. IV.1); dots indicate the positions used to fit the ring shown. Cross and open circle indicate the position of the center of the ring and the location of λ Ori, respectively; the observed proper motion of the star implies that when the star formed 2 Myrs ago it was located at the position marked by a *.

Figure V.10. (a) Position-velocity diagram (right ascension versus velocity) integrated over the range in declination of the λ Ori system of clouds. (Instead of adding actual spectra, Gaussian profiles were fitted to the data, and then added.) Dots indicate positions used to fit the ring shown. The + and circle respectively indicate the position of the center of the ring and the right ascension and radial velocity of λ Ori.

(b) Same as (a), except declination versus velocity is plotted and the integration was over the range in right ascension for the system of clouds.

Figure V.11 The *'s indicate angular coordinates (ξ and ψ), relative to the best-fitted center of the ring, of points used to fit the ring (i.e., the dots in Figs. V.9-V.10); The angle ψ is the position angle of the points (= $\tan^{-1} [(\delta_i - \delta_0)/(\alpha_i - \alpha_0)]$) and ξ the angle between the plane of the sky and those points (= $\tan^{-1} [R_x (V_i-V_0) / V_x([\alpha_i - \alpha_0]^2 + [\delta_i - \delta_0]^2)^{1/2}]$). The sine curve depicts the best-fitted ring.

Figure V.12. Radio continuum observations at 1.4 GHz toward the λ Ori system of clouds; displayed in galactic coordinates and not in the original equatorial coordinates, the figure, copied from Reich (1978), has a noticeable distortion. Contour values are as labeled; the figure is not to the same scale as Fig. V.12.

Figure V.13. Same as Figure V.9, but in galactic coordinates and to the same scale as Figs. V.14-V.15.

Figure V.14. H I emission integrated between -5 and 16 km s^{-1} toward the λ Ori system of clouds (Heiles and Habing 1974). Contour levels are 100 K km s^{-1} apart; the figure is on the same scale as Fig. V.12.

Figure V.15. IRAS 100μm observations toward the λ Ori system of clouds (Boulanger 1985; the same scale as in Fig. V.12. Contour levels are at 26, 33, 40, 50, 60, 73.5 and 91.7 MJy and every other level is dashed. Moonlight contaminated the data in the blank region that runs diagonally across the plot.

Figure V.16. The evolution of the λ Orionis system as seen from Earth (column 1) and from a position at right angles to the line of sight (column 2). The star and the border of the H II region it produced are shown by the * and the thick dashed line, respectively; molecular clouds are outlined by the solid lines.

After the H II region breaks through the cloud (b), remnants of the molecular clouds are accelerated and atomic gas begins to be swept up, as shown, by the expanding edge of the H II region (c and d). Low mass stars, shown as dots, may have been created in areas of clouds compressed by expansion of the H II region (c) and left behind when the clouds were further accelerated by the H II region (d).

Figure V.17. (a) The Orion and Monoceros complexes as they would appear at six times their actual distances (or 3 kpc) and as if observed with the full resolution of the Columbia telescope with the same noise level as in the outer galaxy survey. This figure can be compared with Figs. IV.17-IV.20 where the contour levels (1.5 K km s^{-1} in steps of 1.5 K km s^{-1}) and scale are the same.

(b) The same as (a) but as if were observed with a 1/4° superbeam.

(c) The same as (a) but as if the complexes were at ten times their actual distances (or 5 kpc) and observed with a 1/4° superbeam.

Figure APPENDIX.1. Comparison between line width determined for a 9 deg^2 section of the Orion A cloud using, the method described in Appendix A,1 (thin line) and that determined by adding actual spectra (thick line).

Figure APPENDIX.2. Same as Figure APPENDIX.1 but for the entire area of Cloud Q (Table IV.3). The spectrum represented by the thick line is the one already shown in Fig. 23a and used in the the calculation of M_{vir} in Table IV.3.

Figure APPENDIX.3. Comparison between calculated N_{LTE} and observed W_{CO}. Solid line is weighted least-square line of best-fit through the origin while the dashed line is the line predicted from results of Bloemen et al. (1984). Circles represent full resolution and crosses 1/2° resolution observations.

Figure APPENDIX.4. (a) Predicted expansion velocity for the λ Ori shell. A, B, and C represent the conclusion of the first, second, and third stages of the model, and D indicates when the shell radius is equals to the observed 34 pc. The numbers along the drawn line indicate the time elapsed since the birth of the star.

(b) The solid line indicates the remaining molecular mass, M_c, in the system. The decrease in M_c corresponds to the increase in ionized mass interior to the shell. The dashed line is the mass of both atomic and molecular gas, M_s, enveloped by the shell. When the radius is greter than 10 pc, the difference between the two lines illustrates the atomic mass swept up in the expansion.
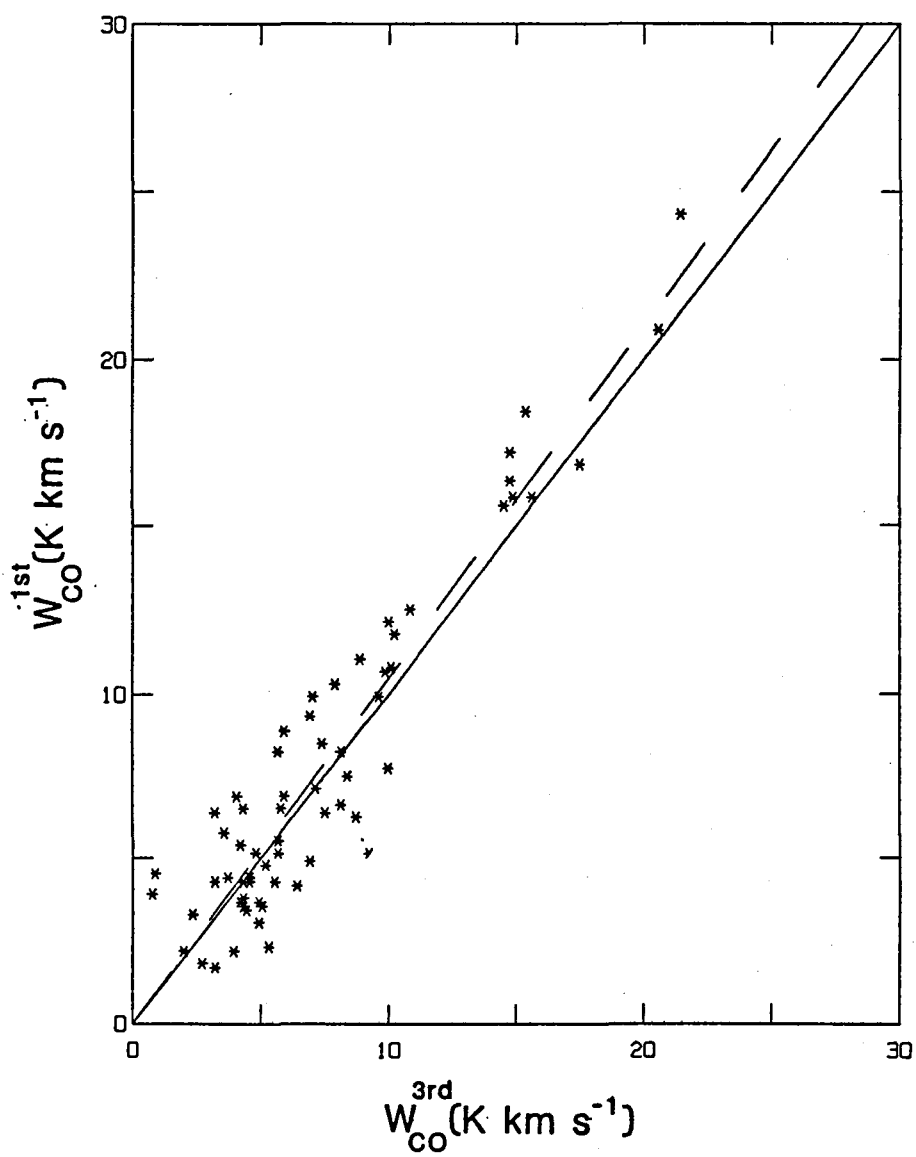
Figure III.1
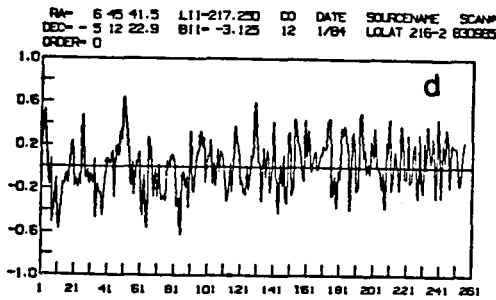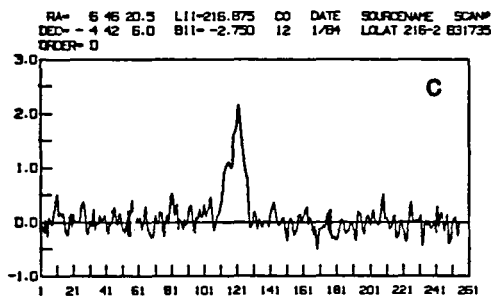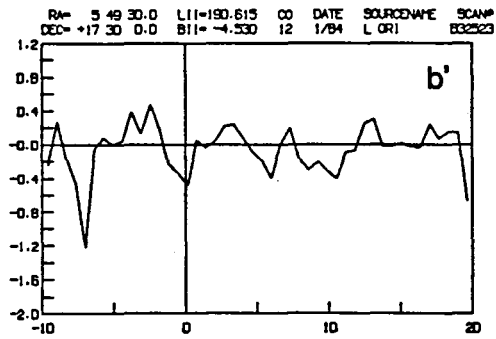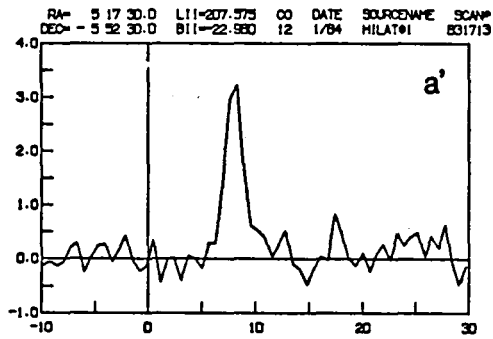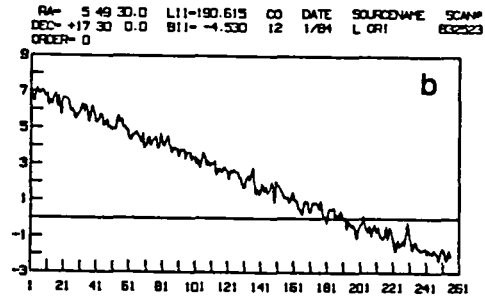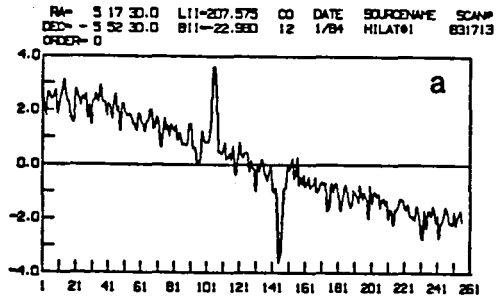
Figure III.2

Figure III.3

Figure III.4

141

Figure III.5

MOLECULAR CLOUDS IN
ORION AND MONOCEROS
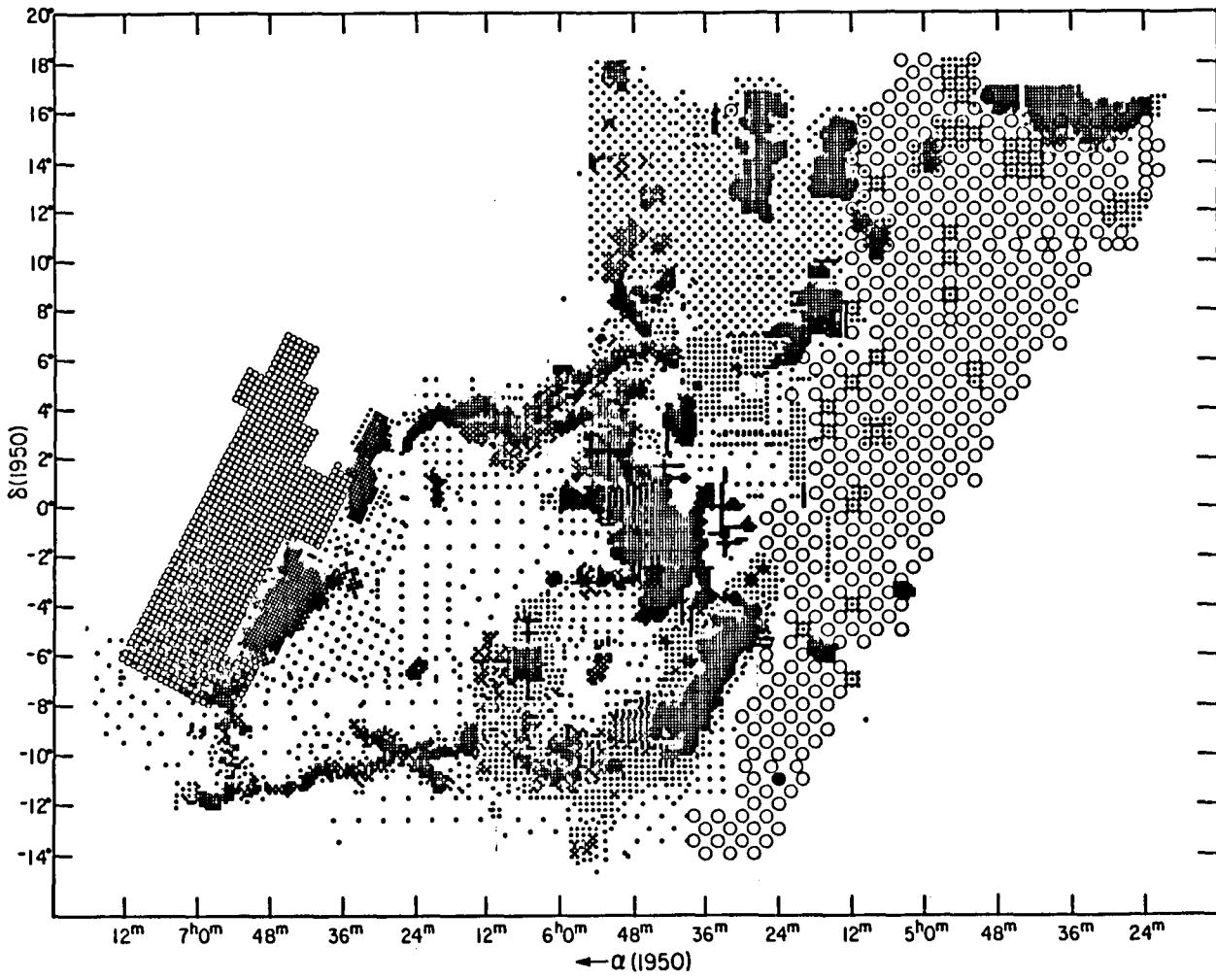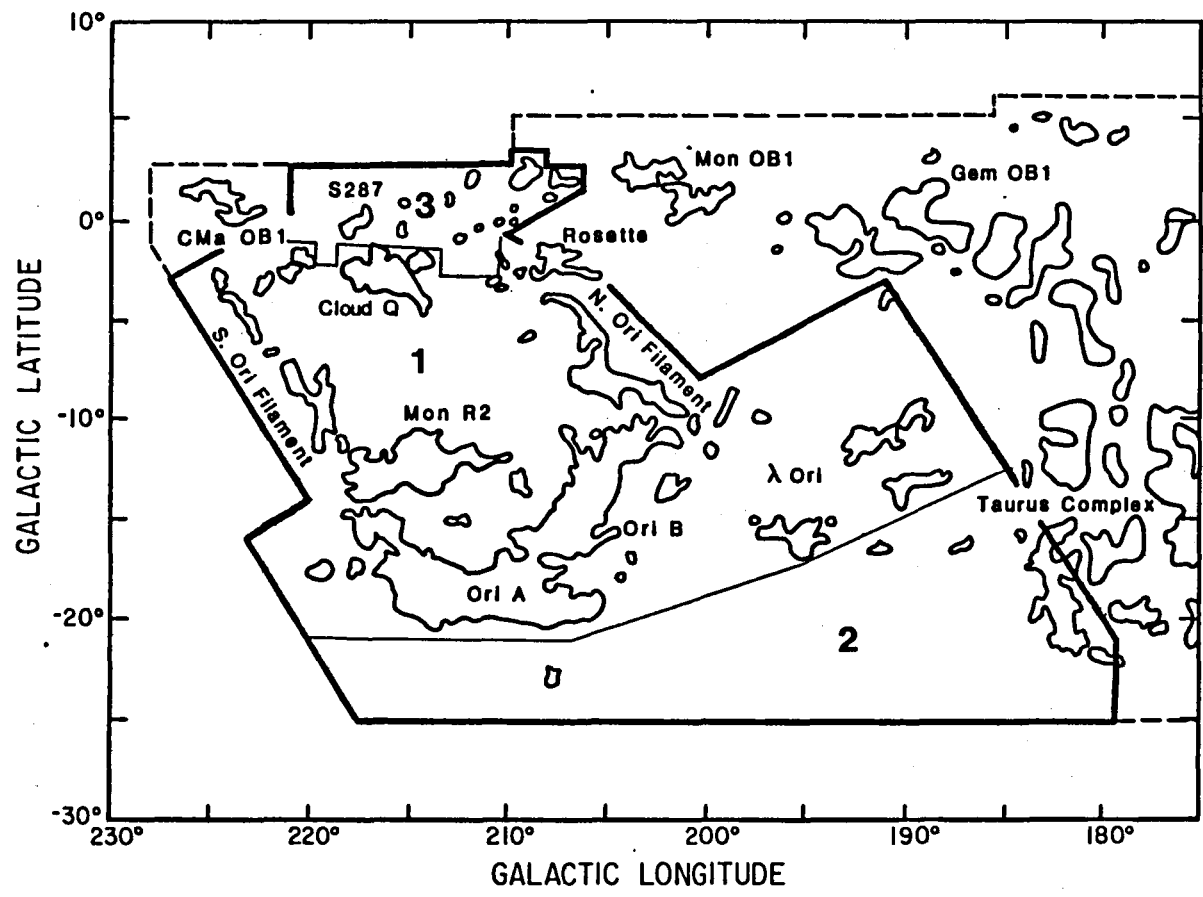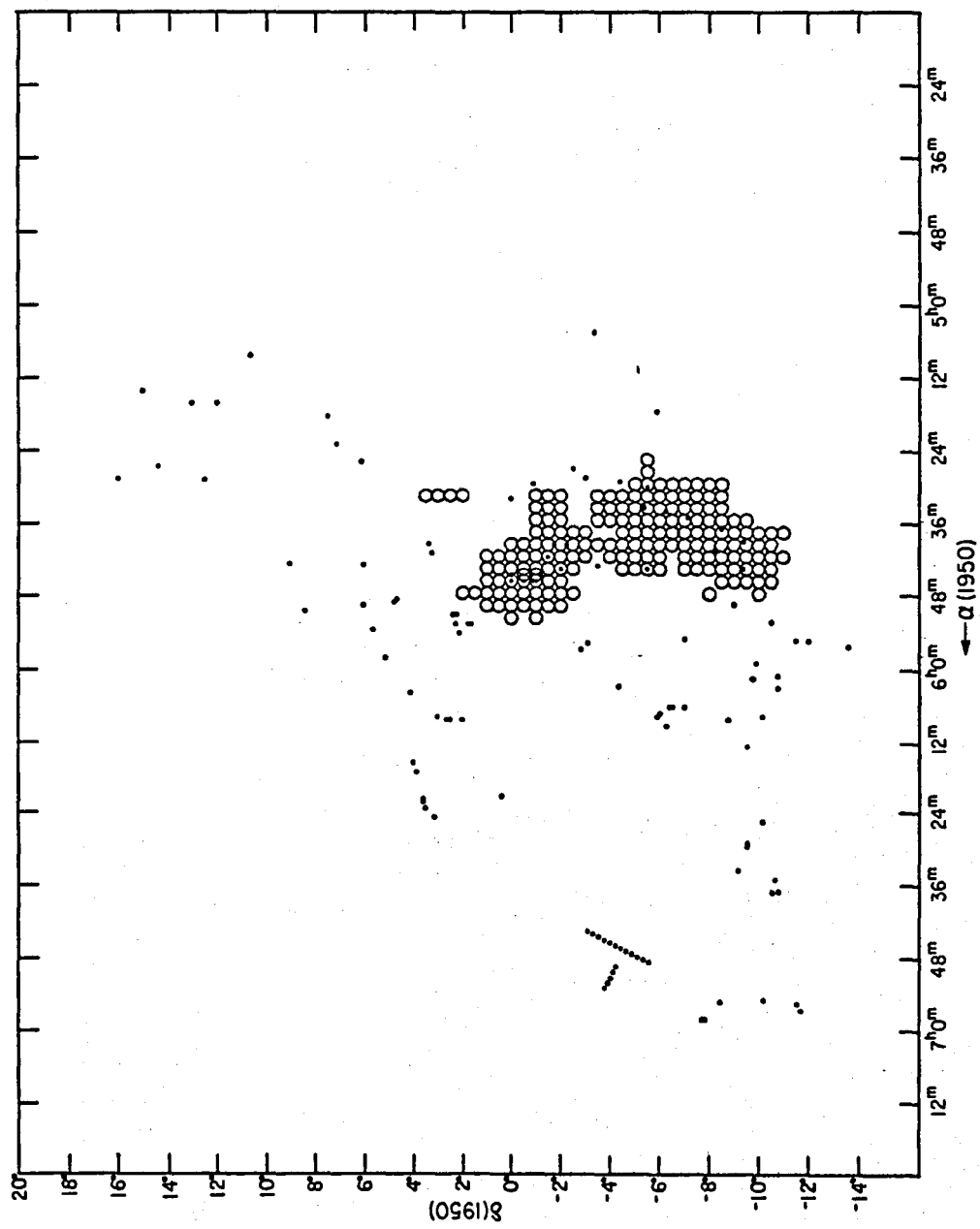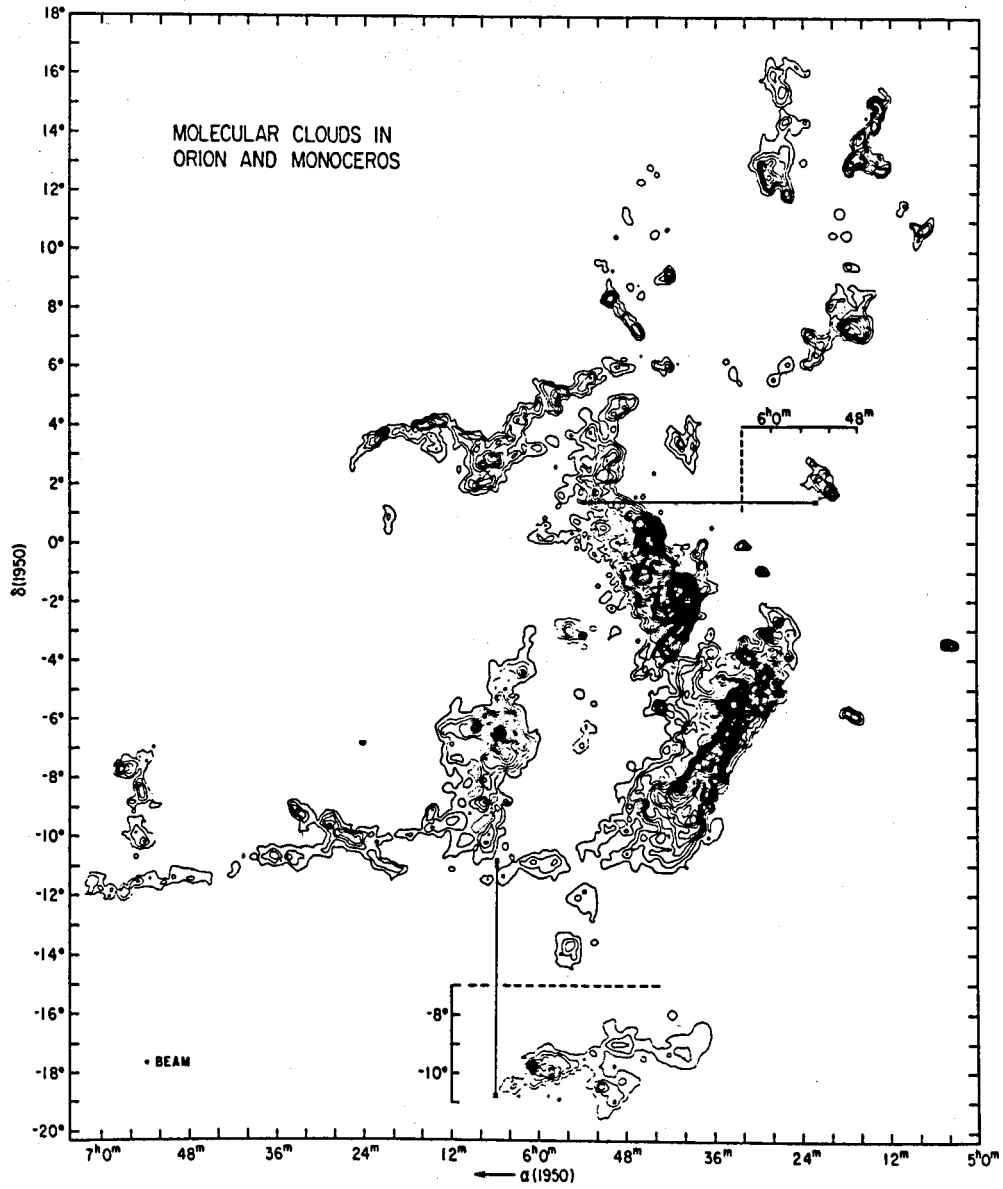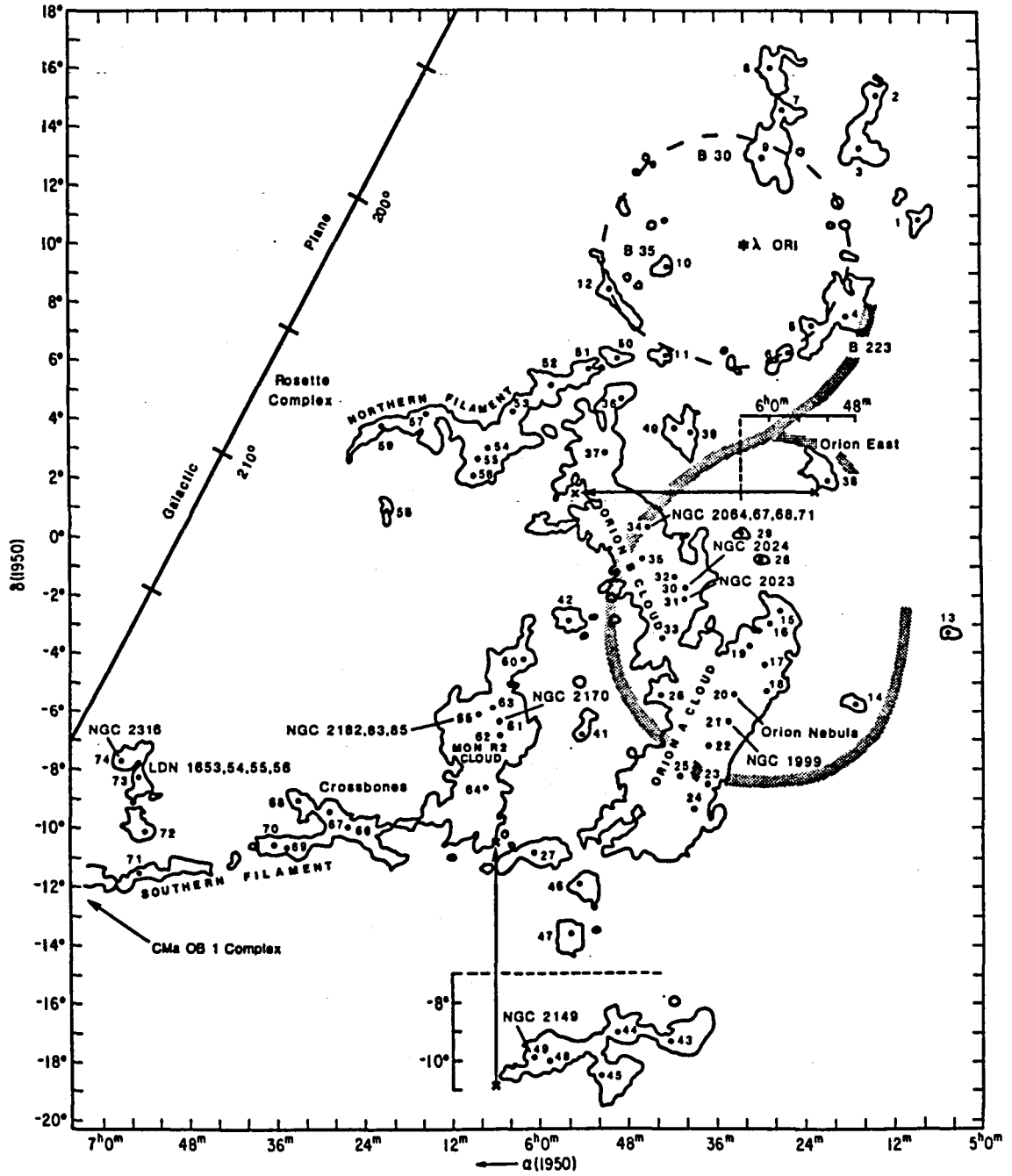
Figure IV.1
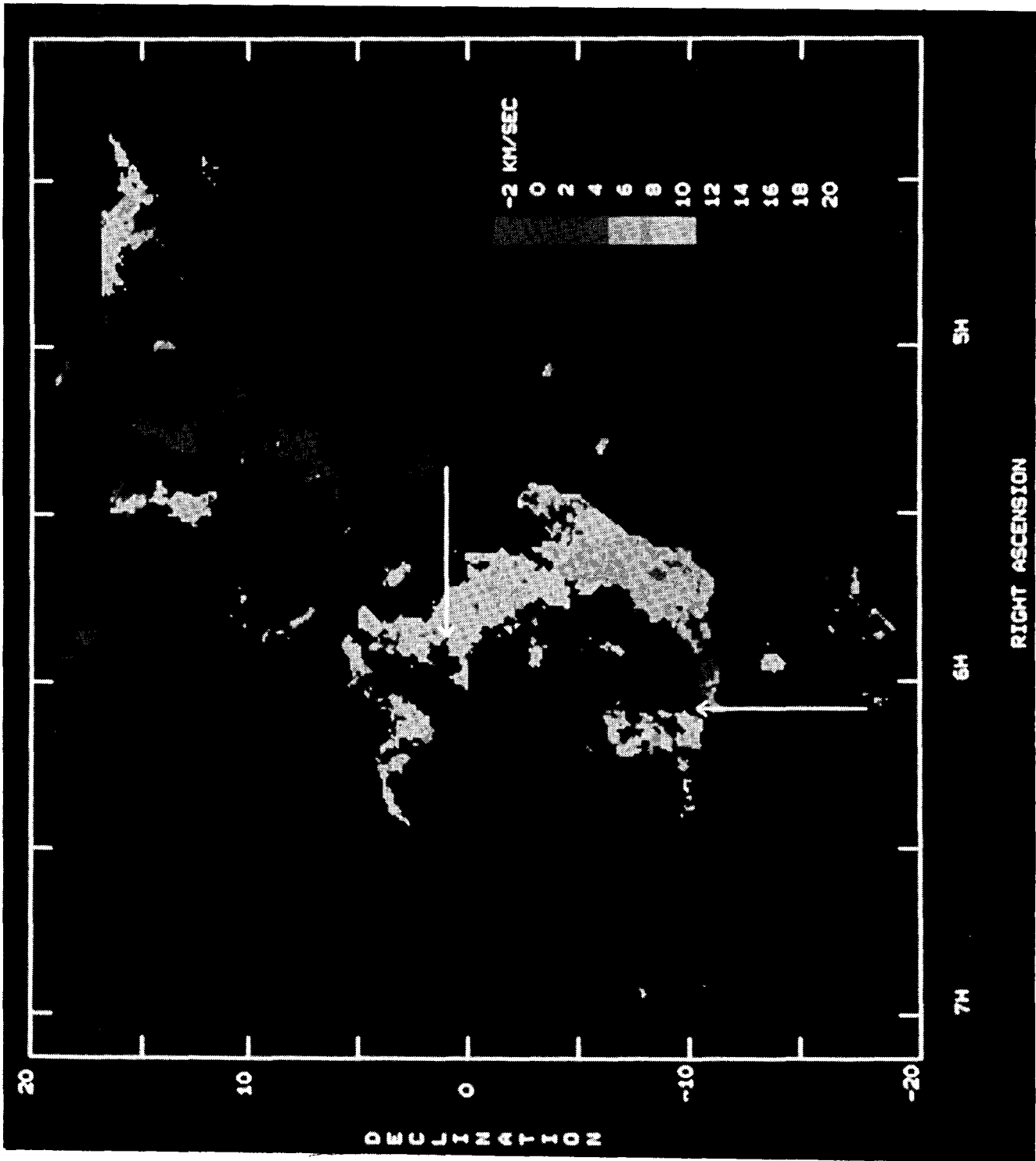
Figure IV.2

Figure IV.3
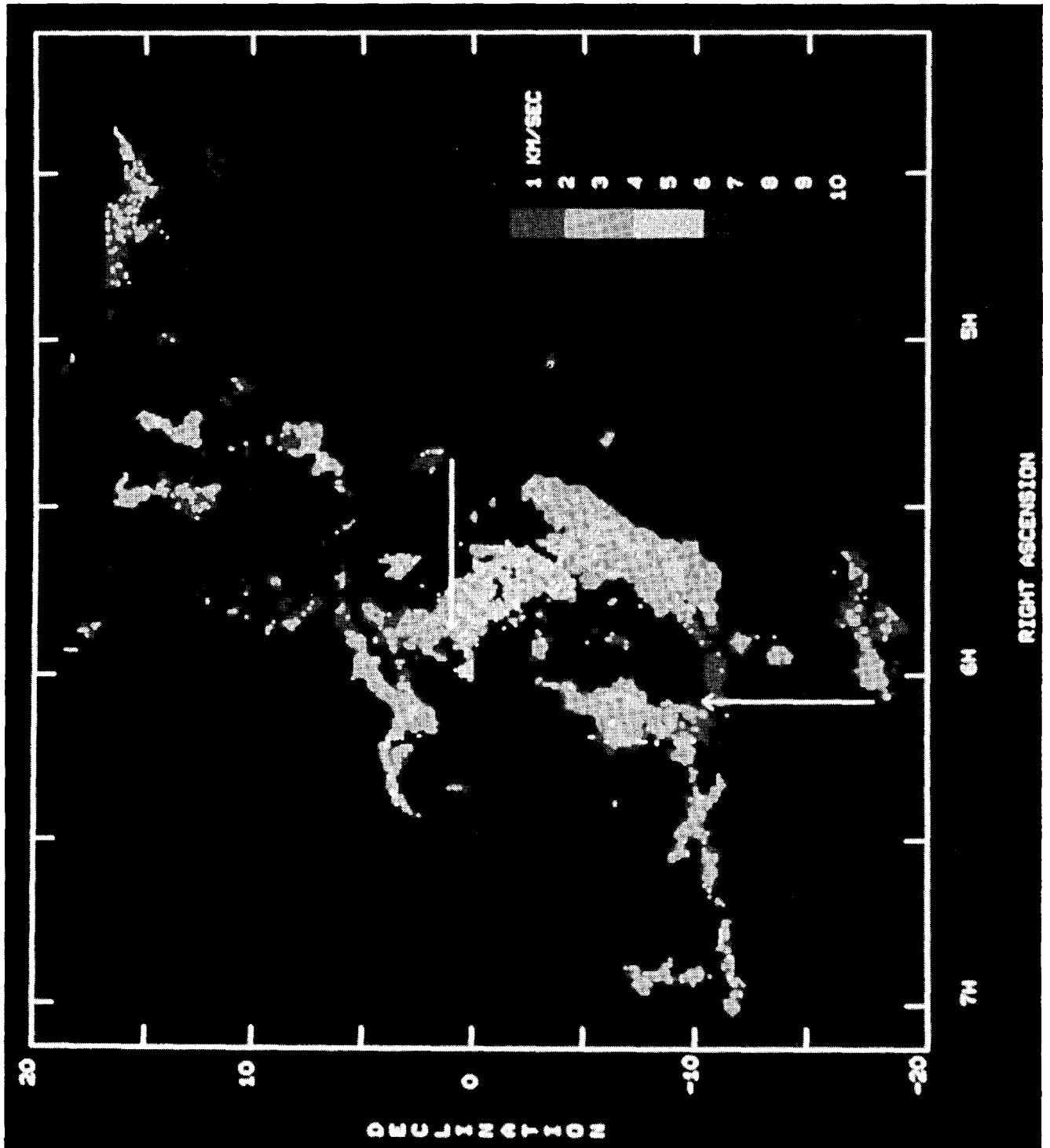
Figure IV.4
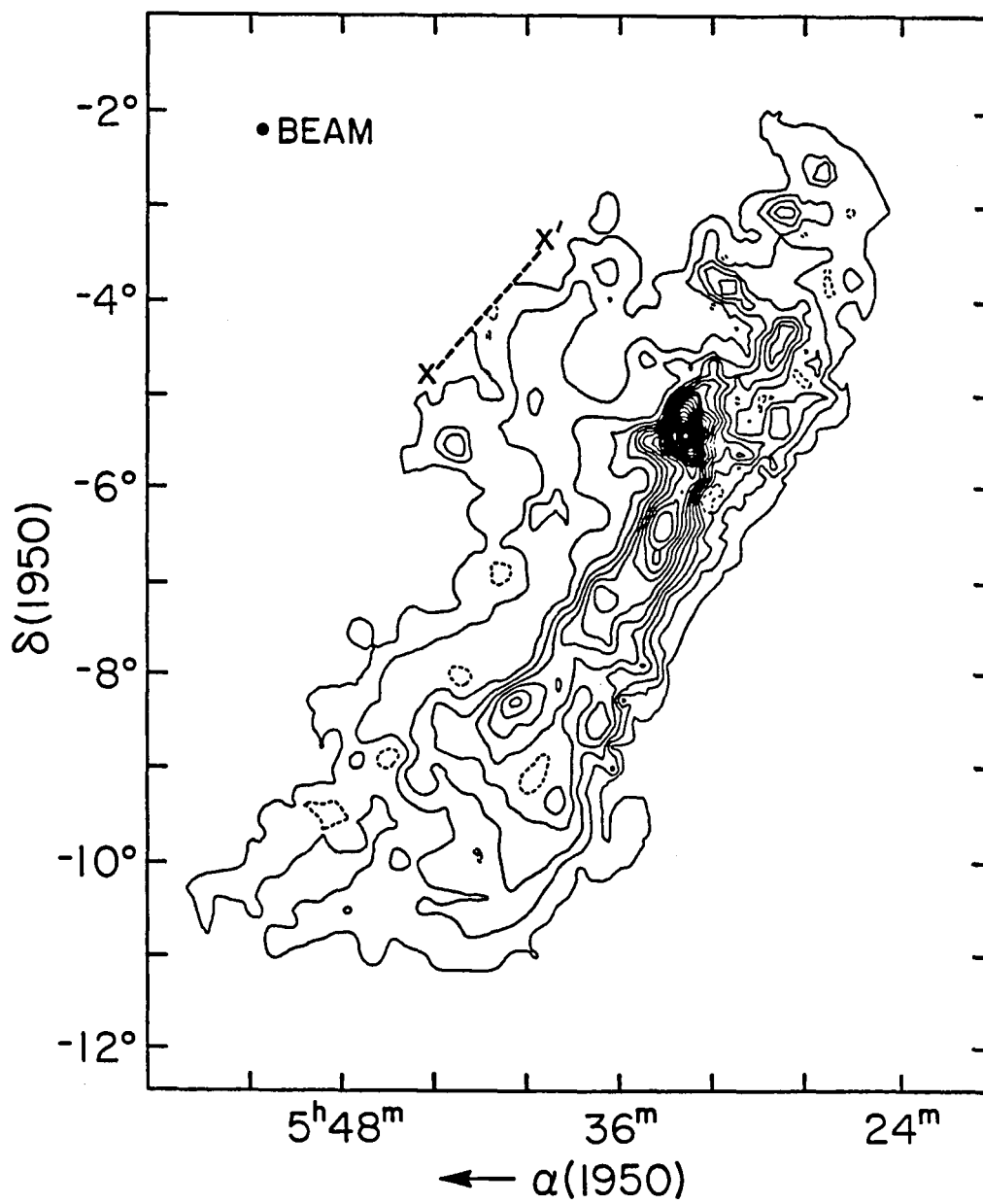
Figure IV.5
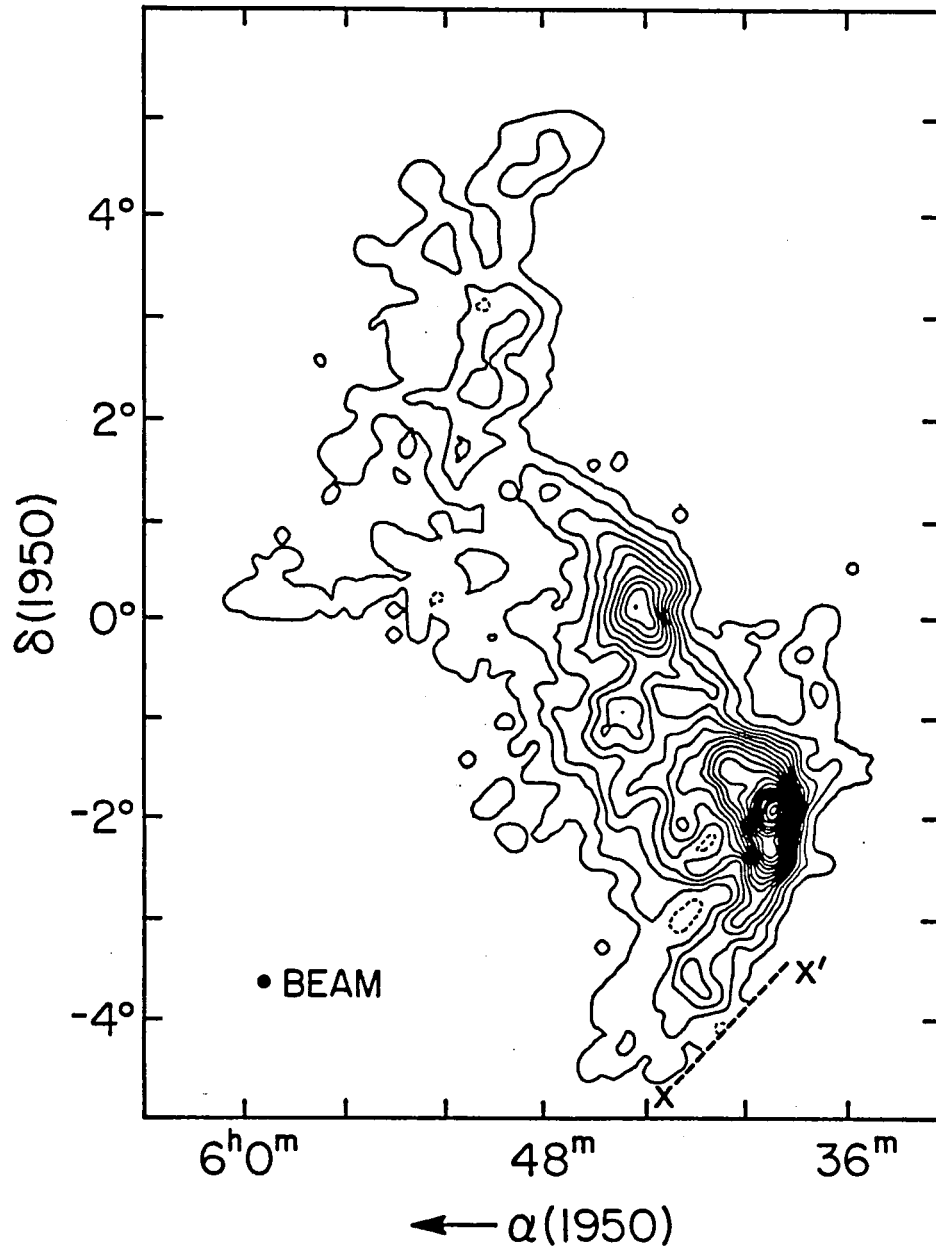
Figure IV.6
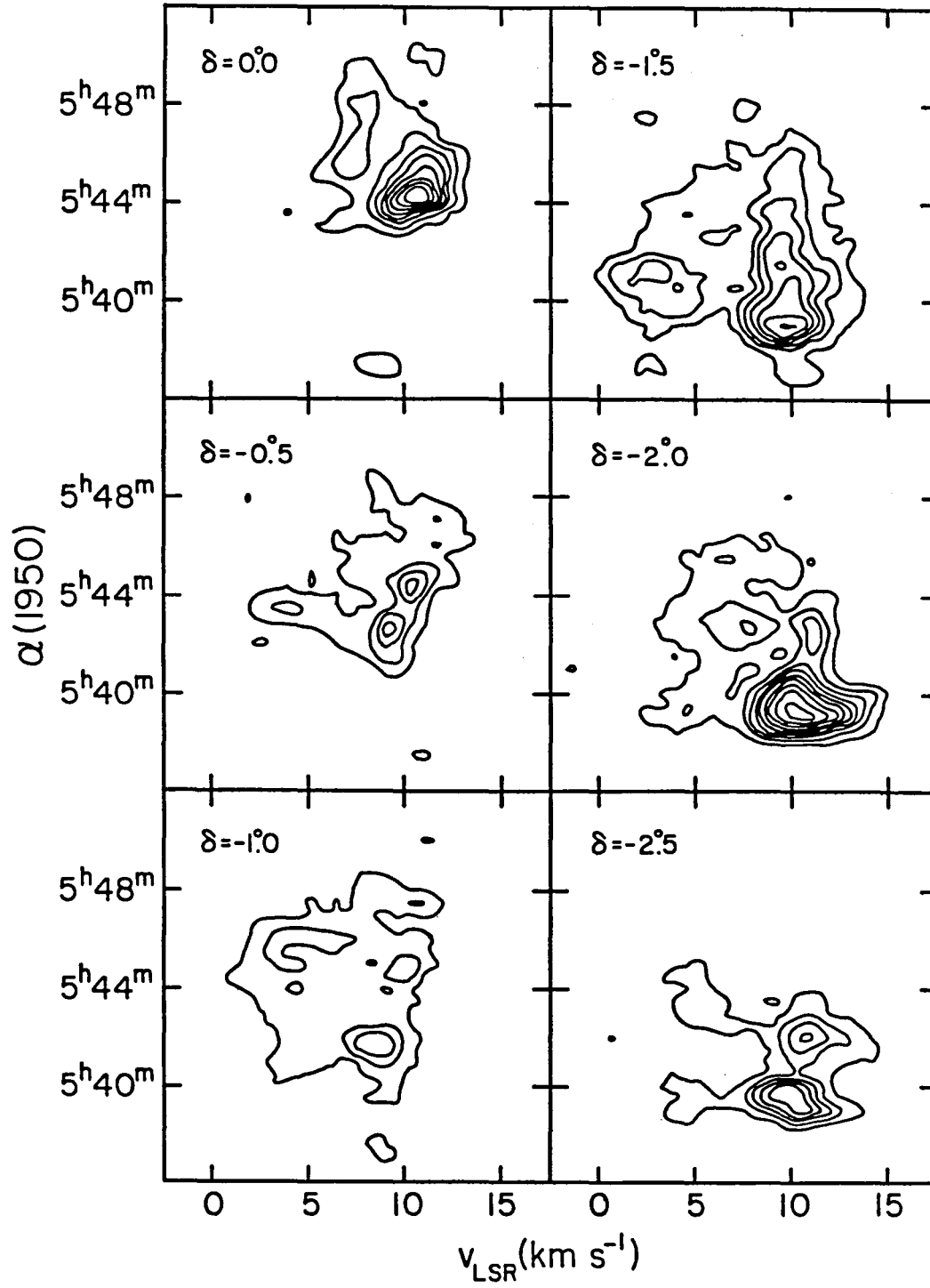
Figure IV.7
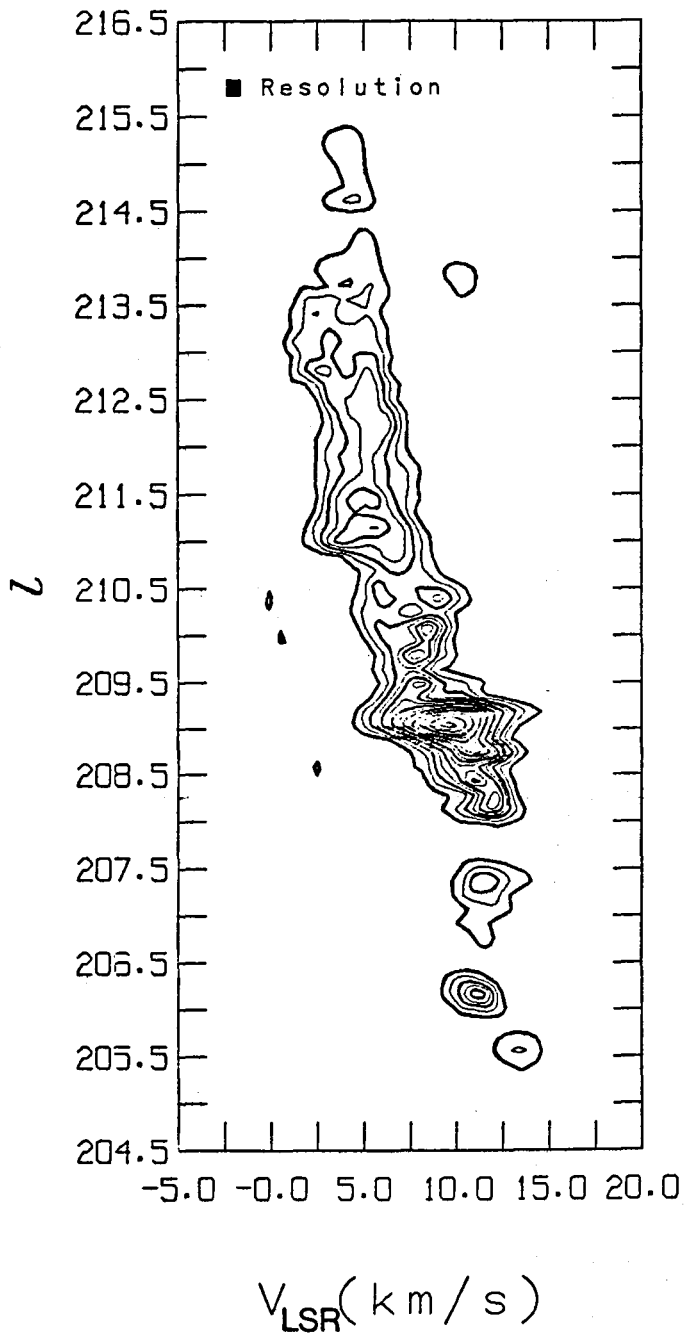
Figure IV.8
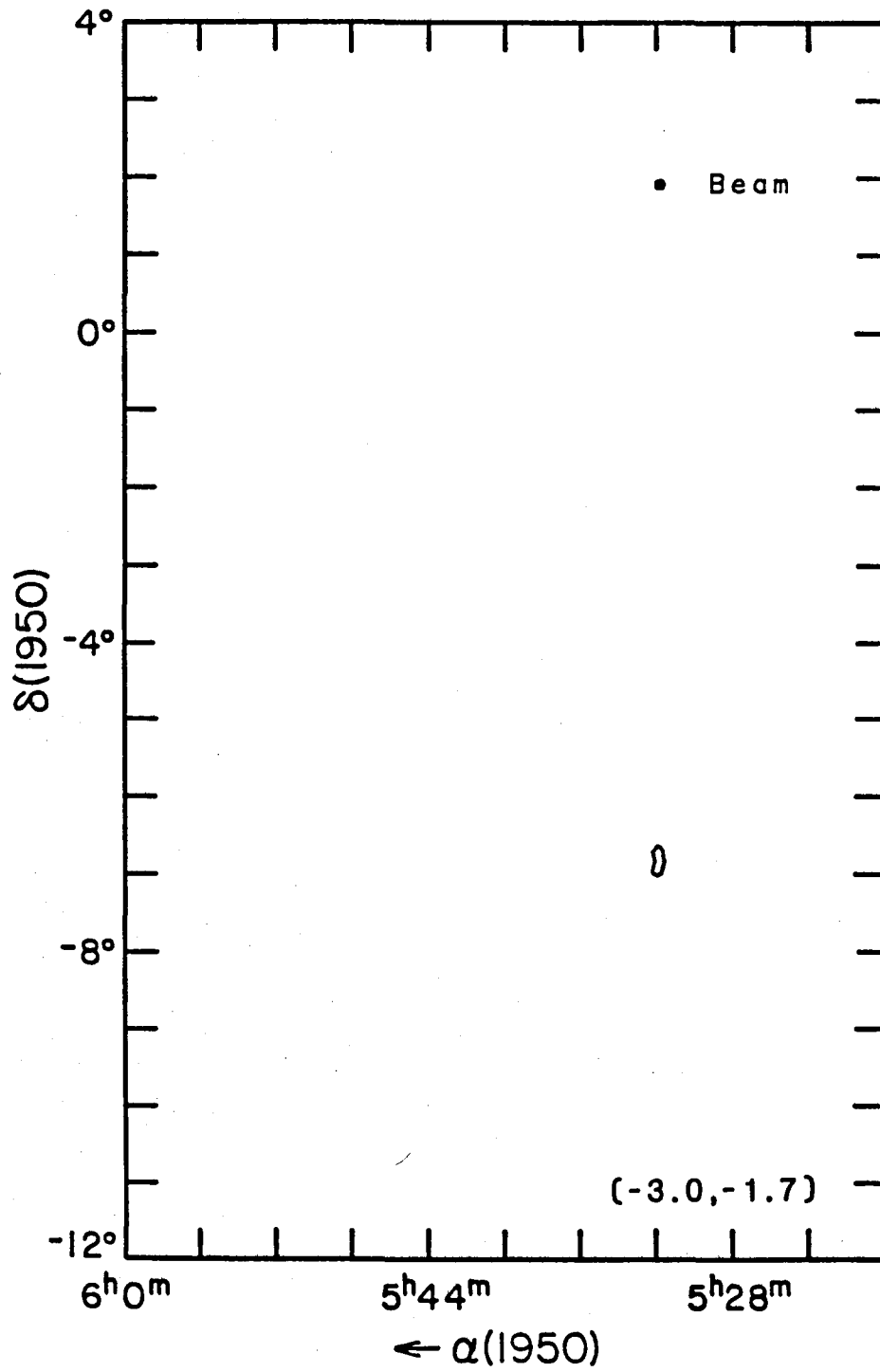
Figure IV.9a
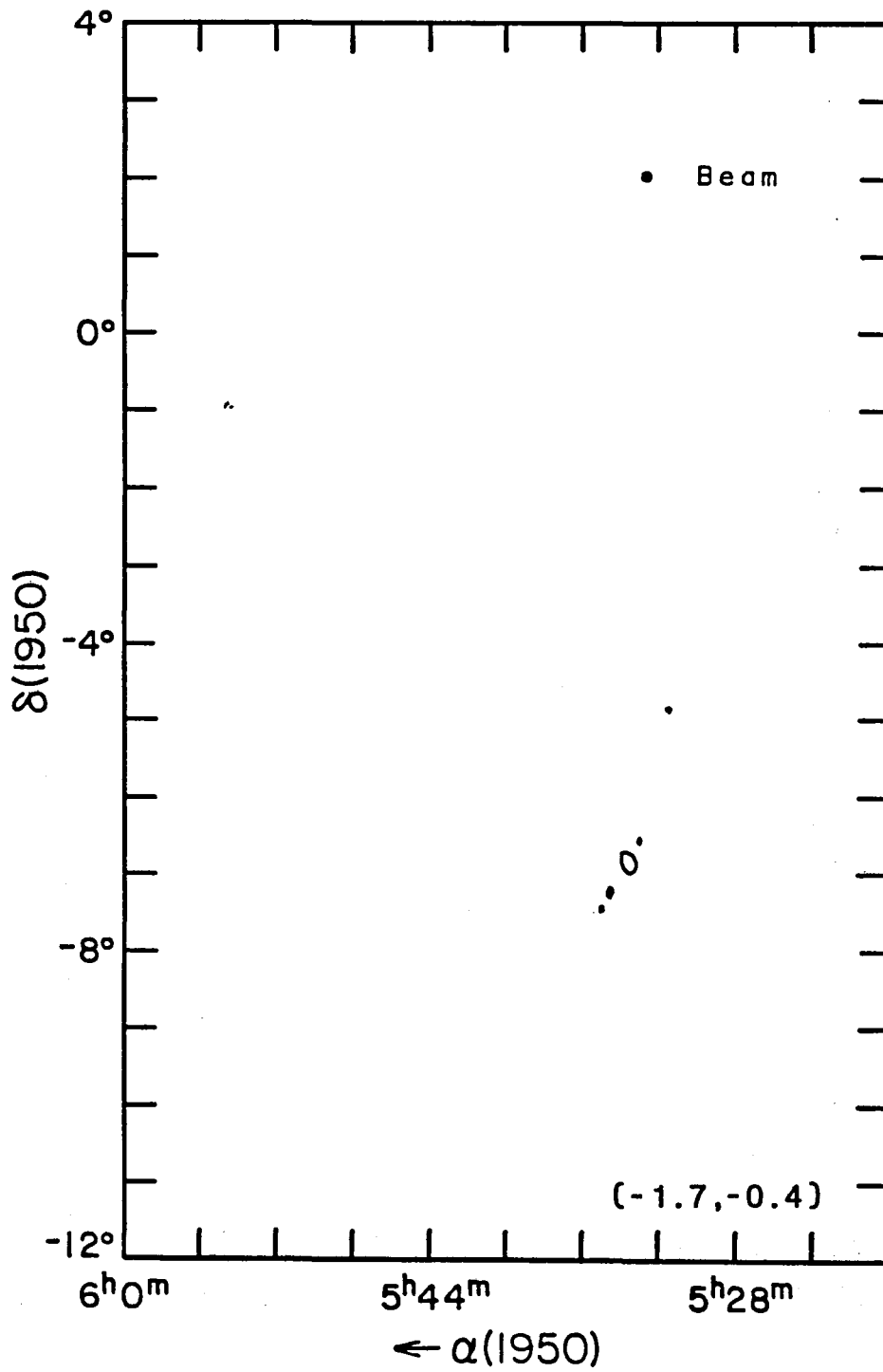
Figure IV.9b
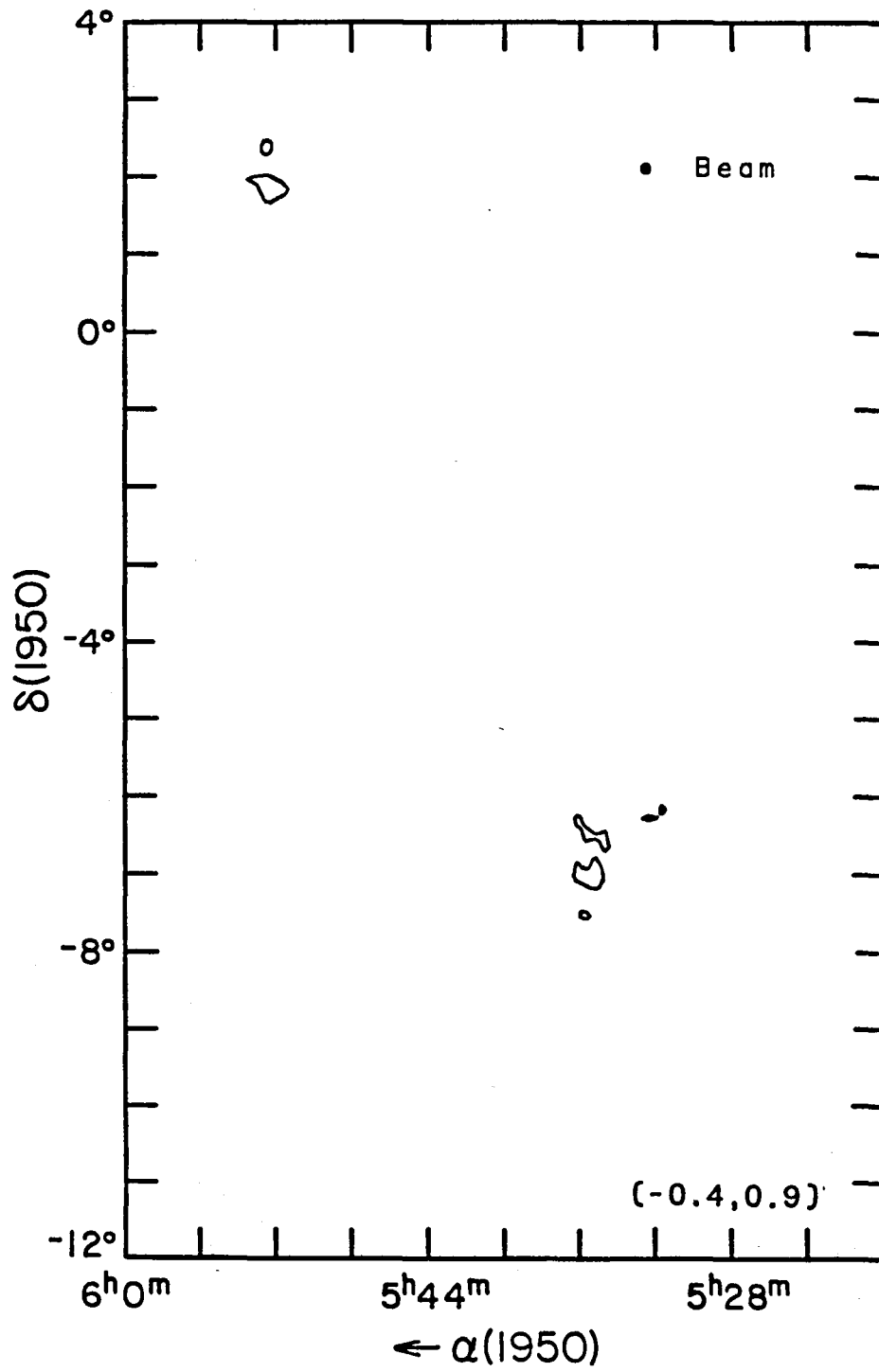
Figure IV.9c
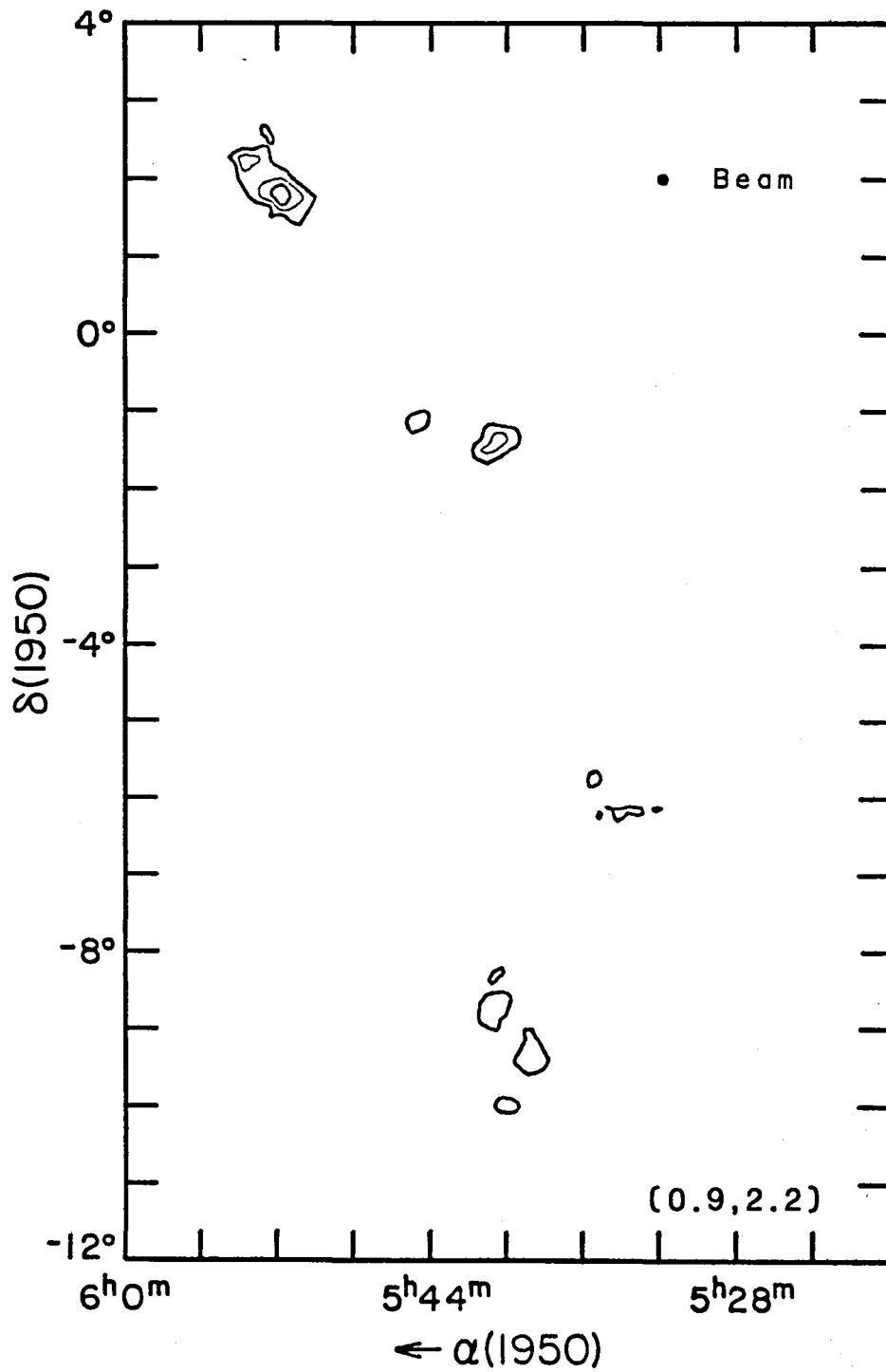
Figure IV.9d
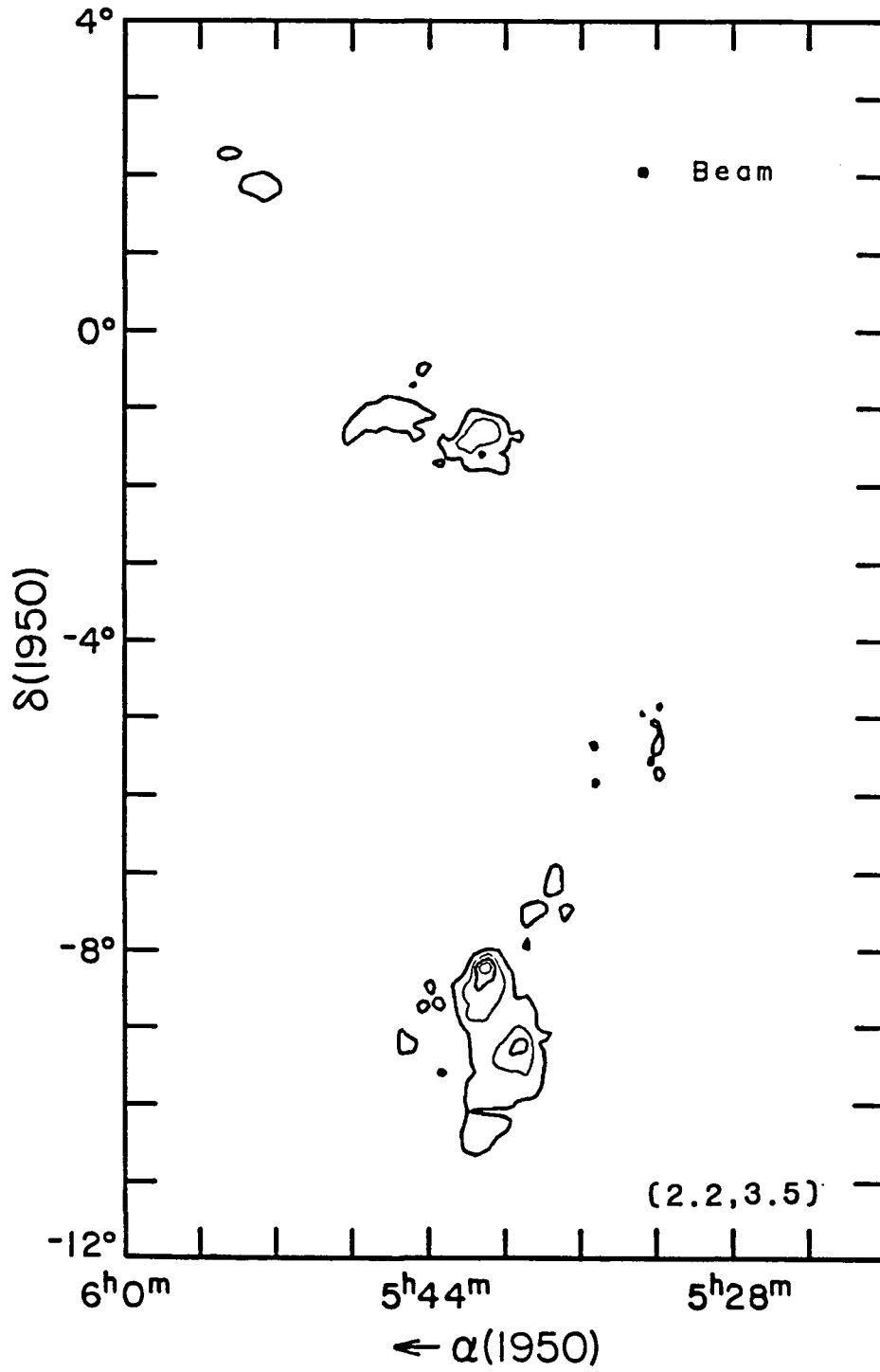
Figure IV.9e
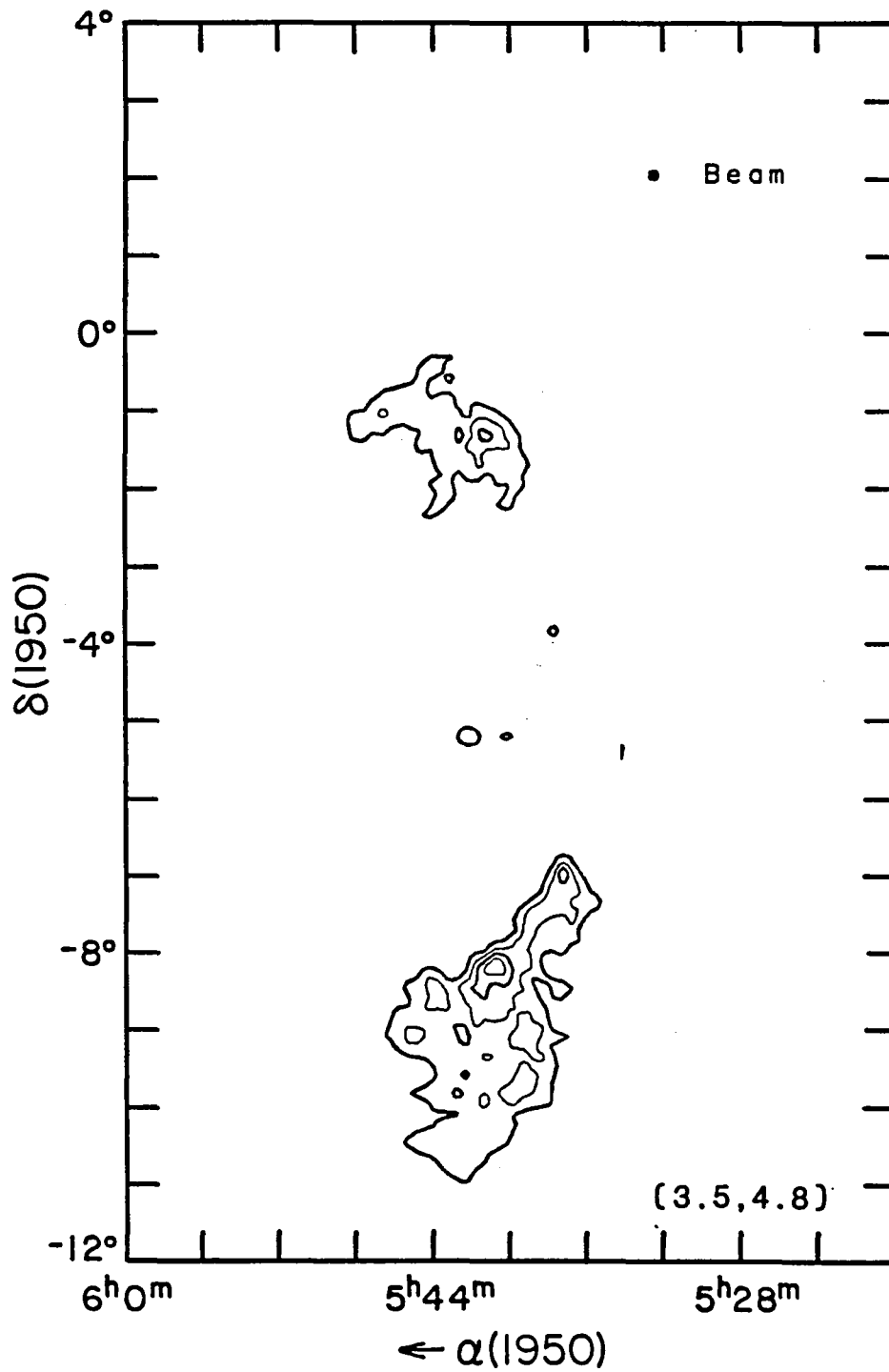
Figure IV.9f

Figure IV.9g

(6.1,7.4)
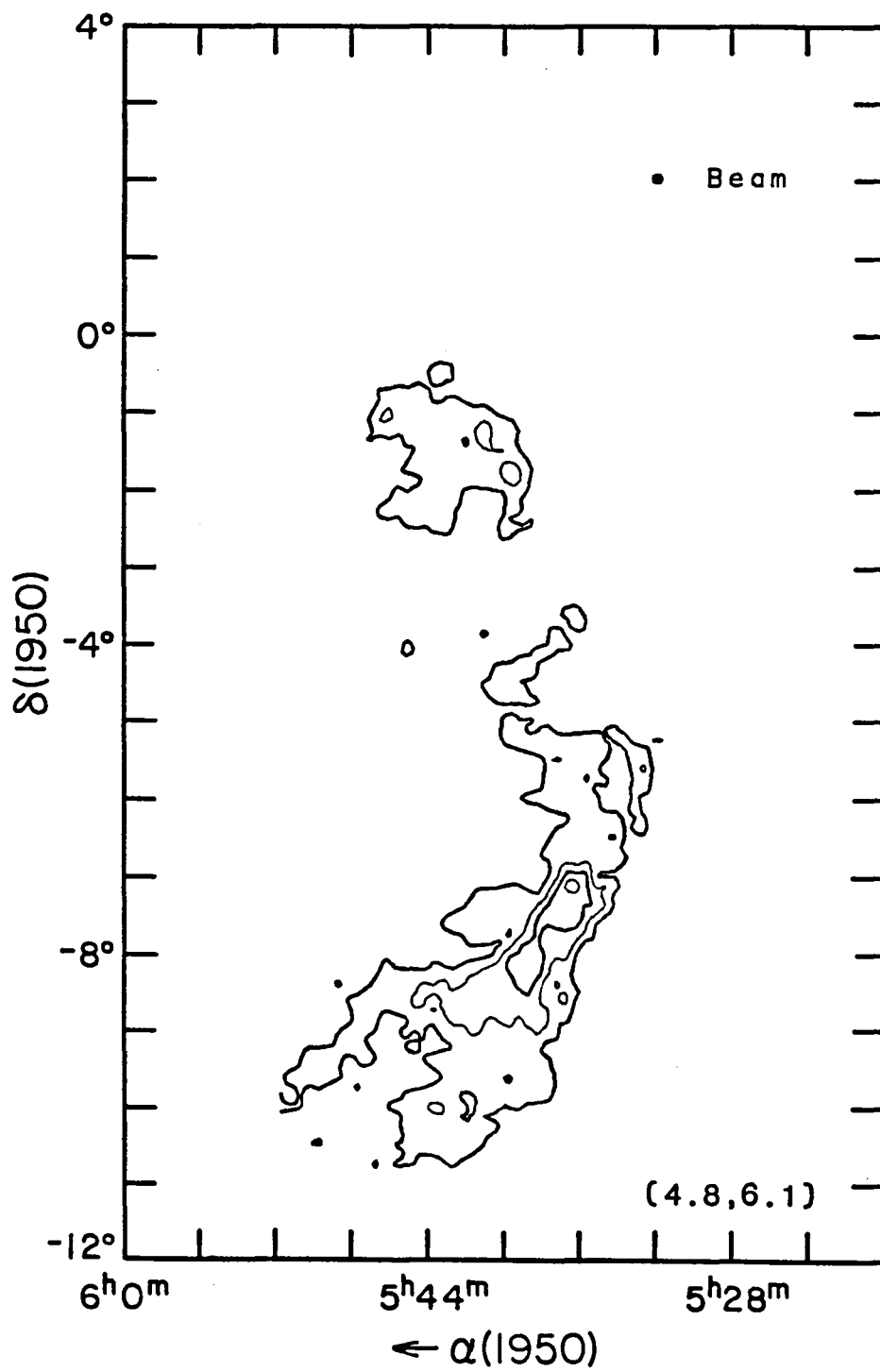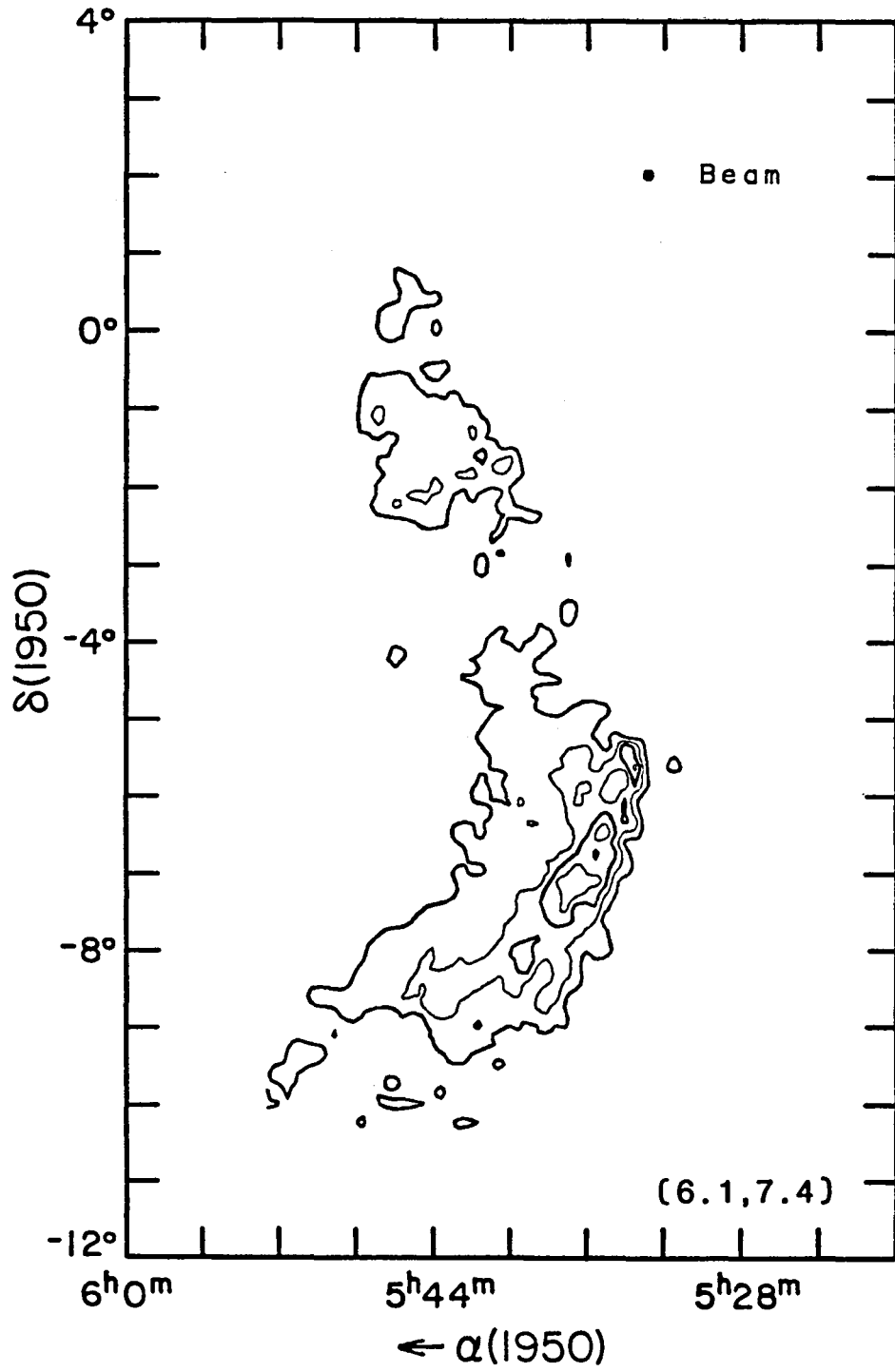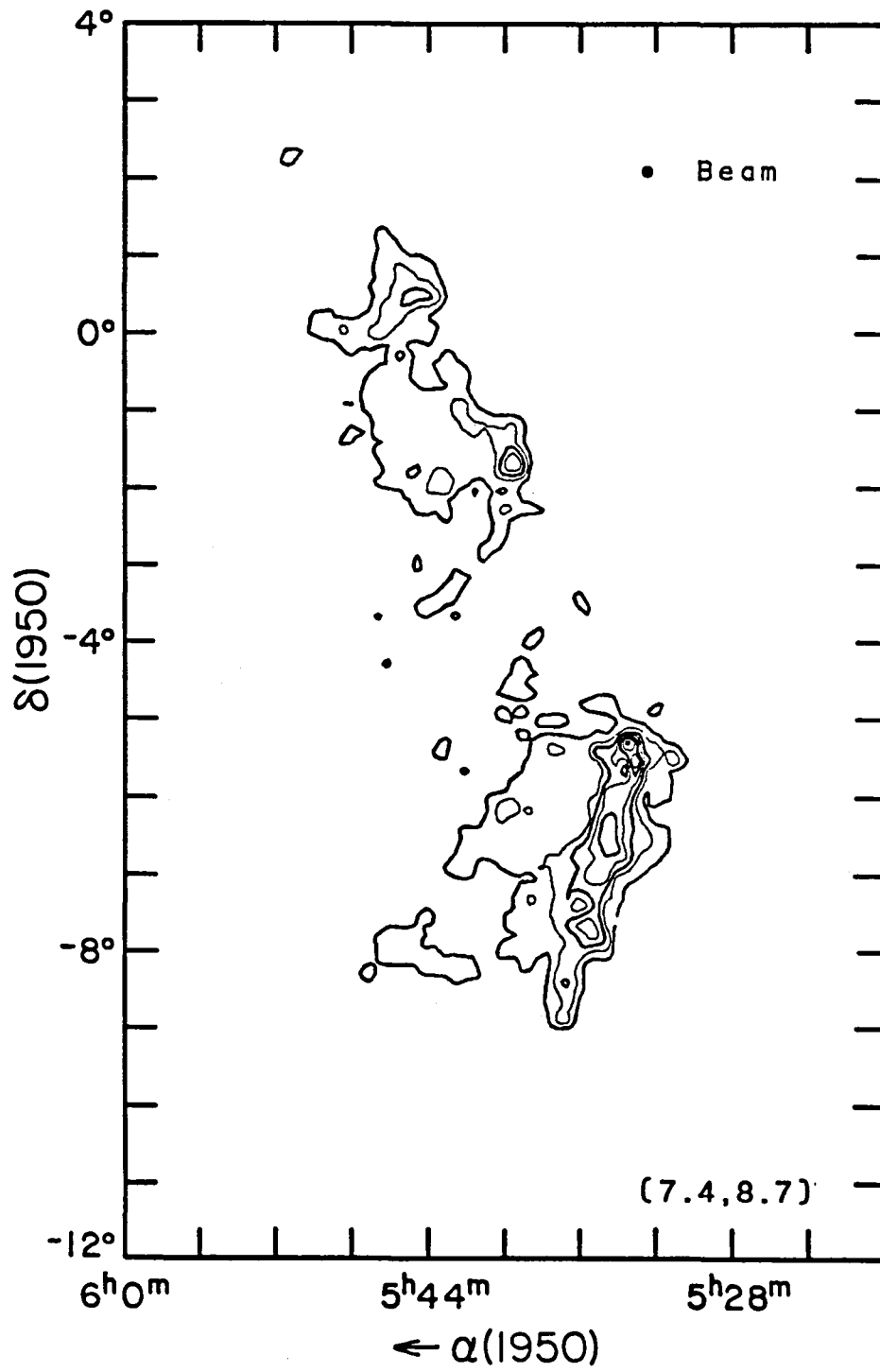
Figure IV.9h

Figure IV.9i
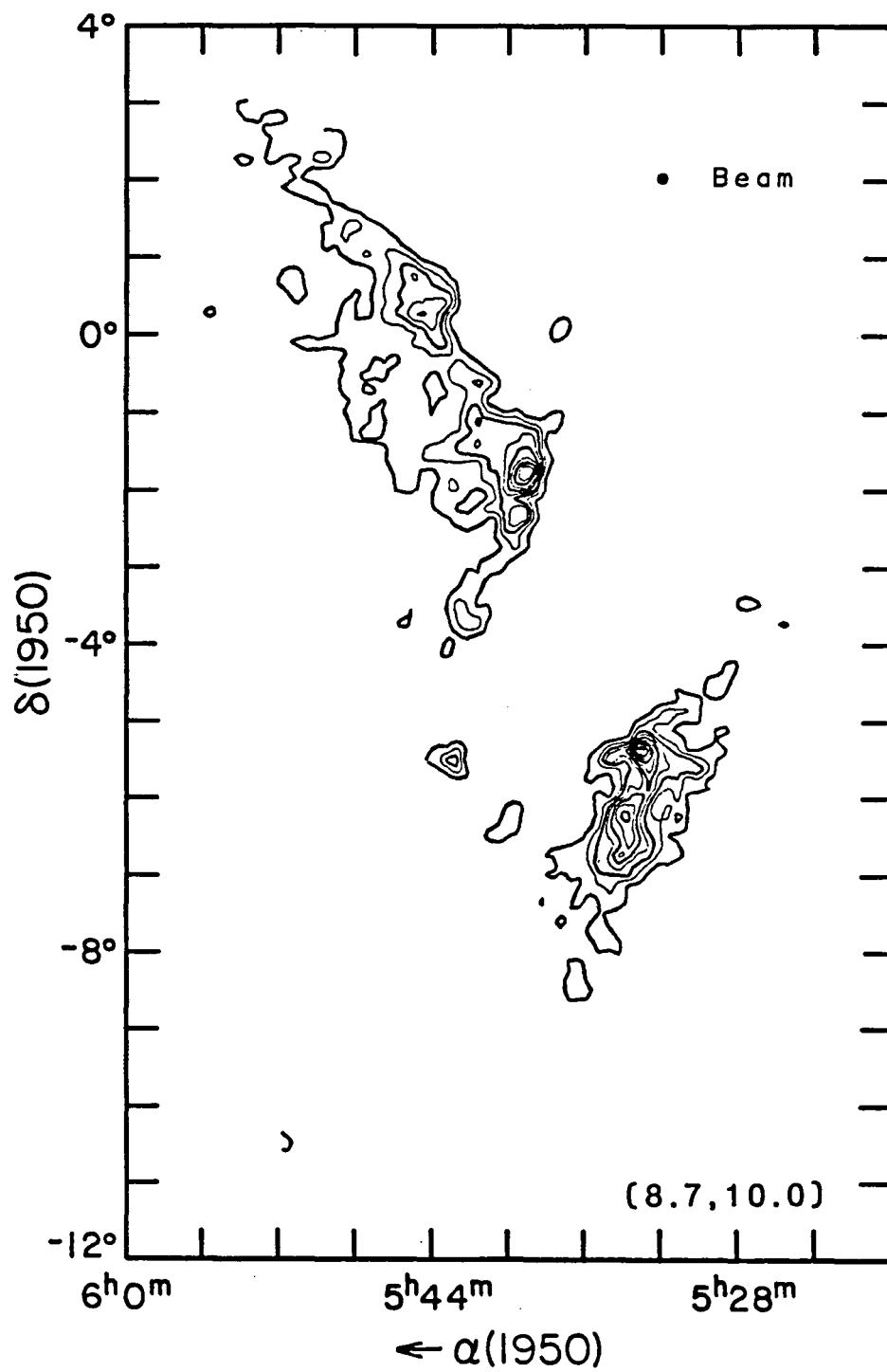
Figure IV.9j

Figure IV.9k

162
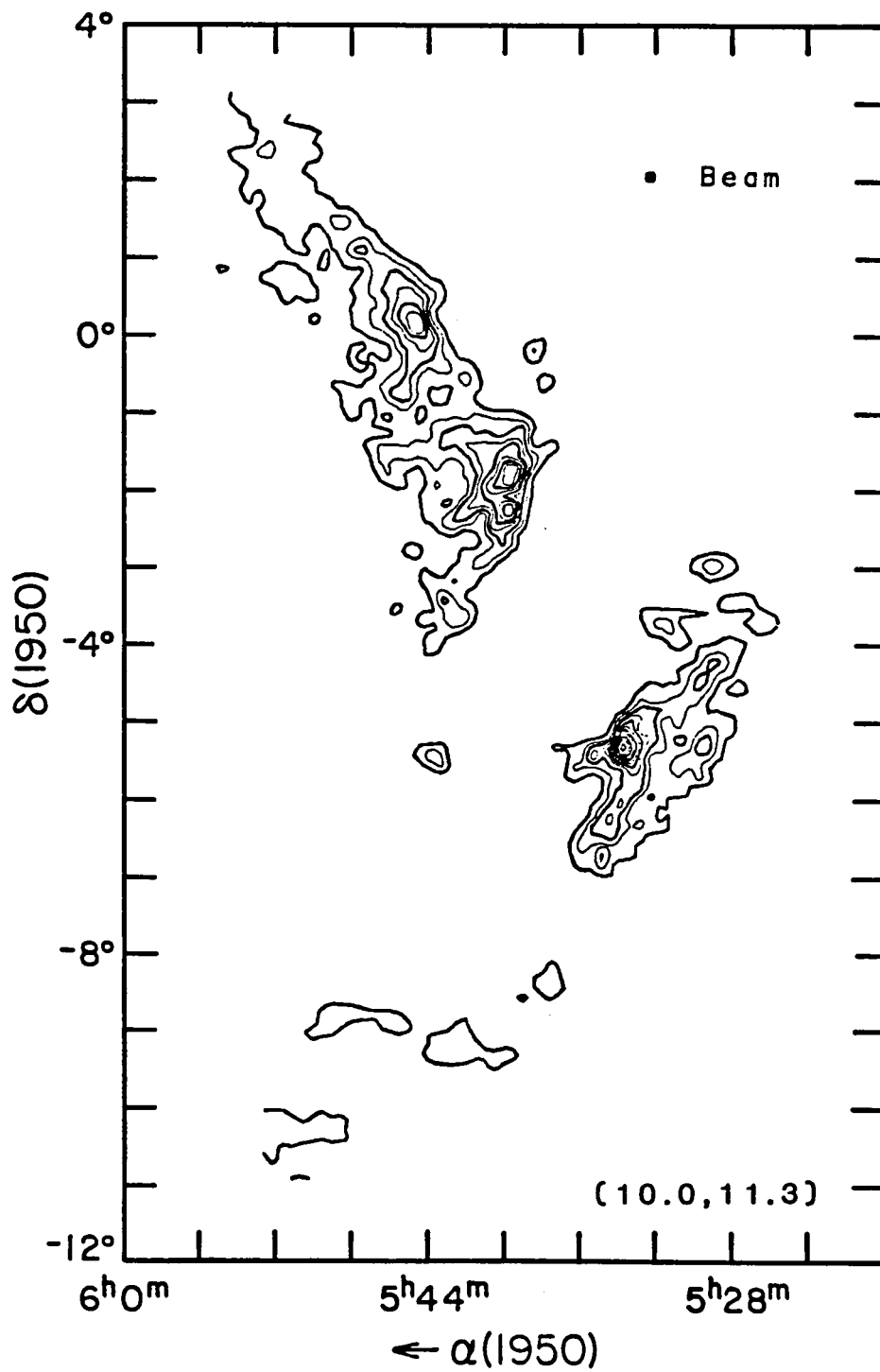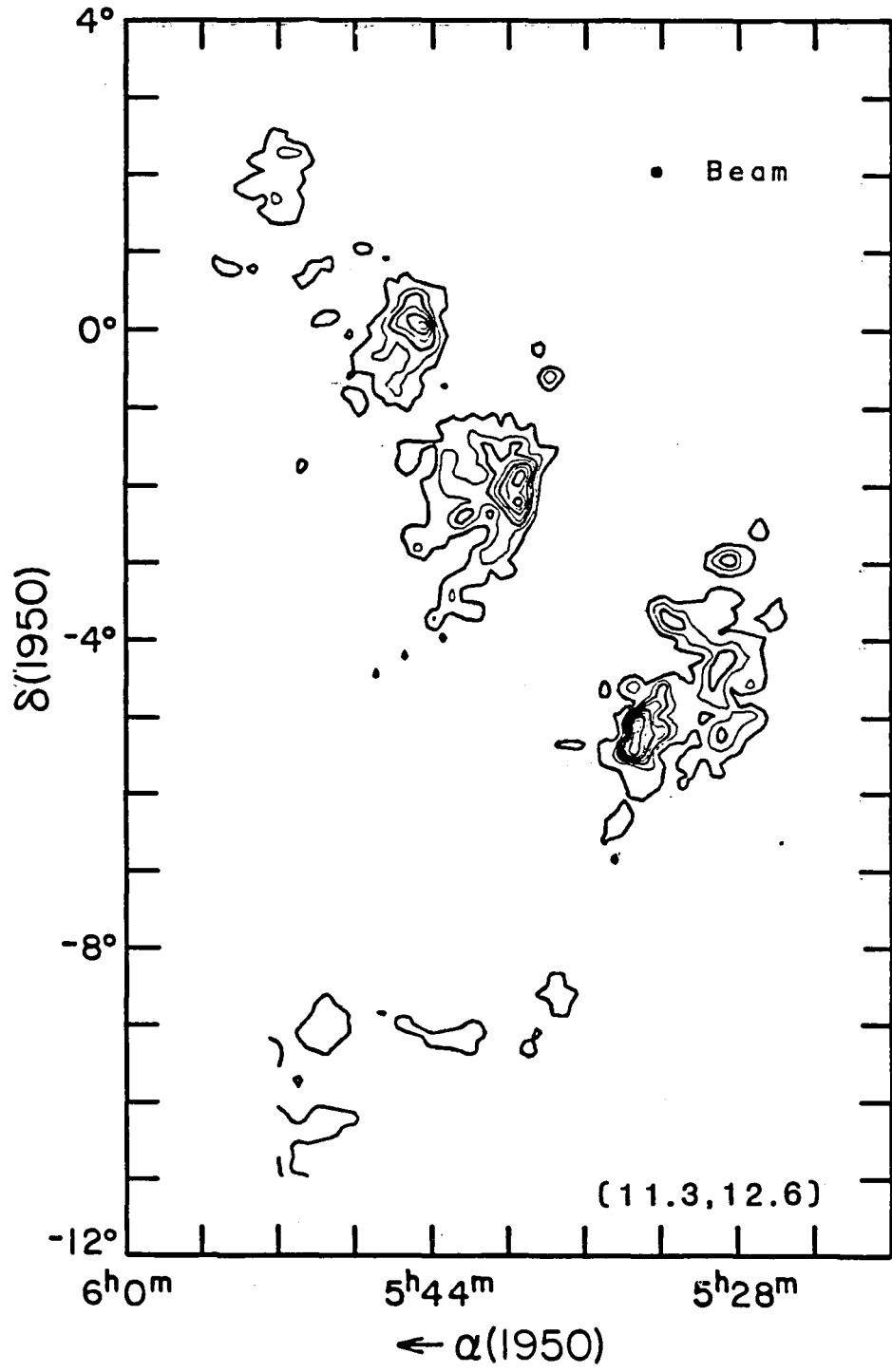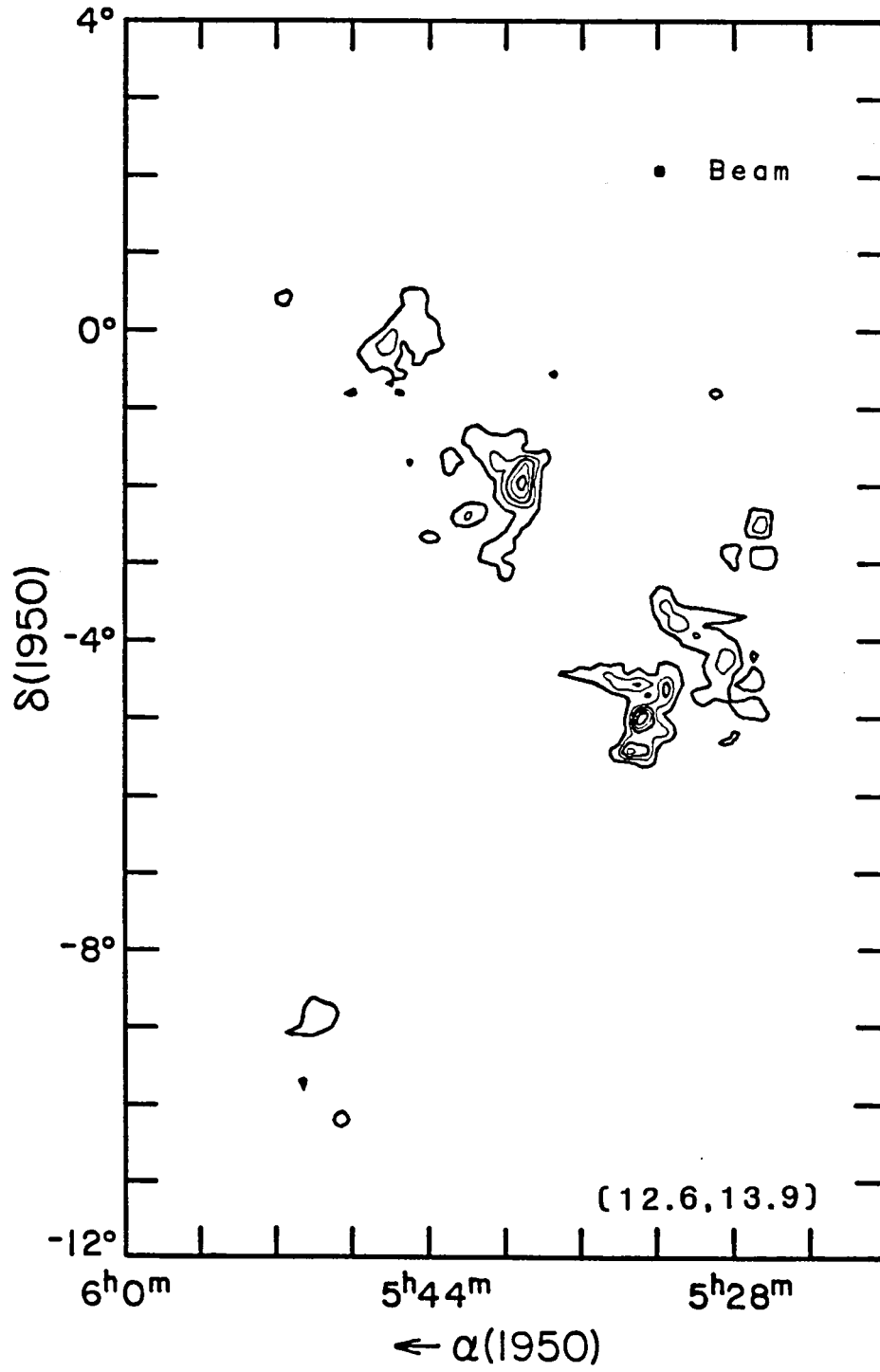
Figure IV.91

Figure IV.9m
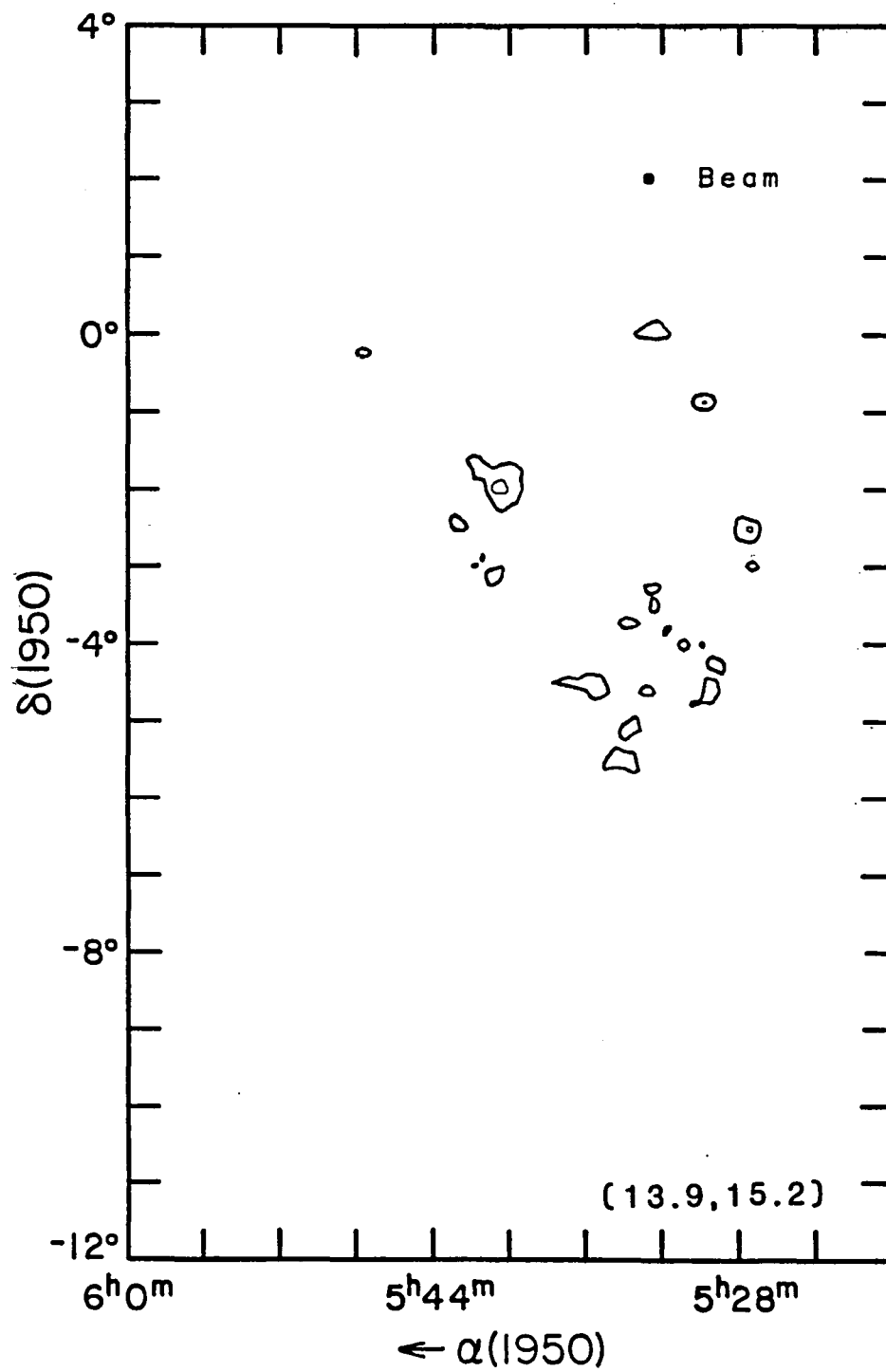
Figure IV.9n
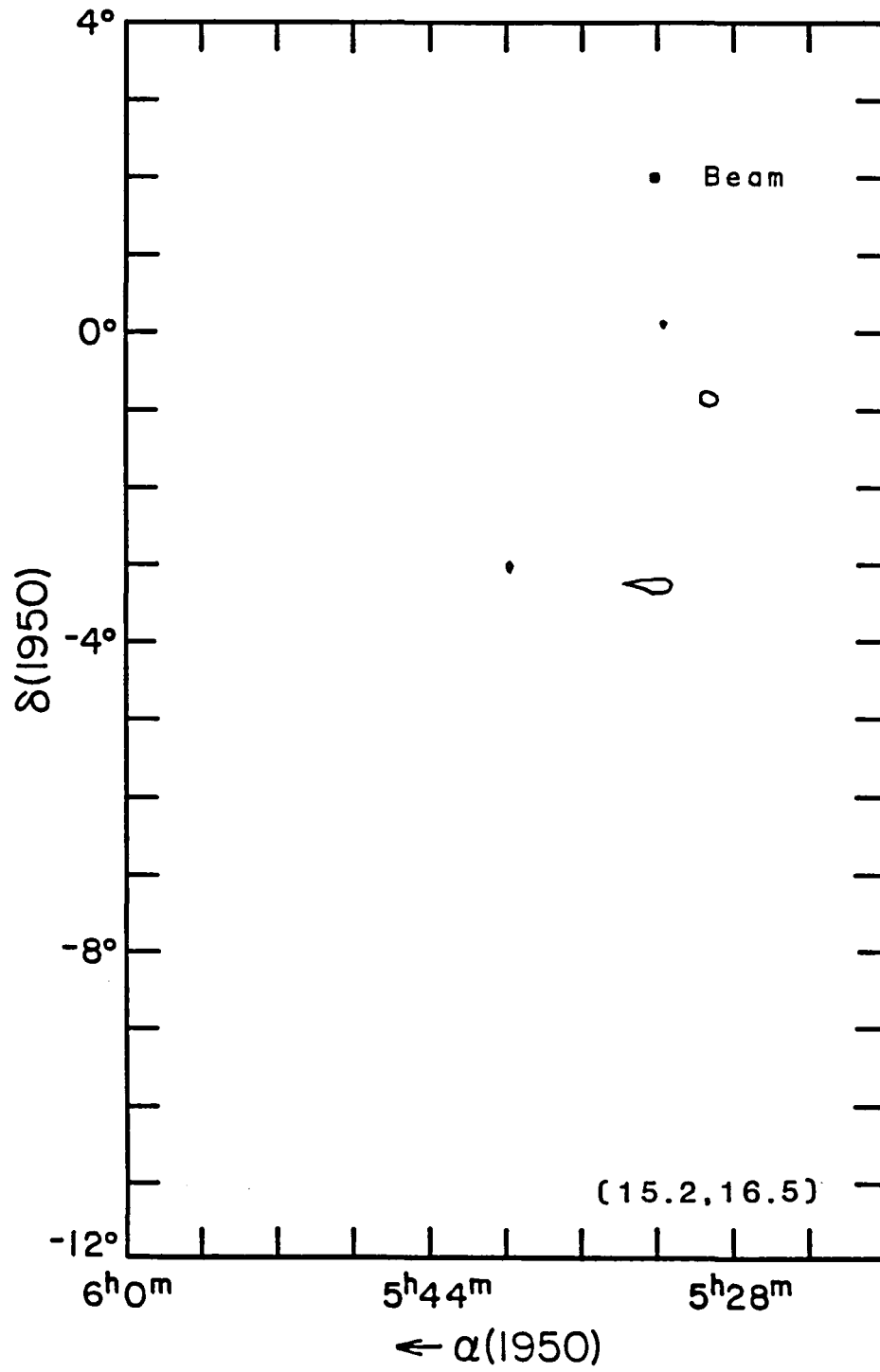
Figure IV.9o
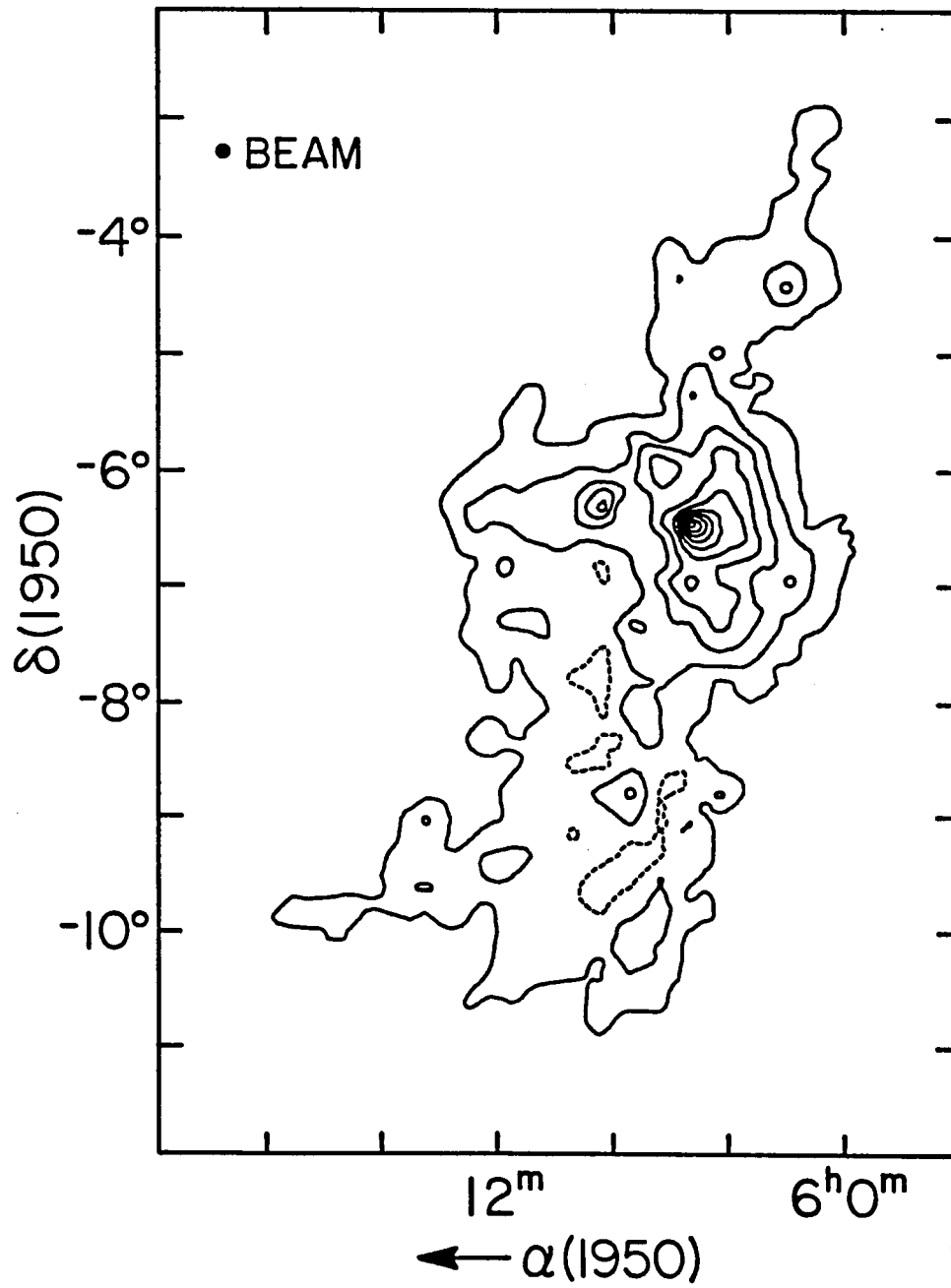
Figure IV.10
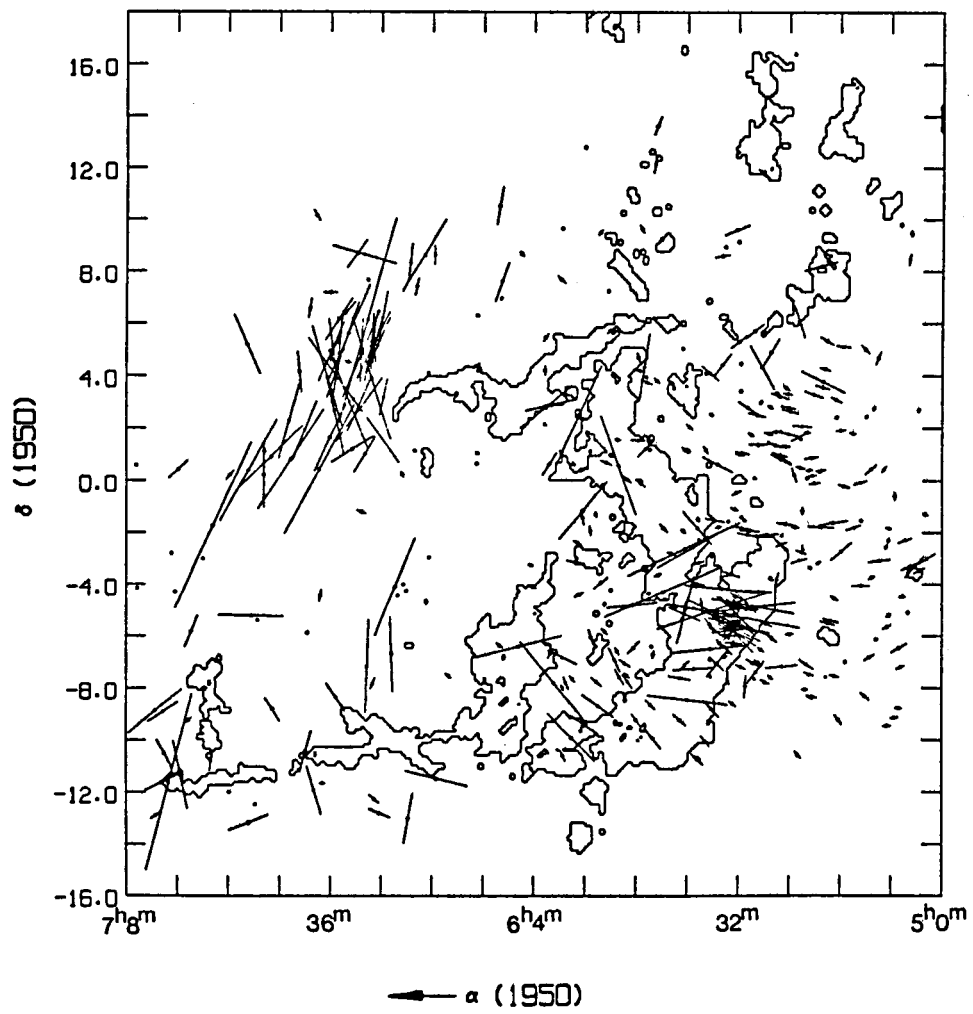
Figure IV.11
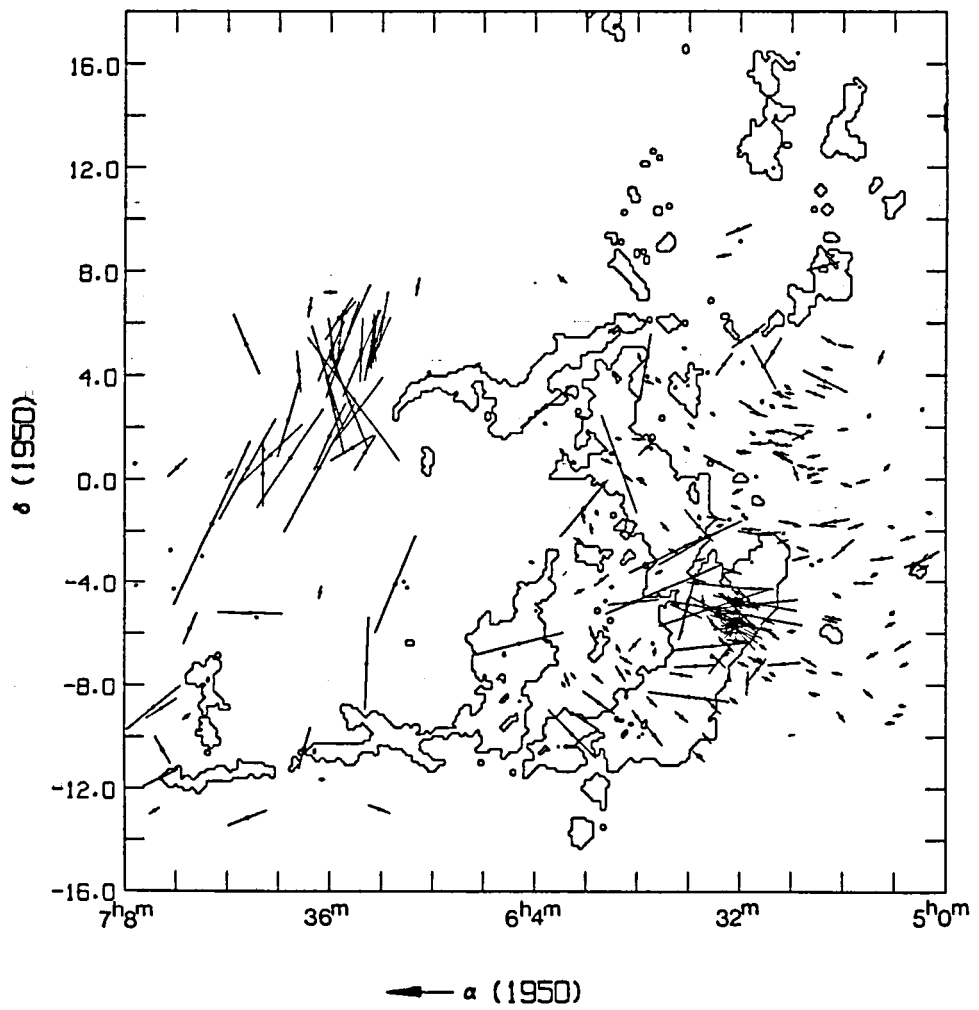
Figure IV.12
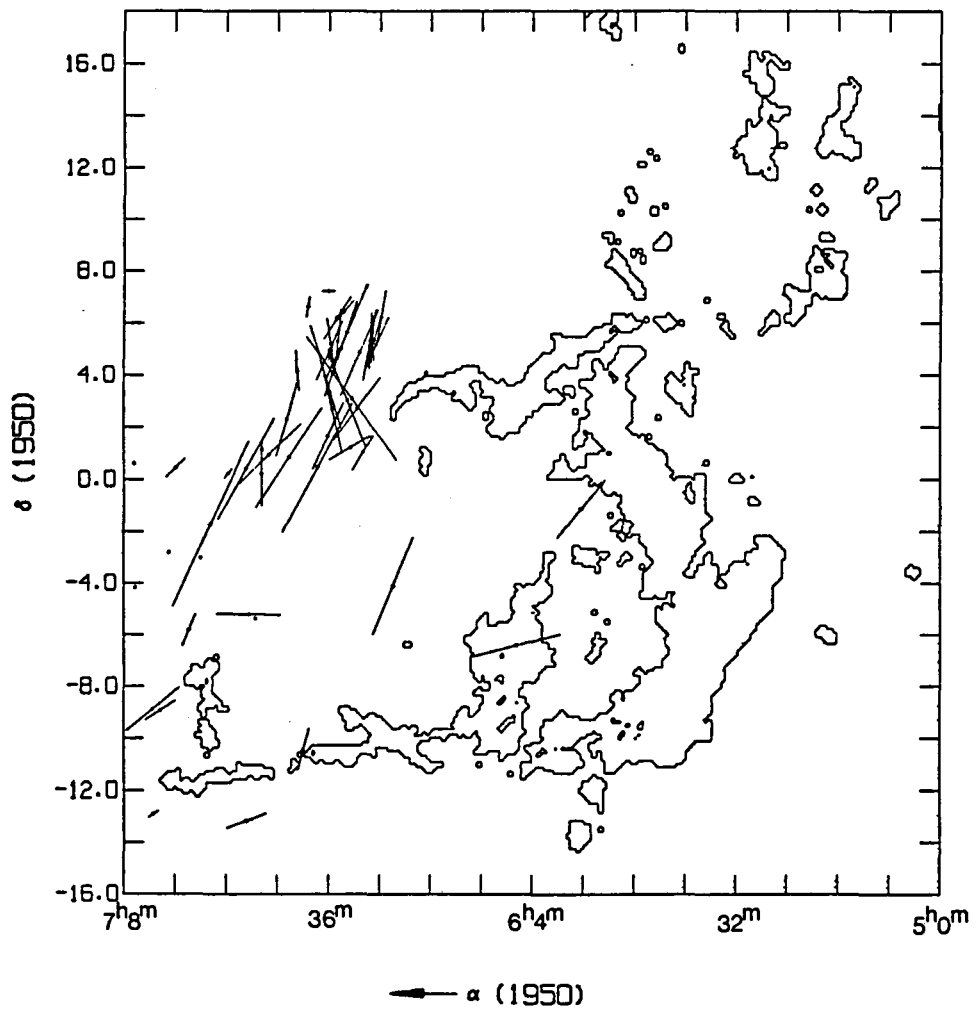
Figure IV.13
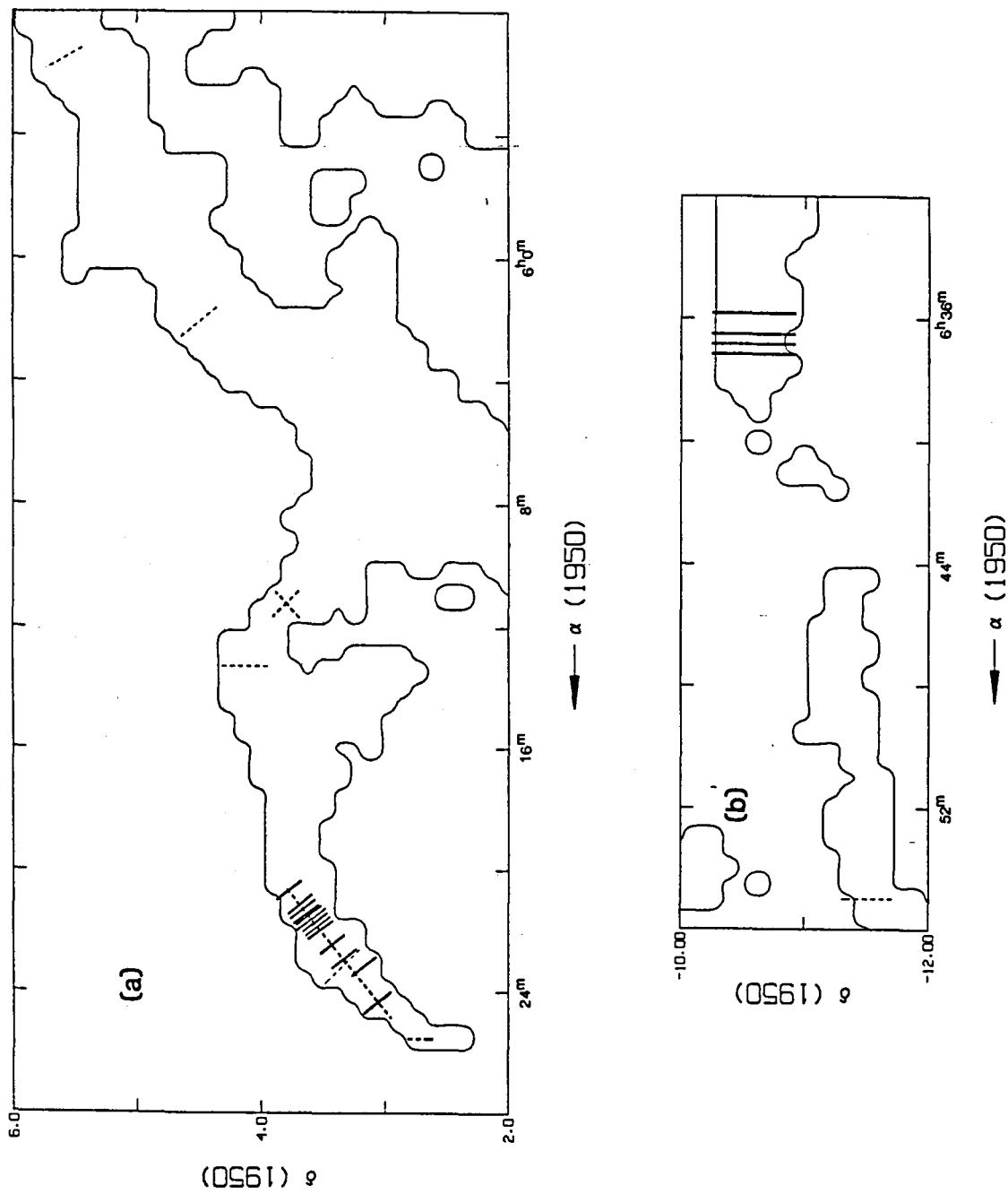
Figure IV.14
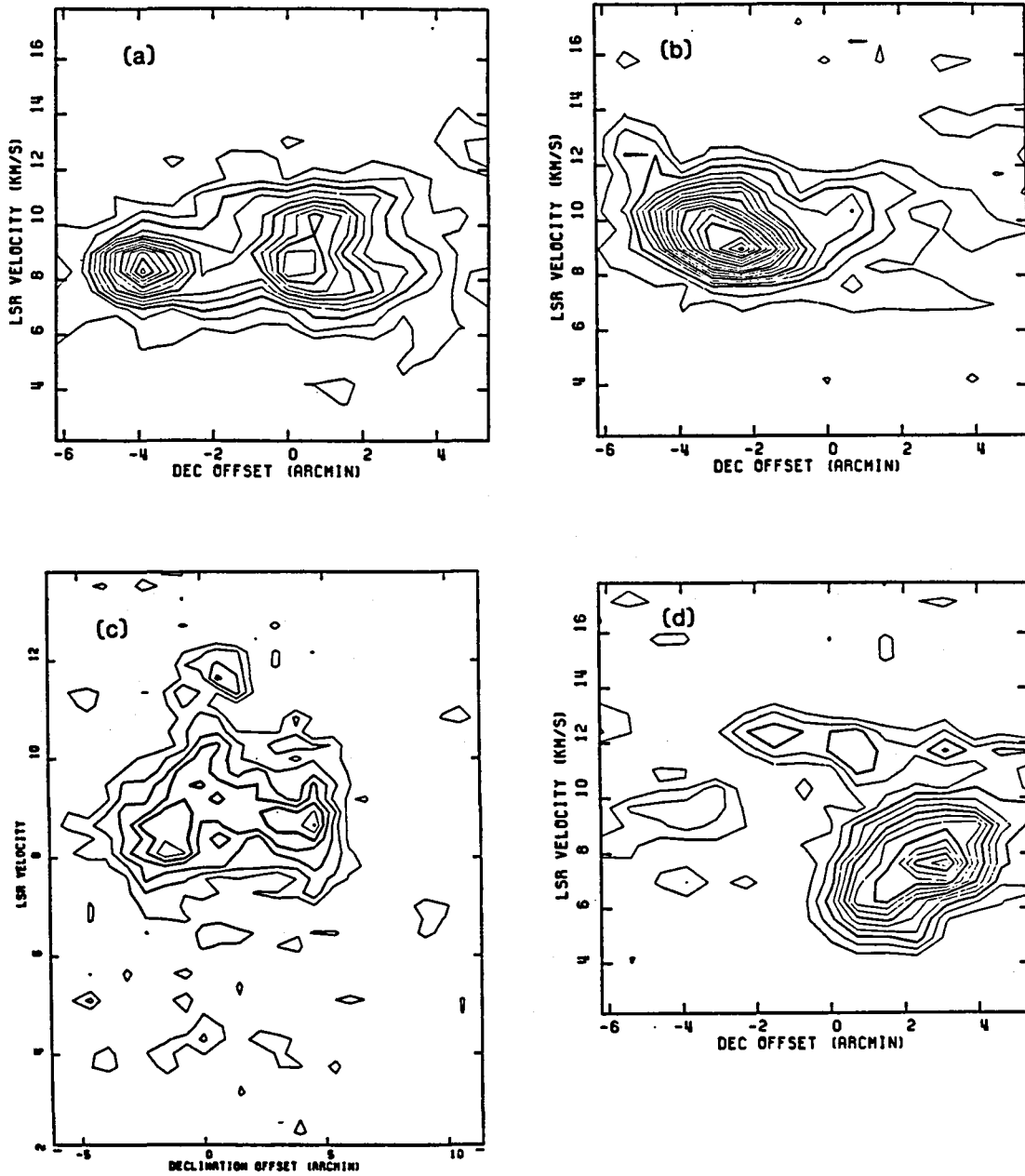
Figure IV.15a-d
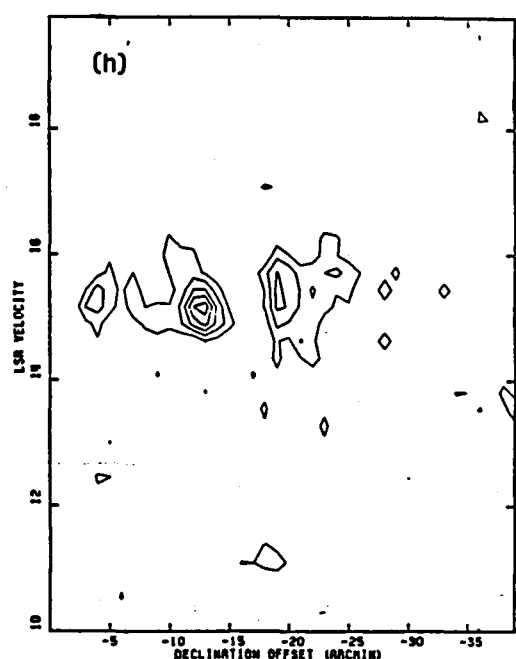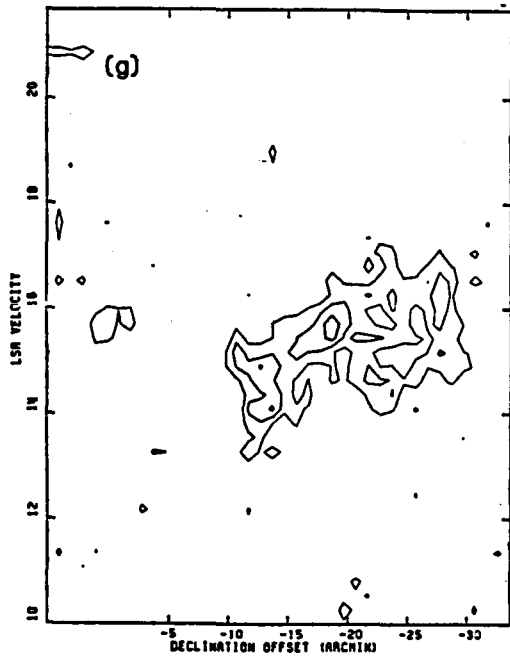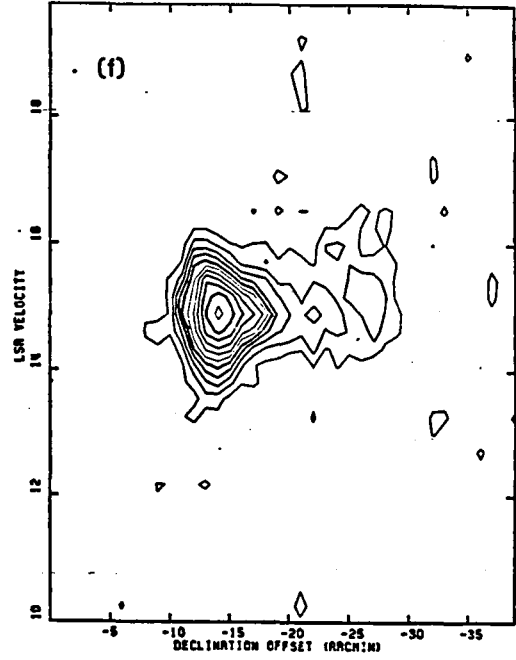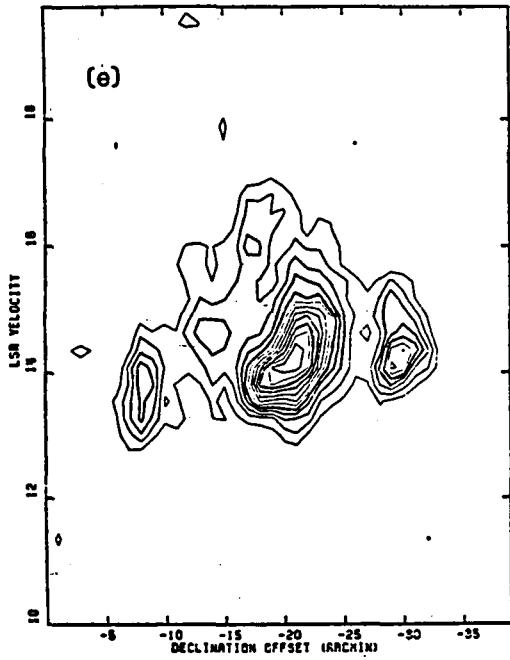
Figure IV.15e-h
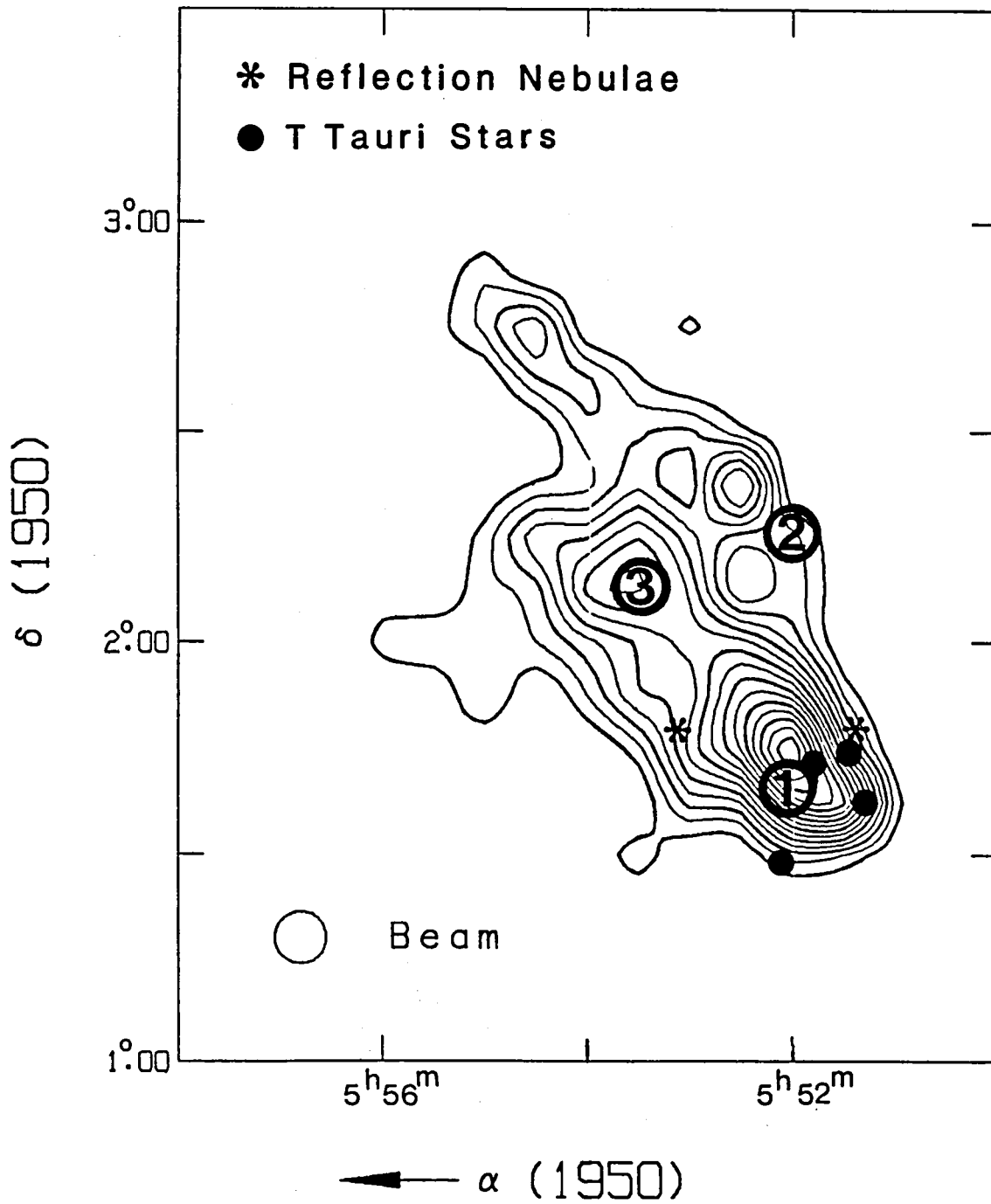
Figure IV.16
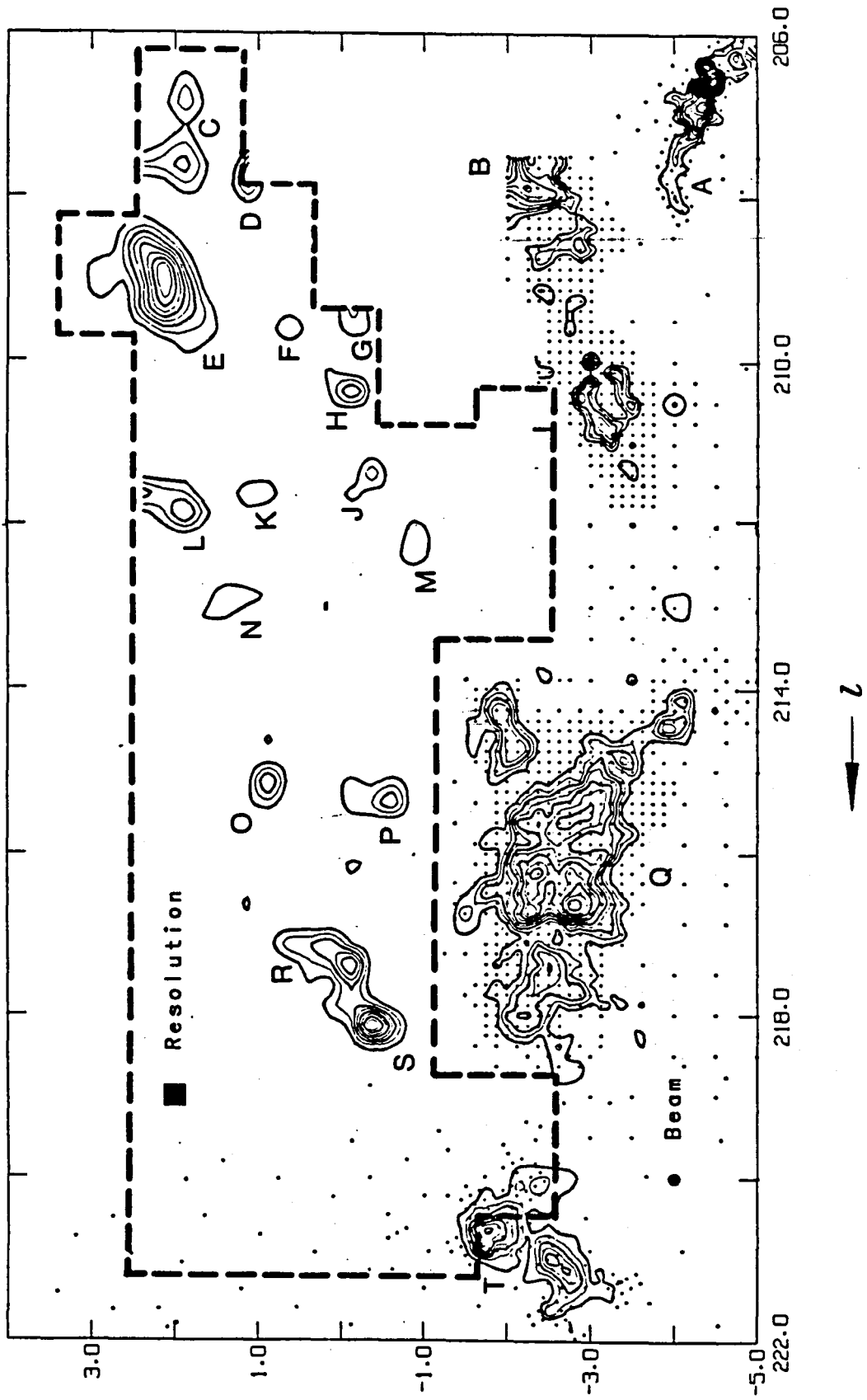
Figure IV.17
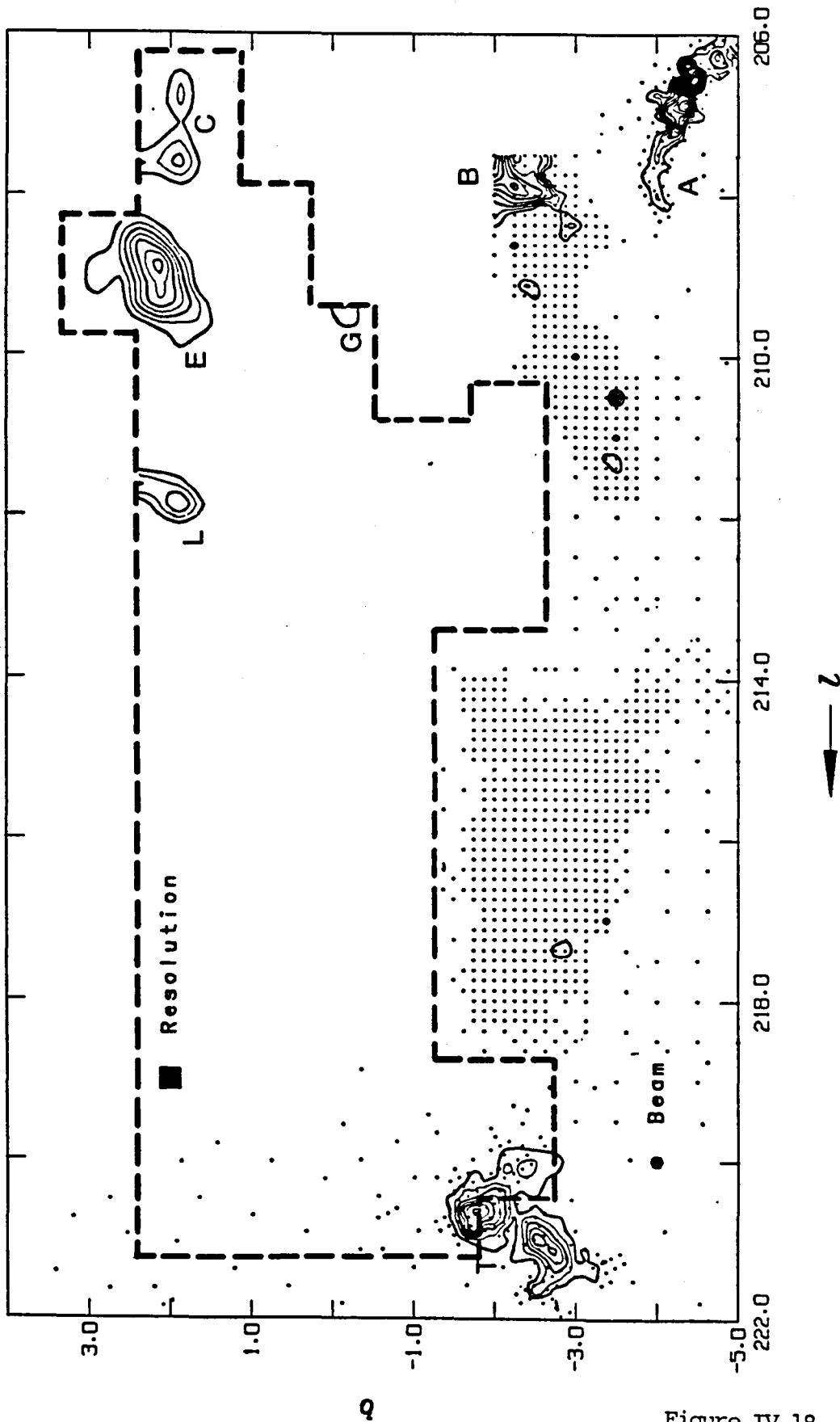
Figure IV.18
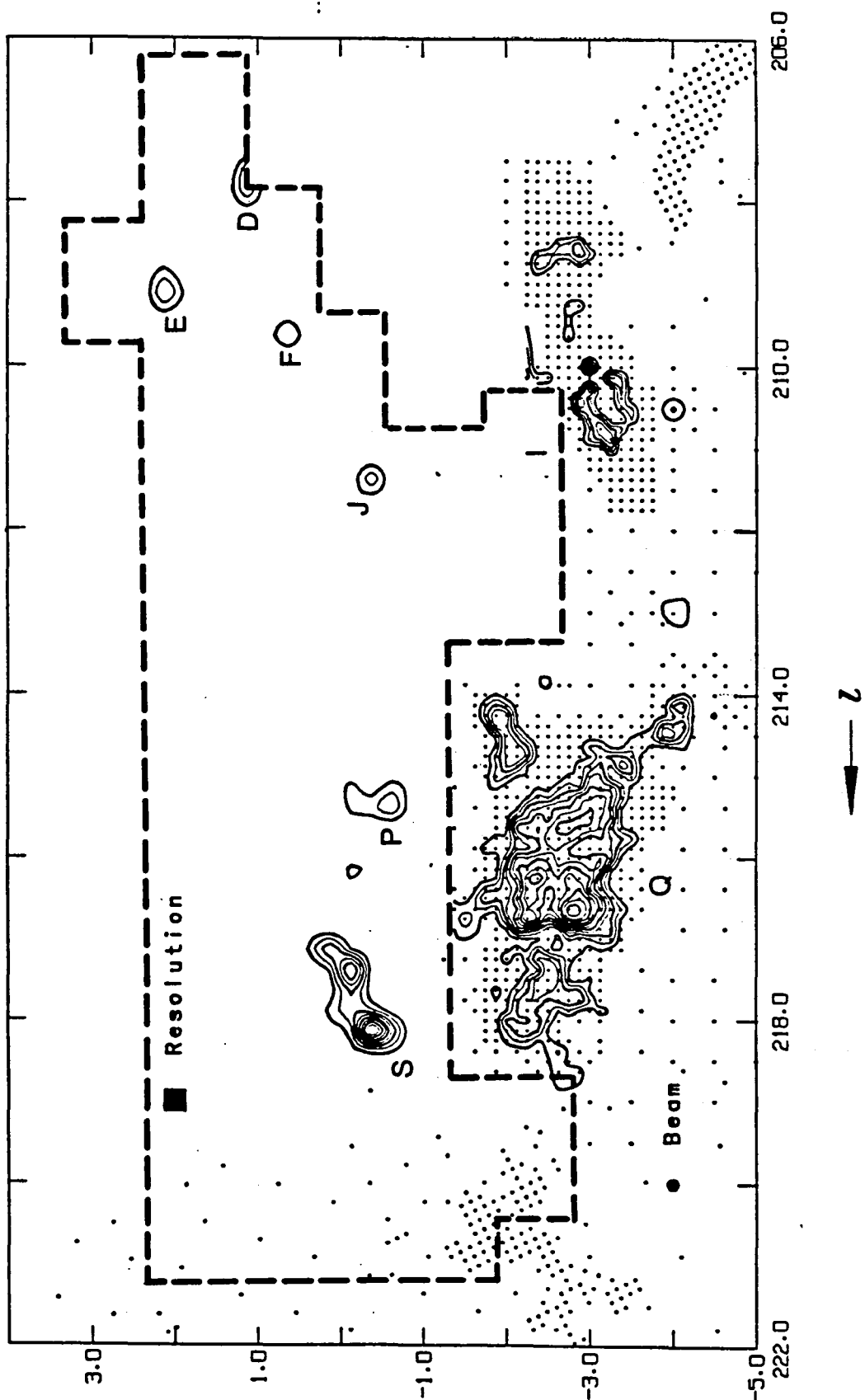
Figure IV.19
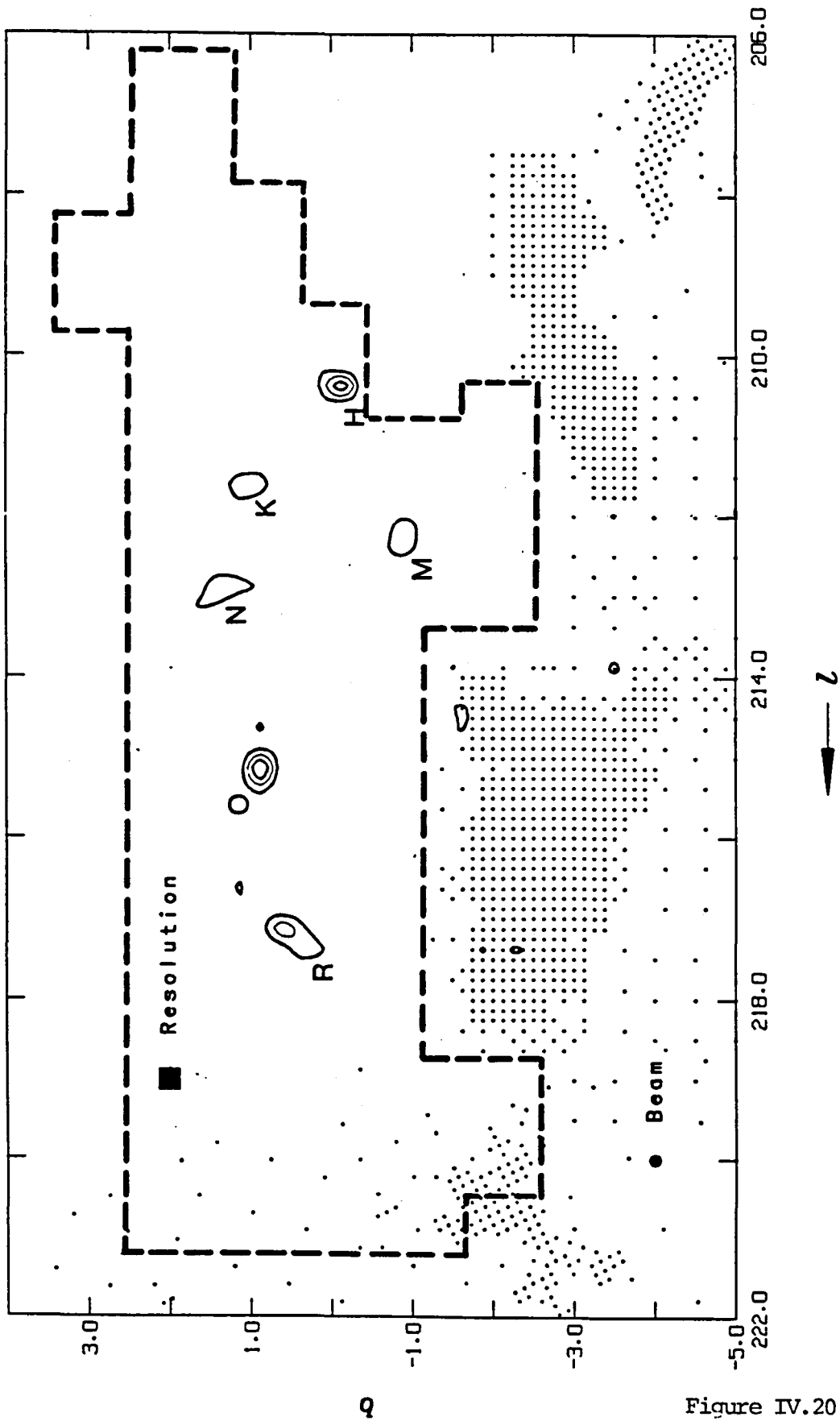
Figure IV.20
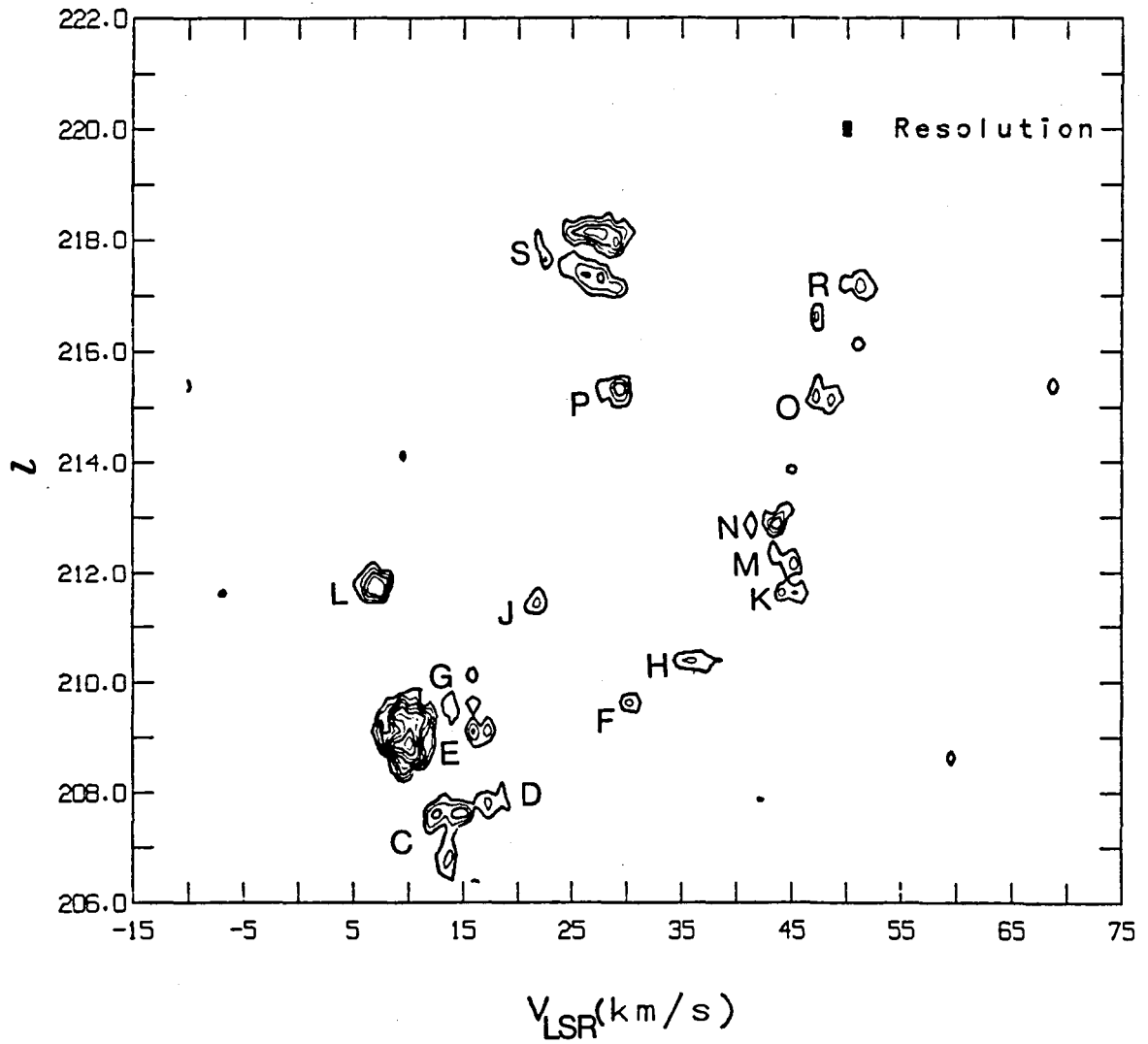
Figure IV.21
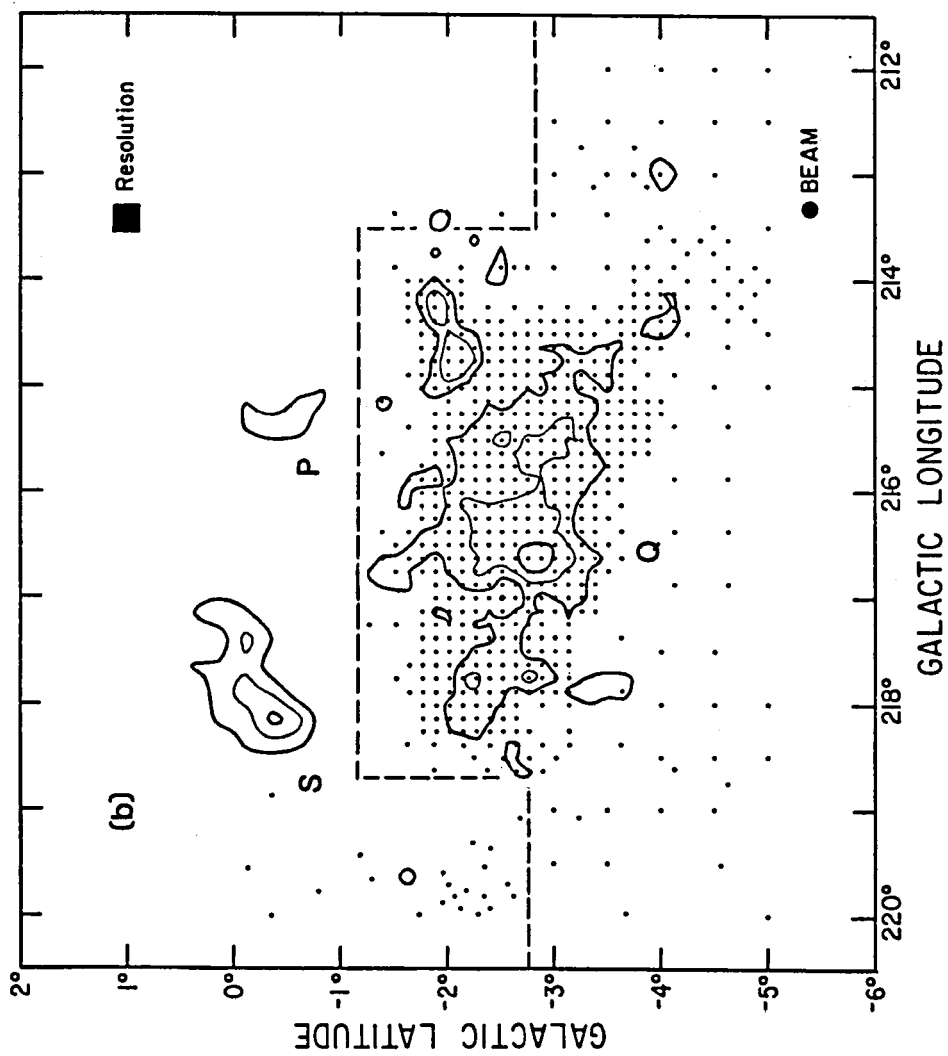
Figure IV.22
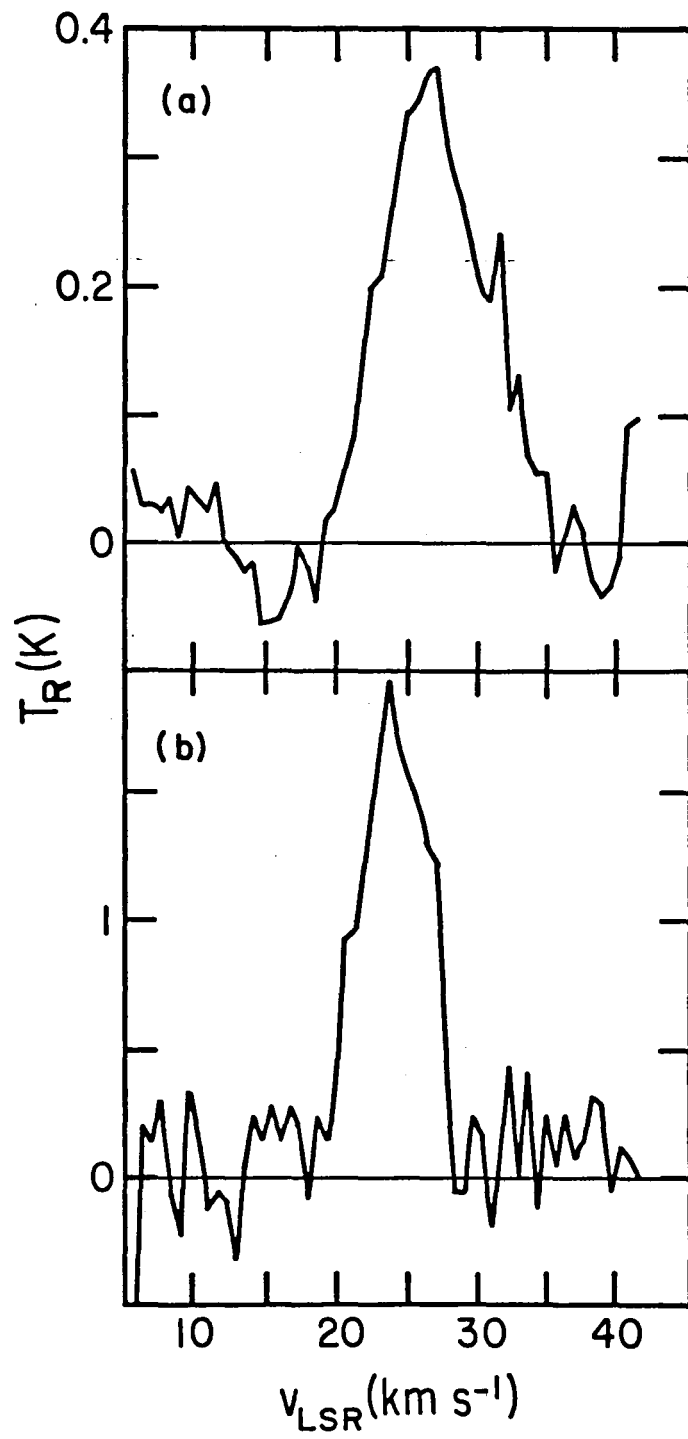
Figure IV.23
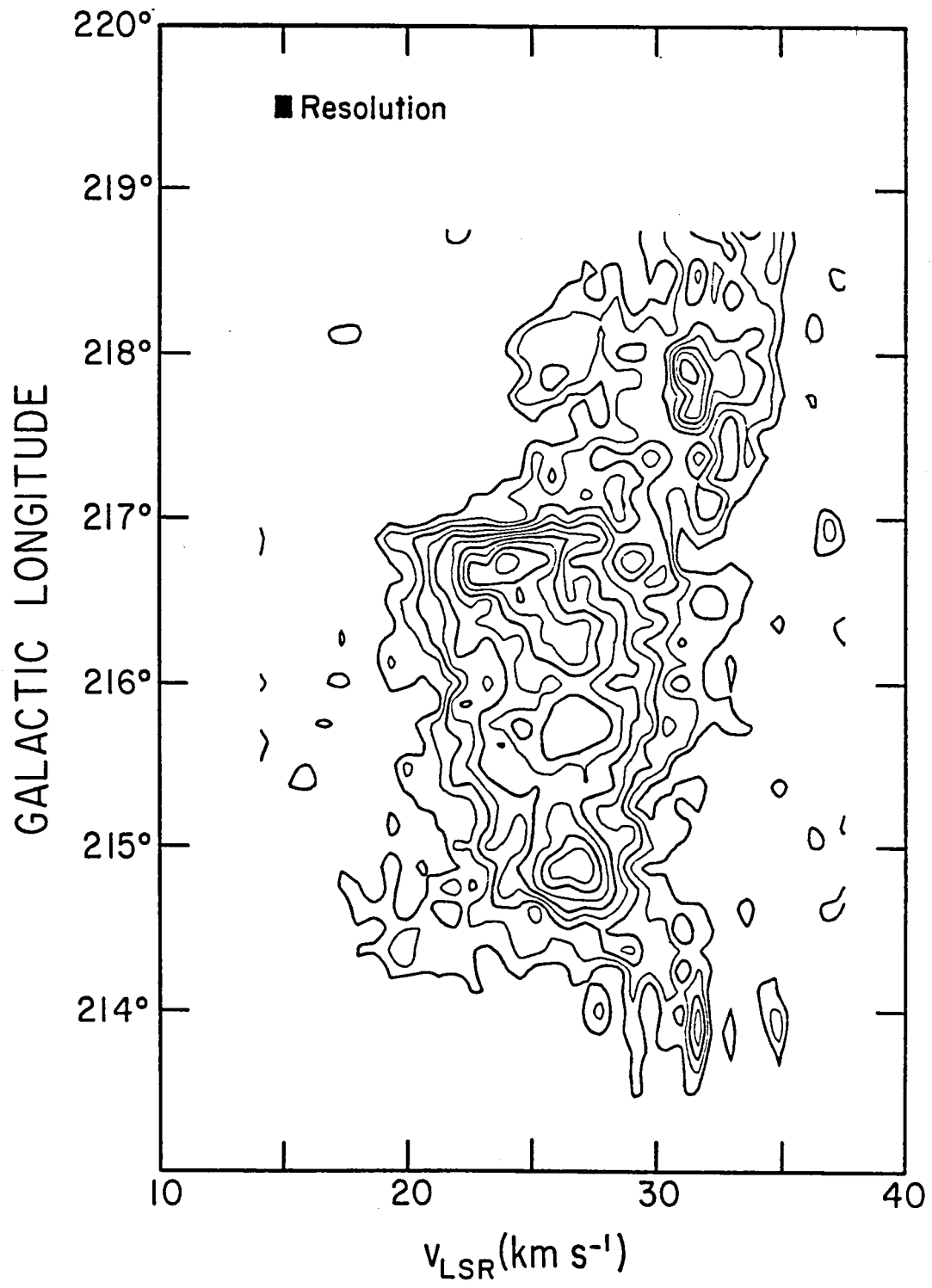
Figure IV.24
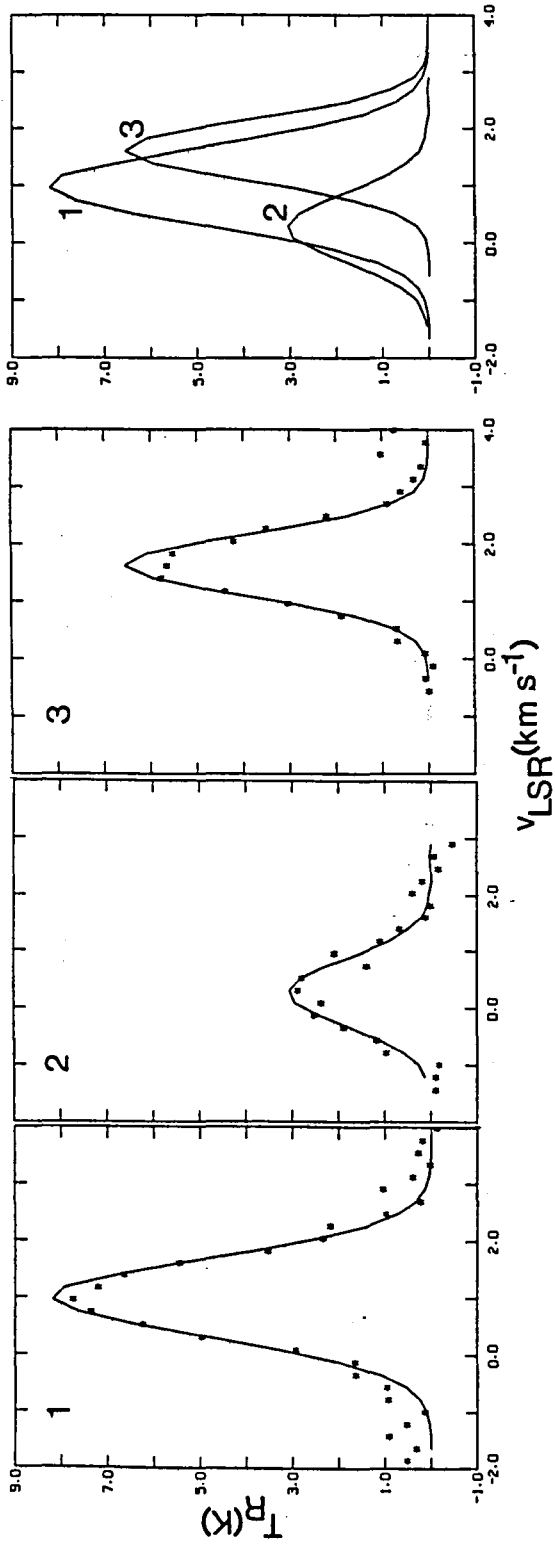
Figure V.1
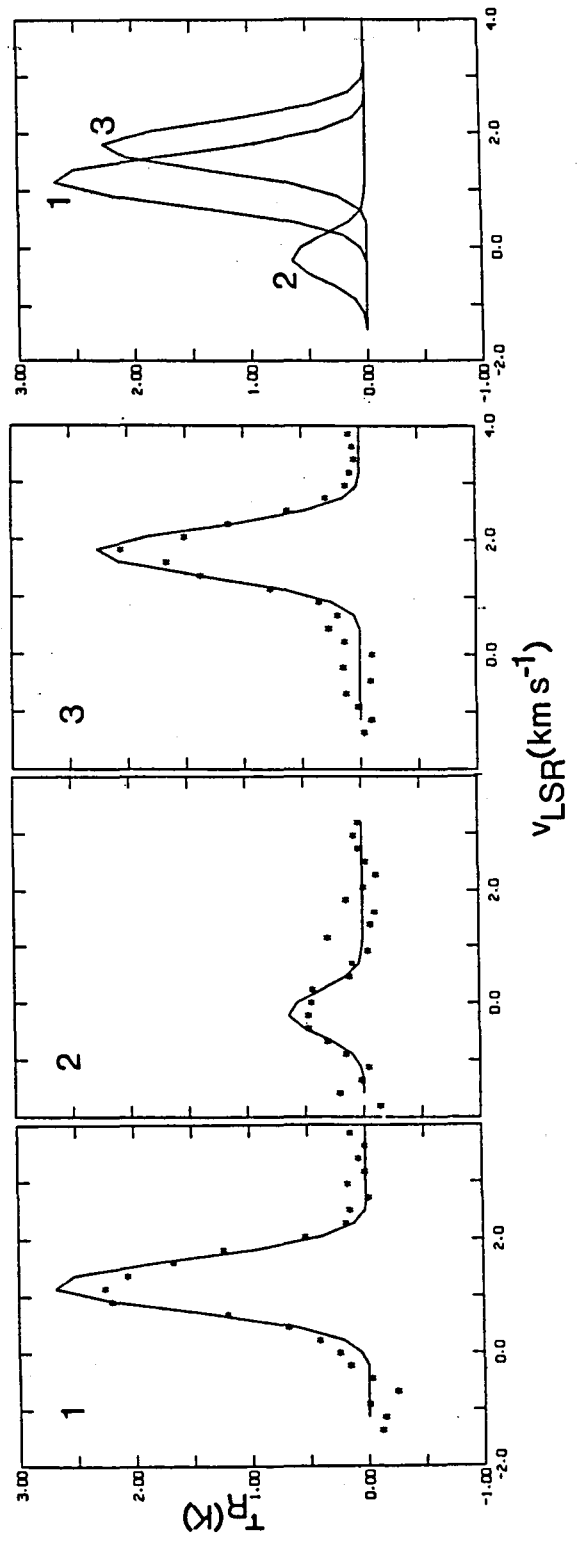
Figure V.2
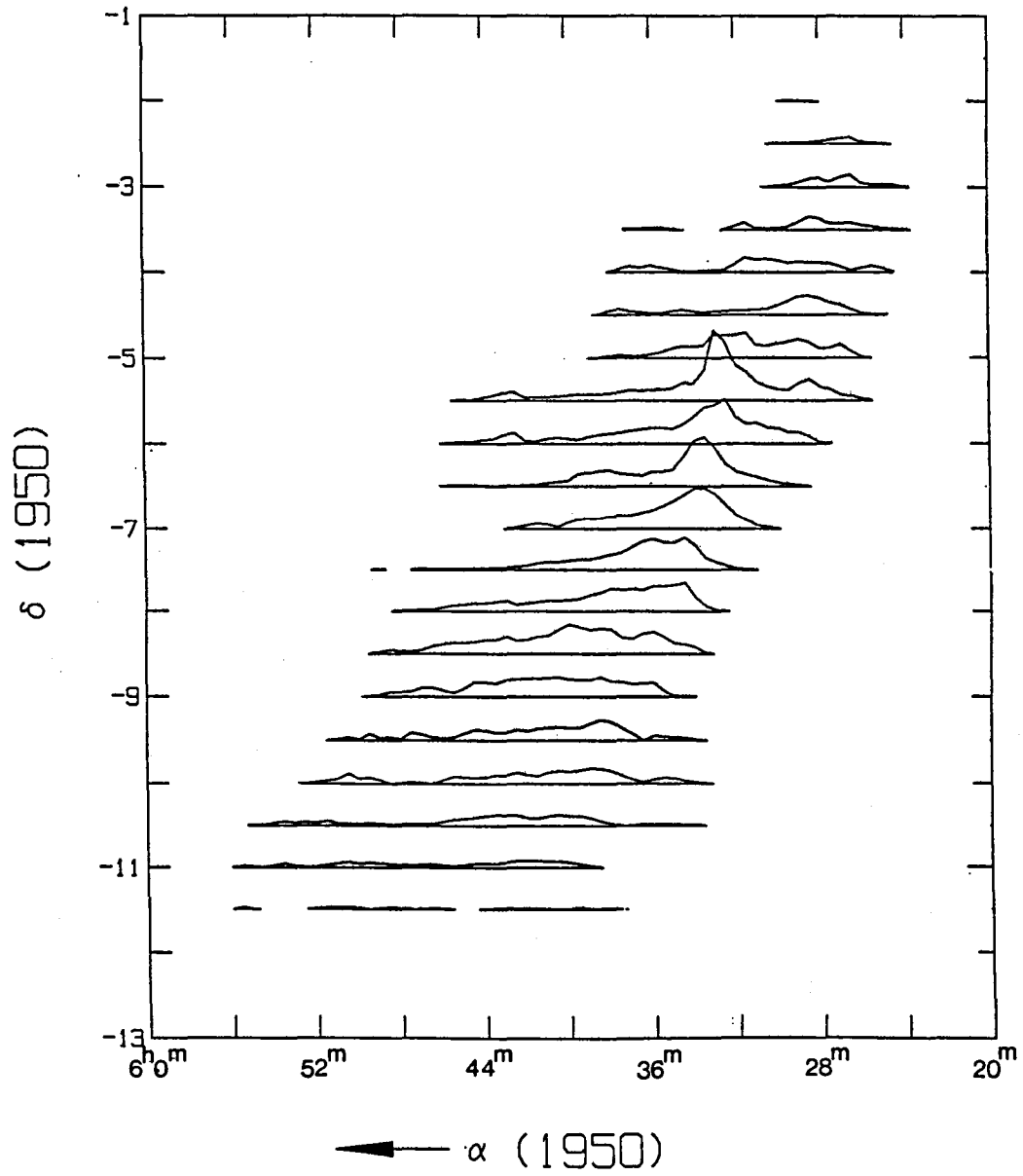
Figure V.3
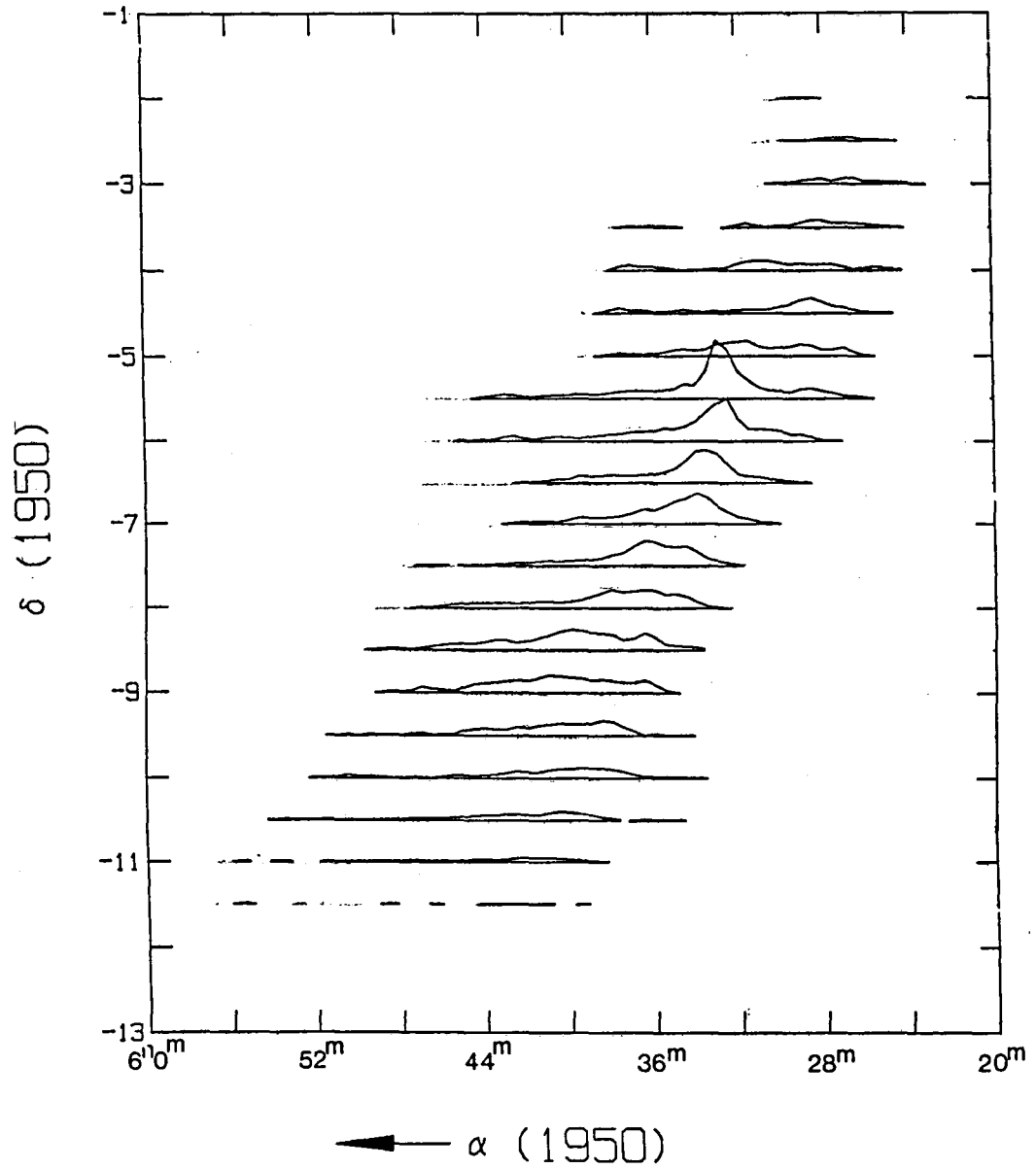
Figure V.4
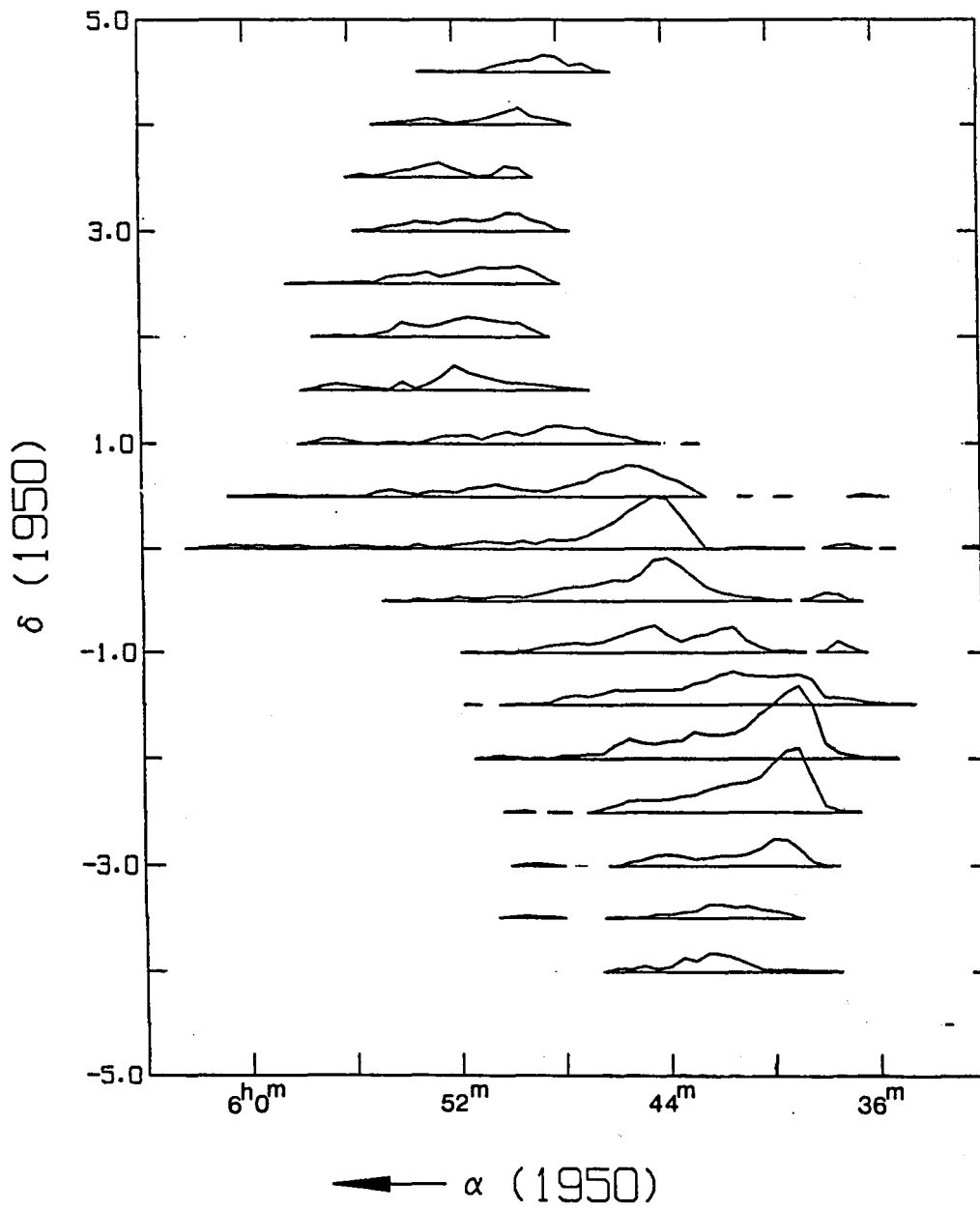
Figure V.5
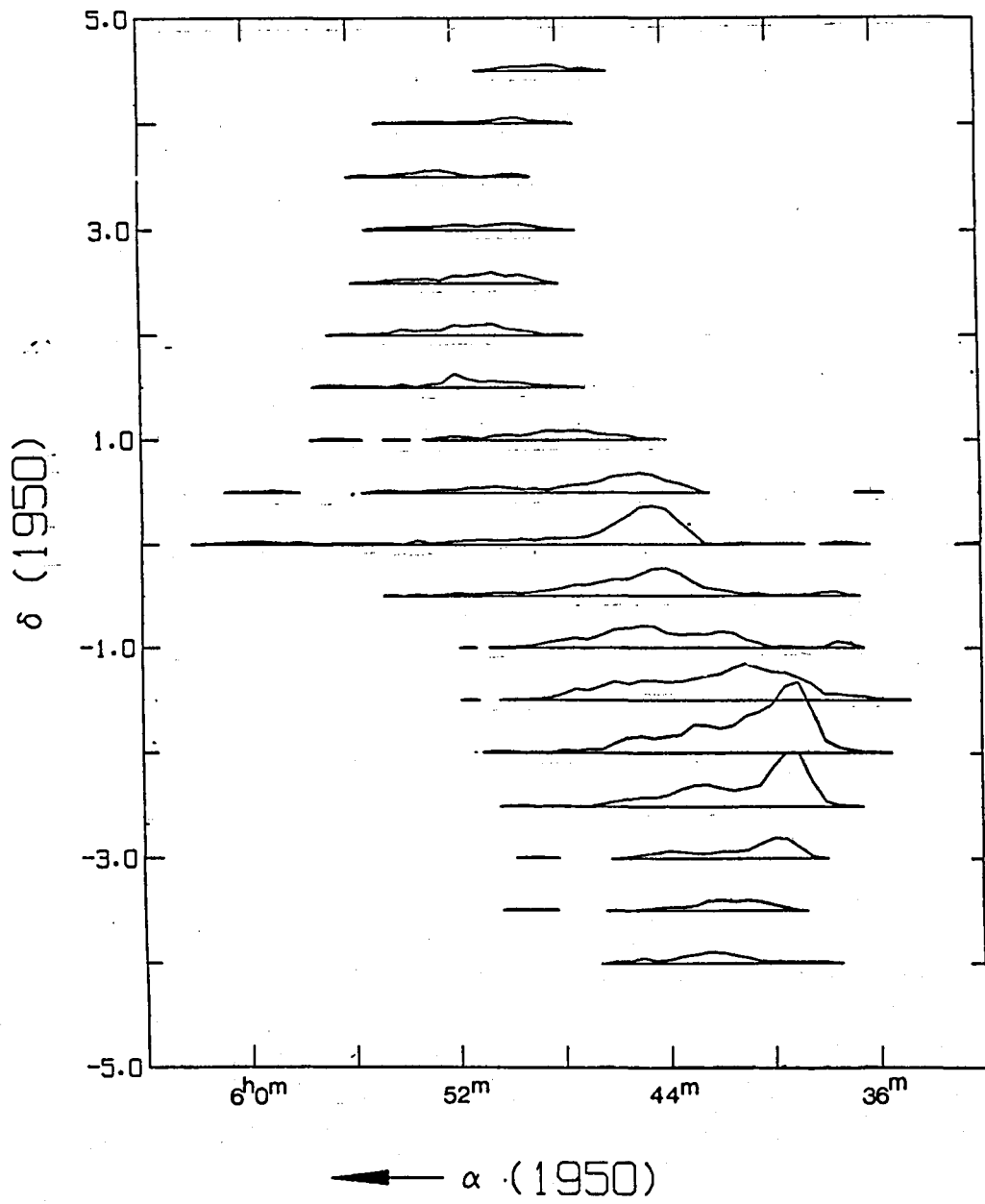
Figure V.6
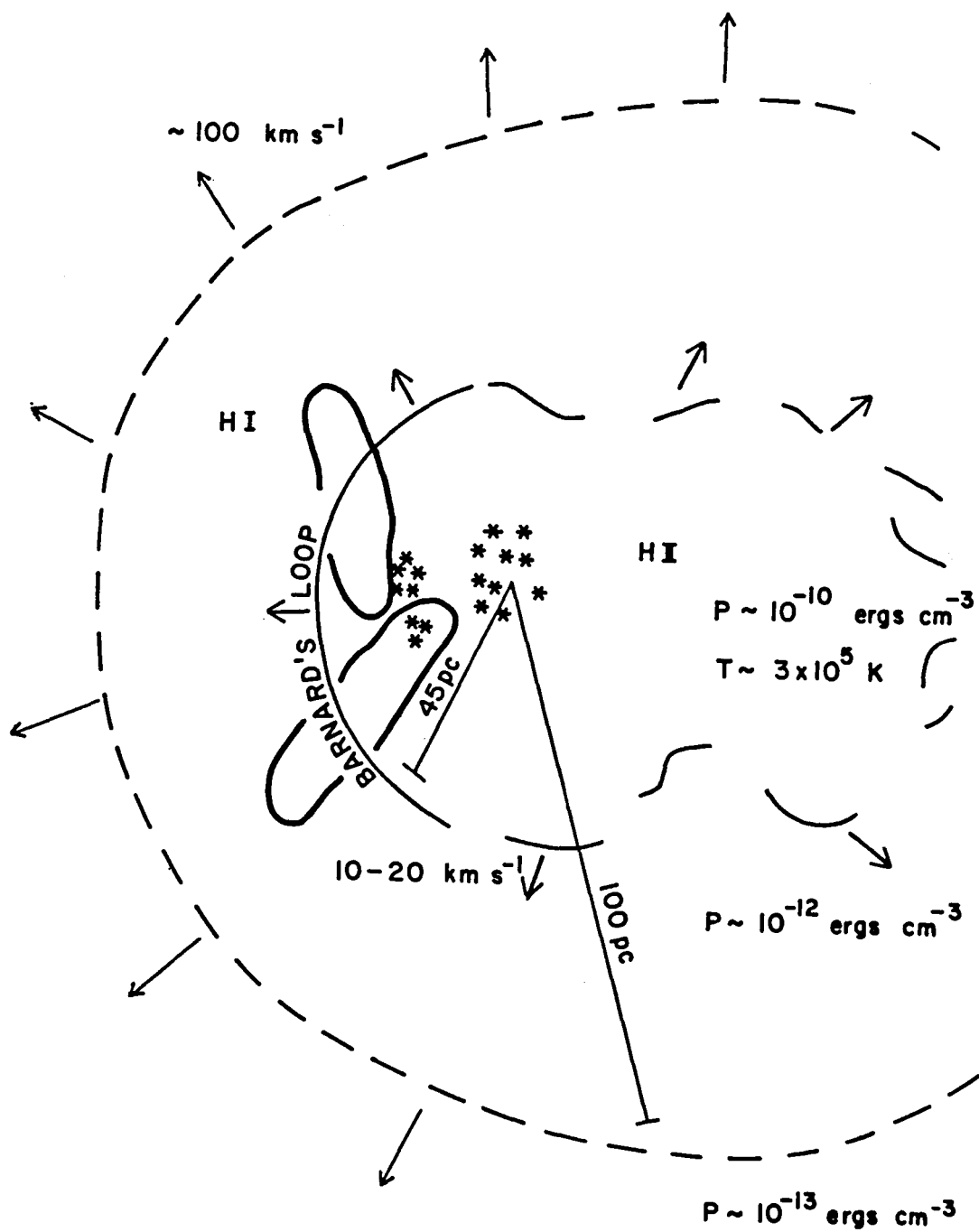
Figure V.7
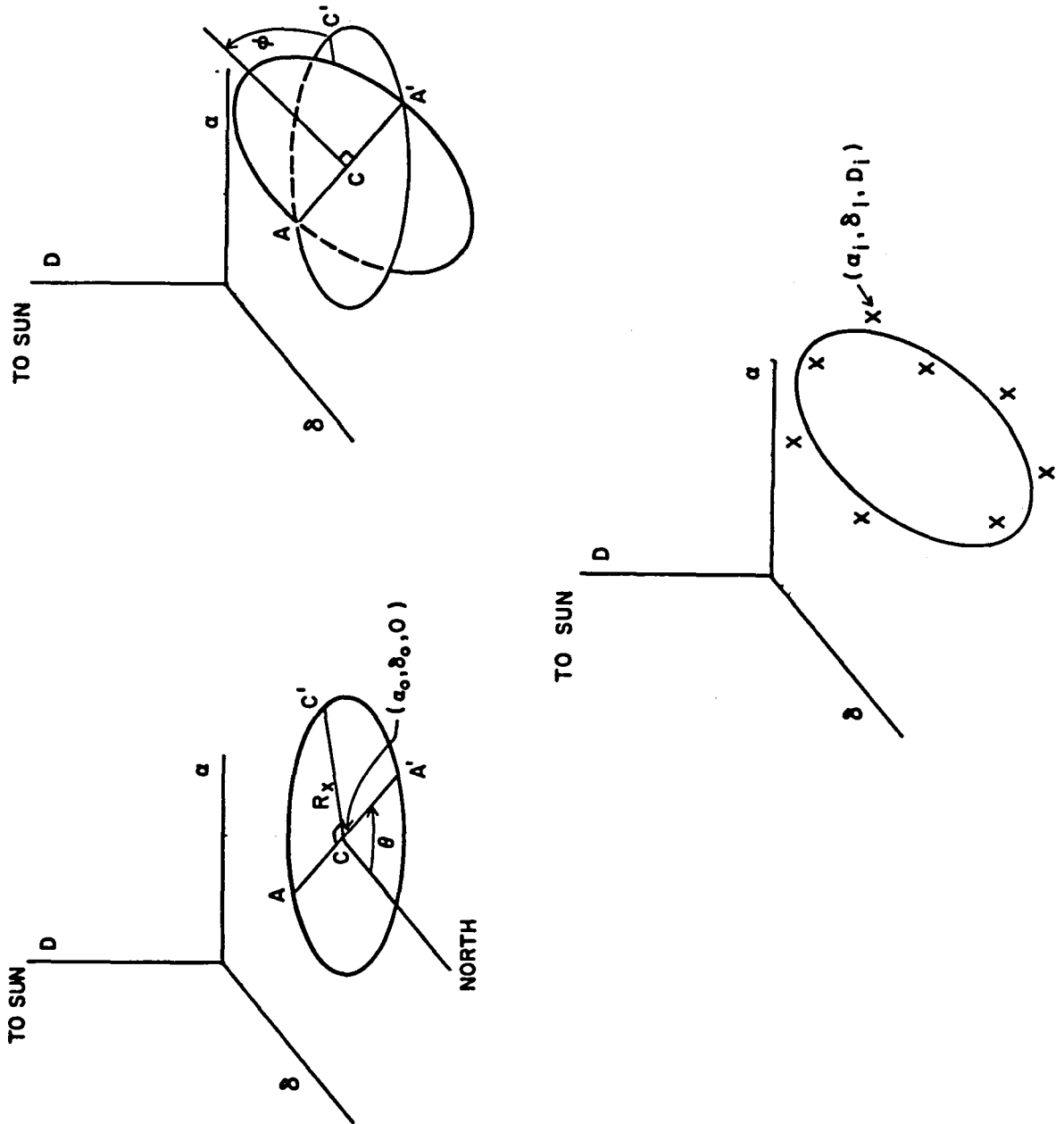
Figure V.8
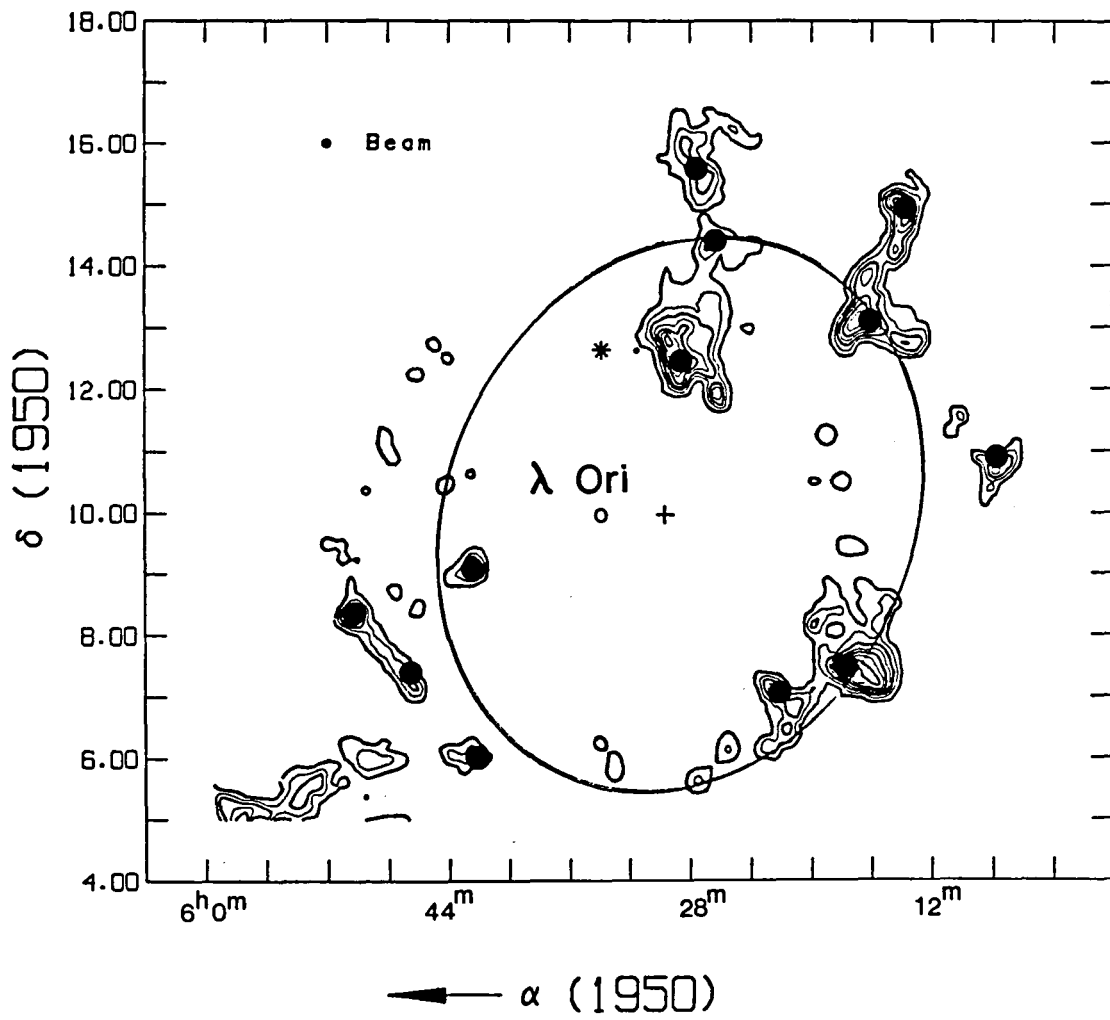
Figure V.9
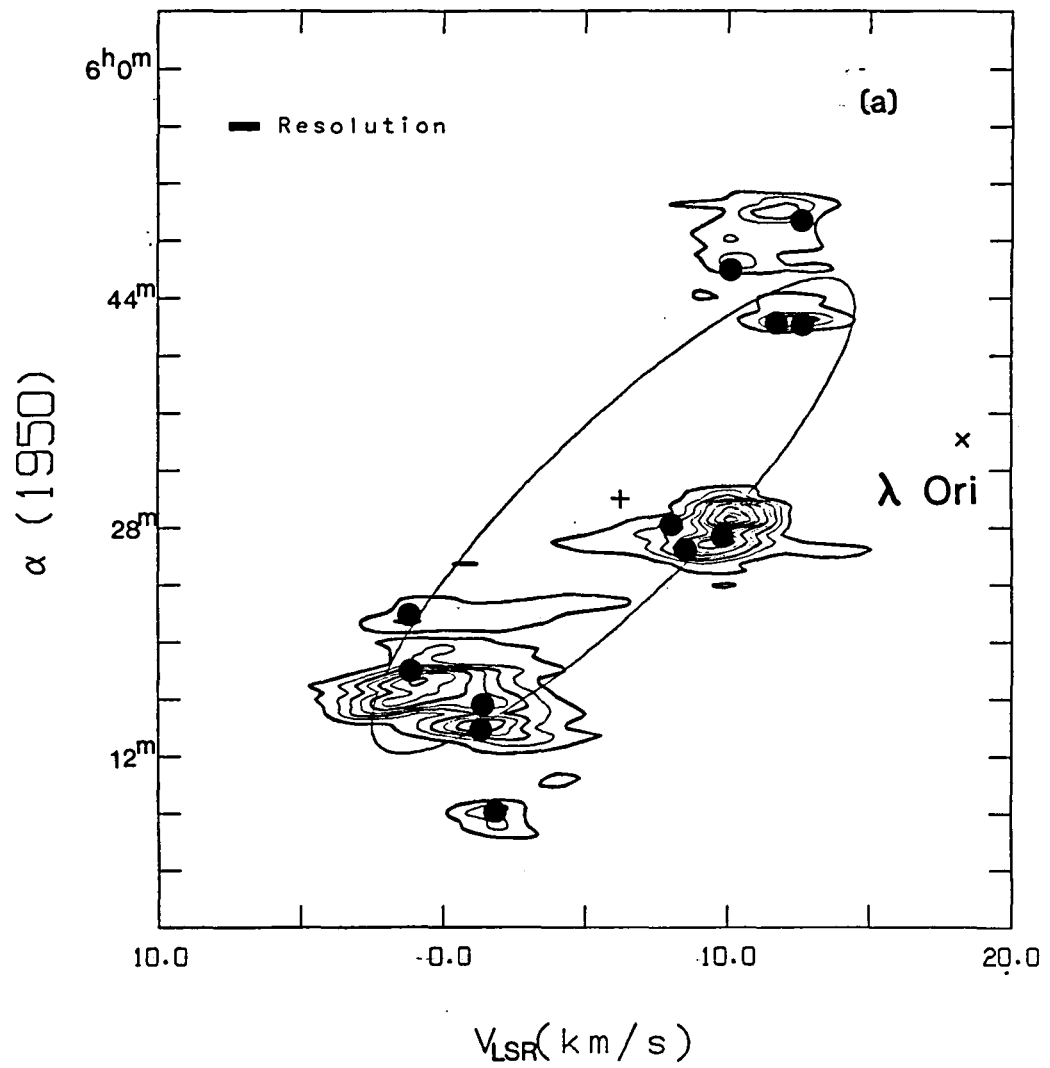
Figure V.10a
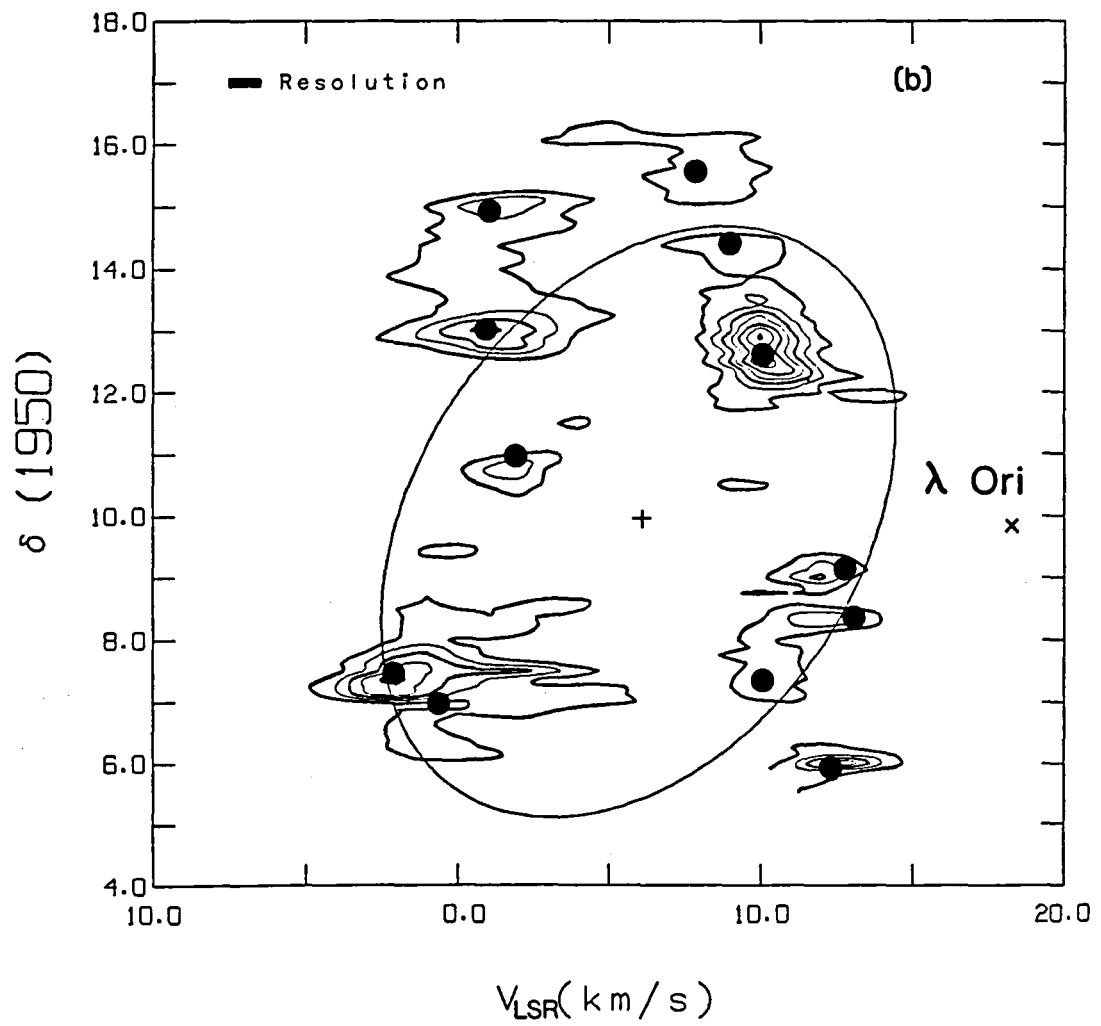
Figure V.10b
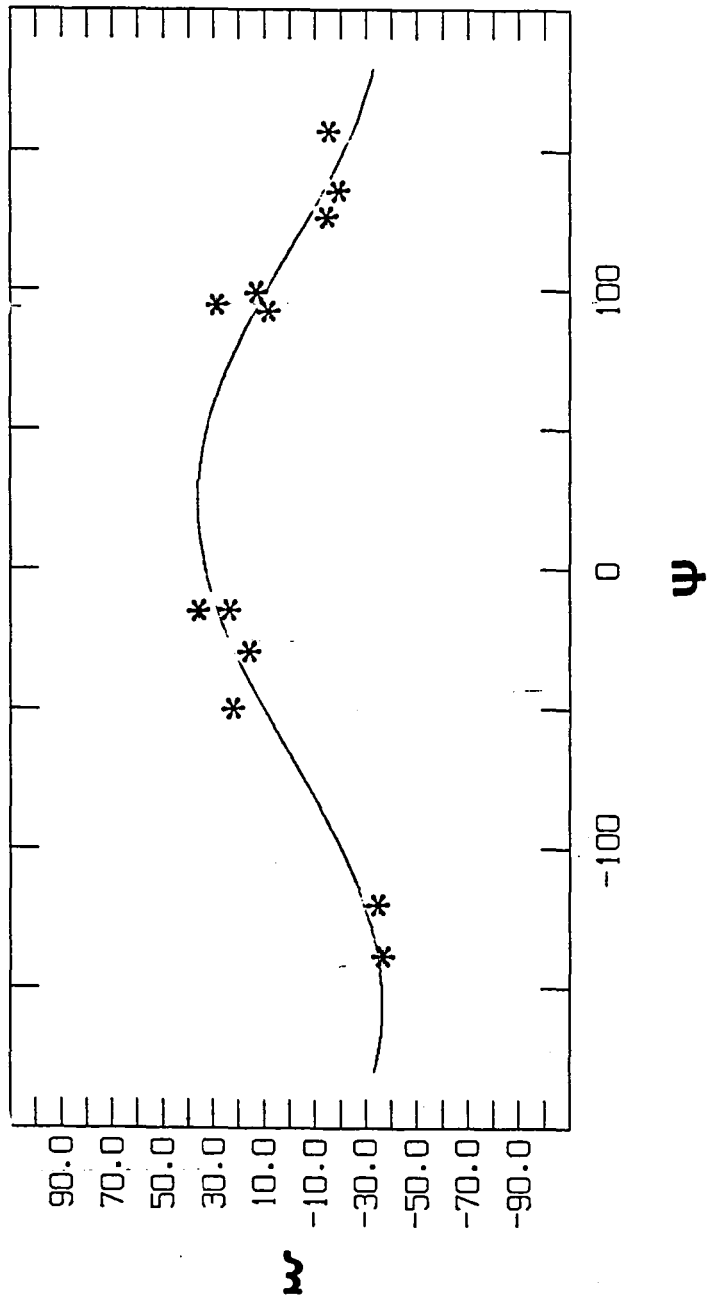
Figure V.11
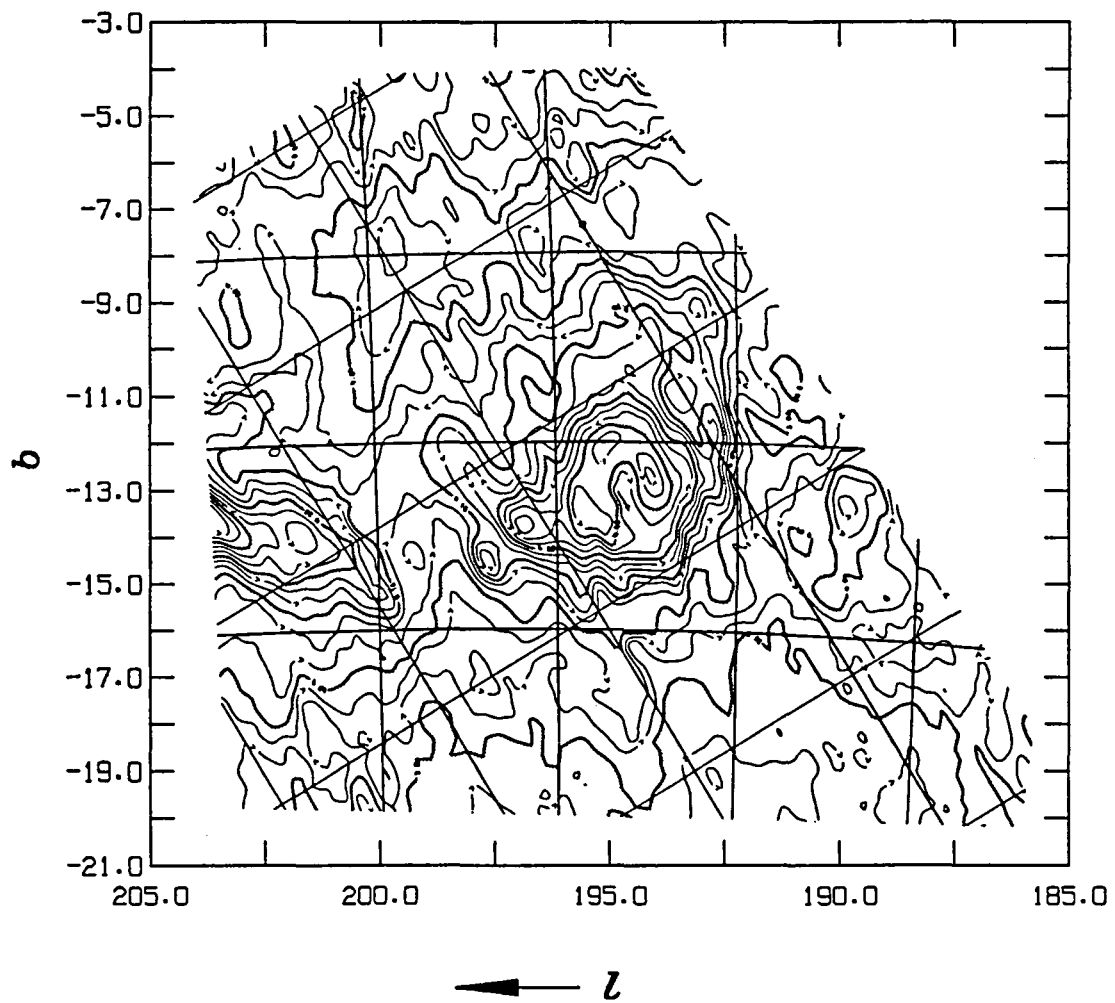
Figure V.12
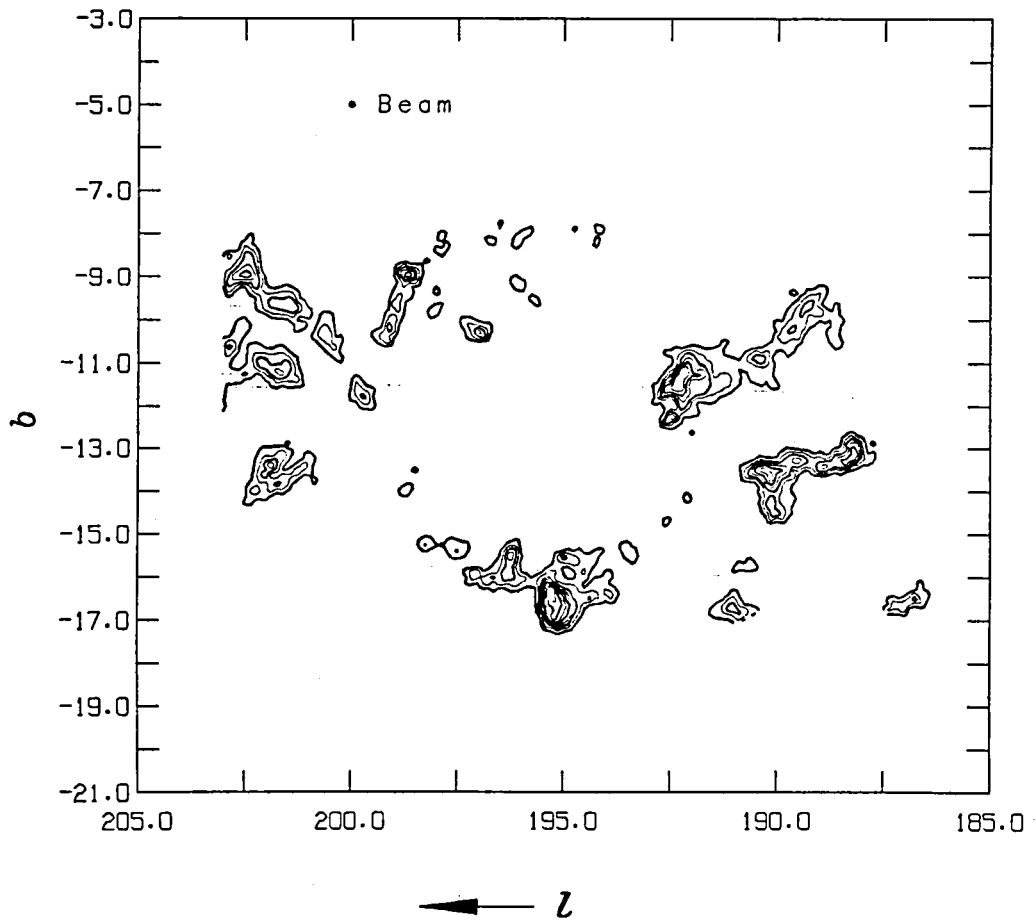
Figure V.13
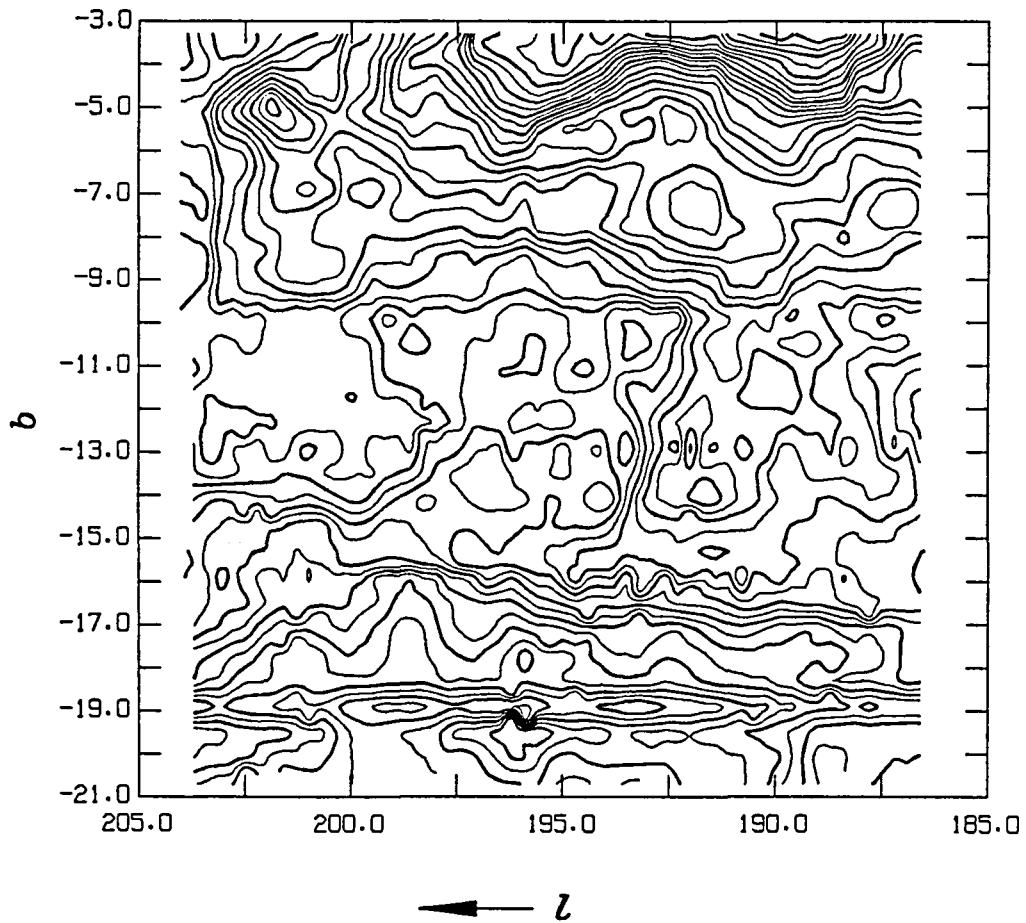
Figure V.14
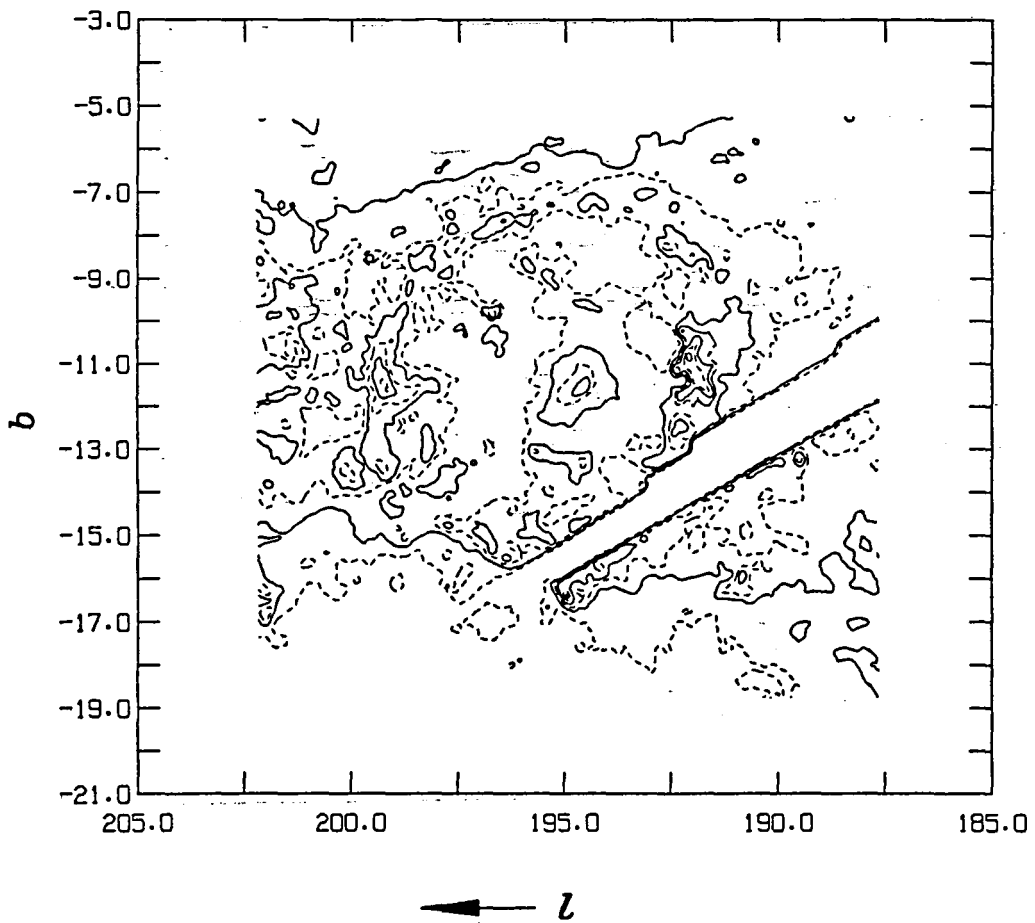
Figure V.15

(a)
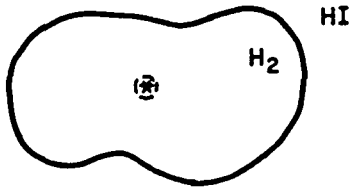
(b)
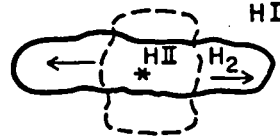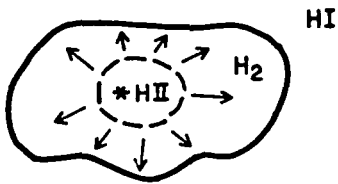
(c)
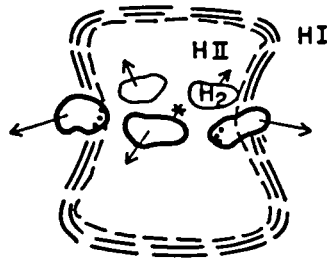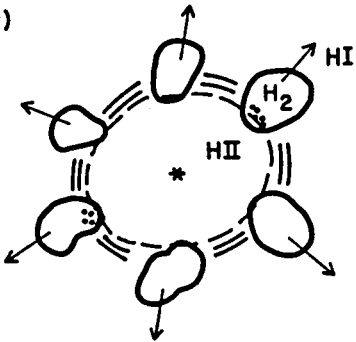
(d)
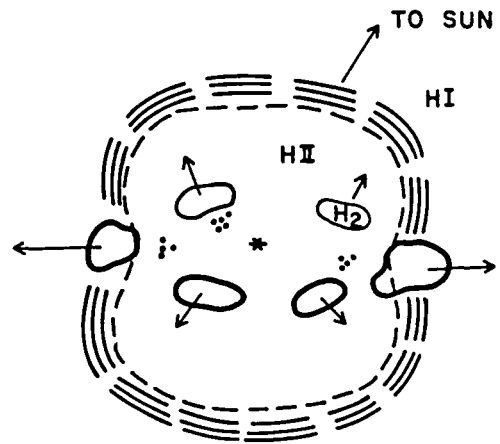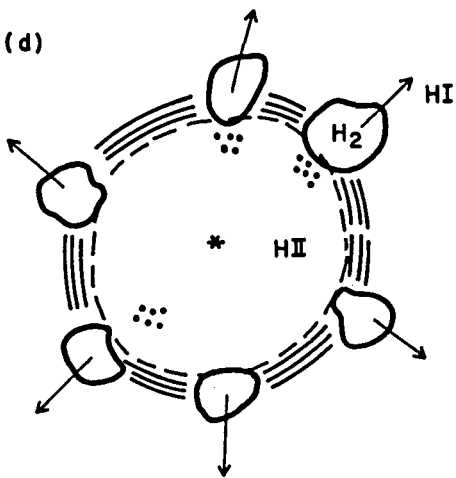
Figure IV.16
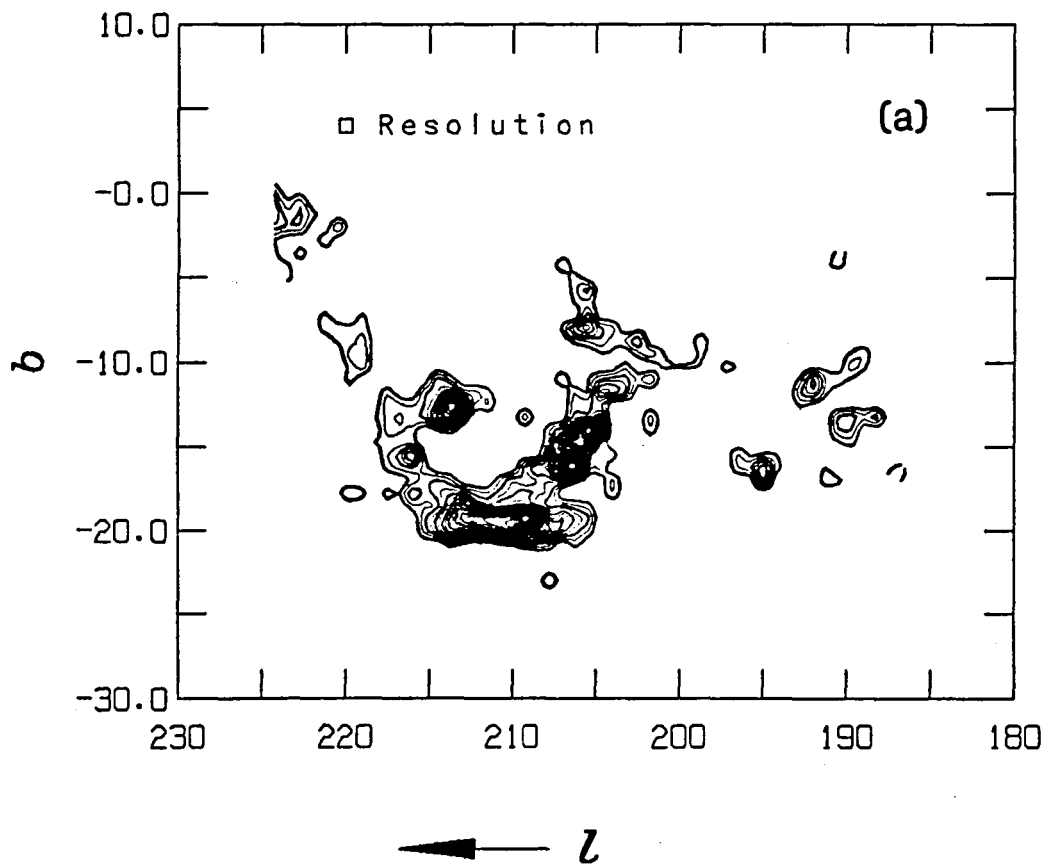
Figure IV.17a
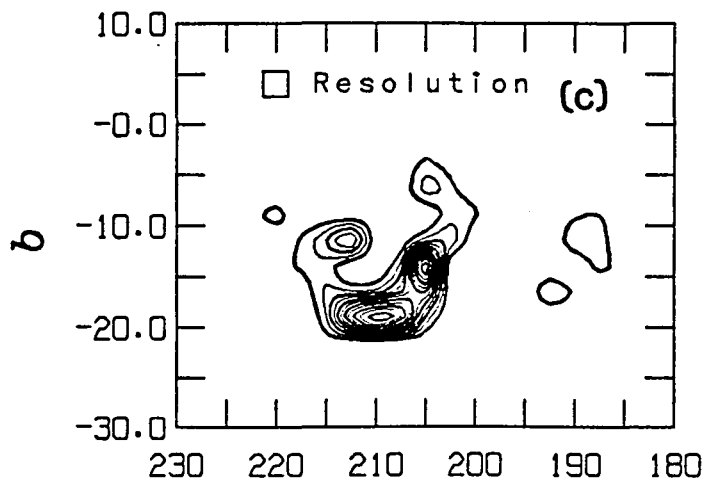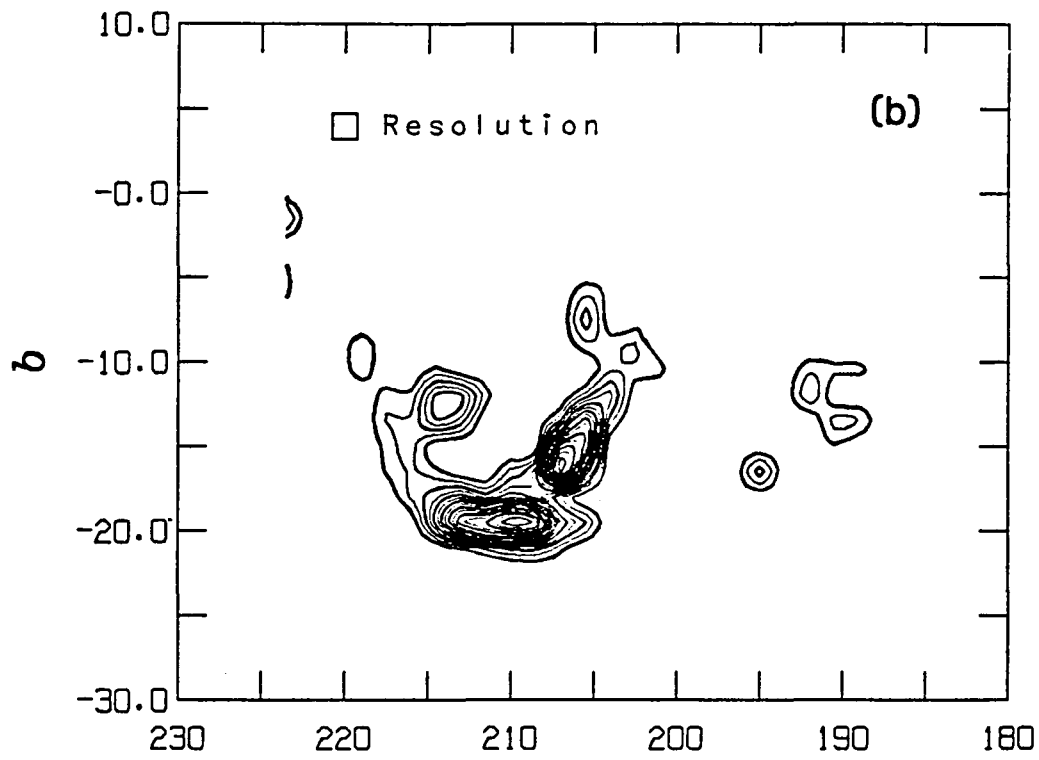
Figure IV.17b-c
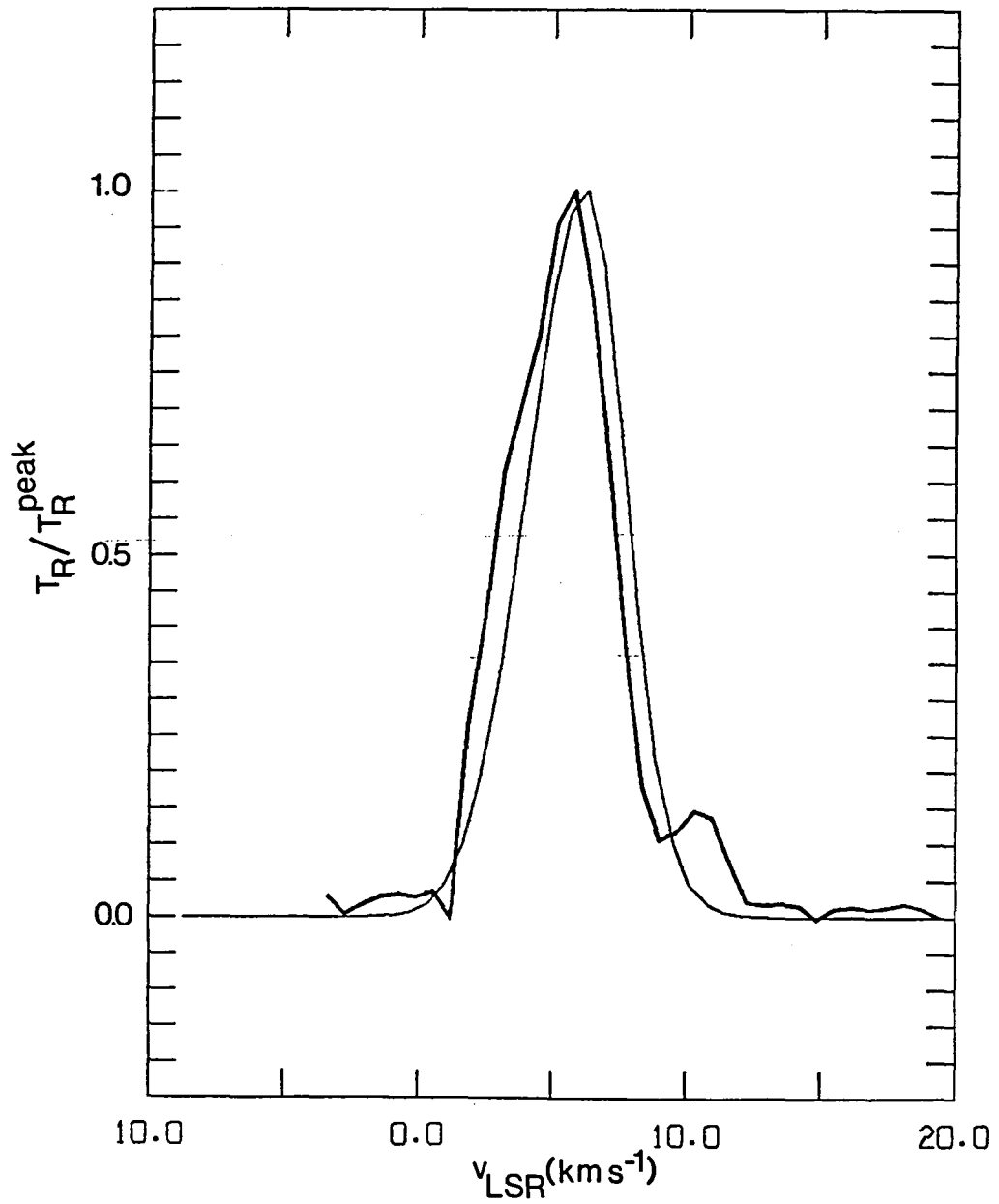
Figure APPENDIX.1

Figure APPENDIX.2
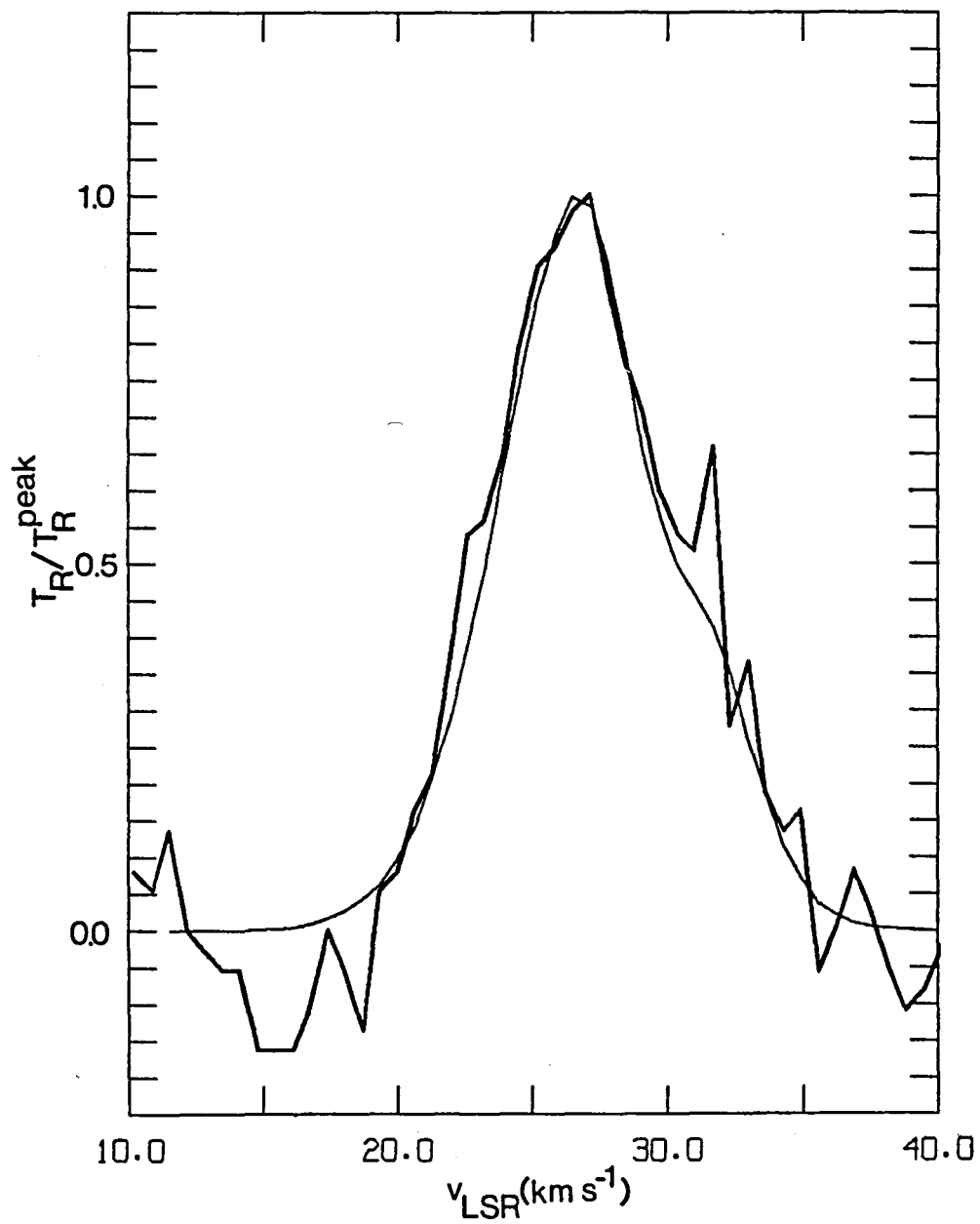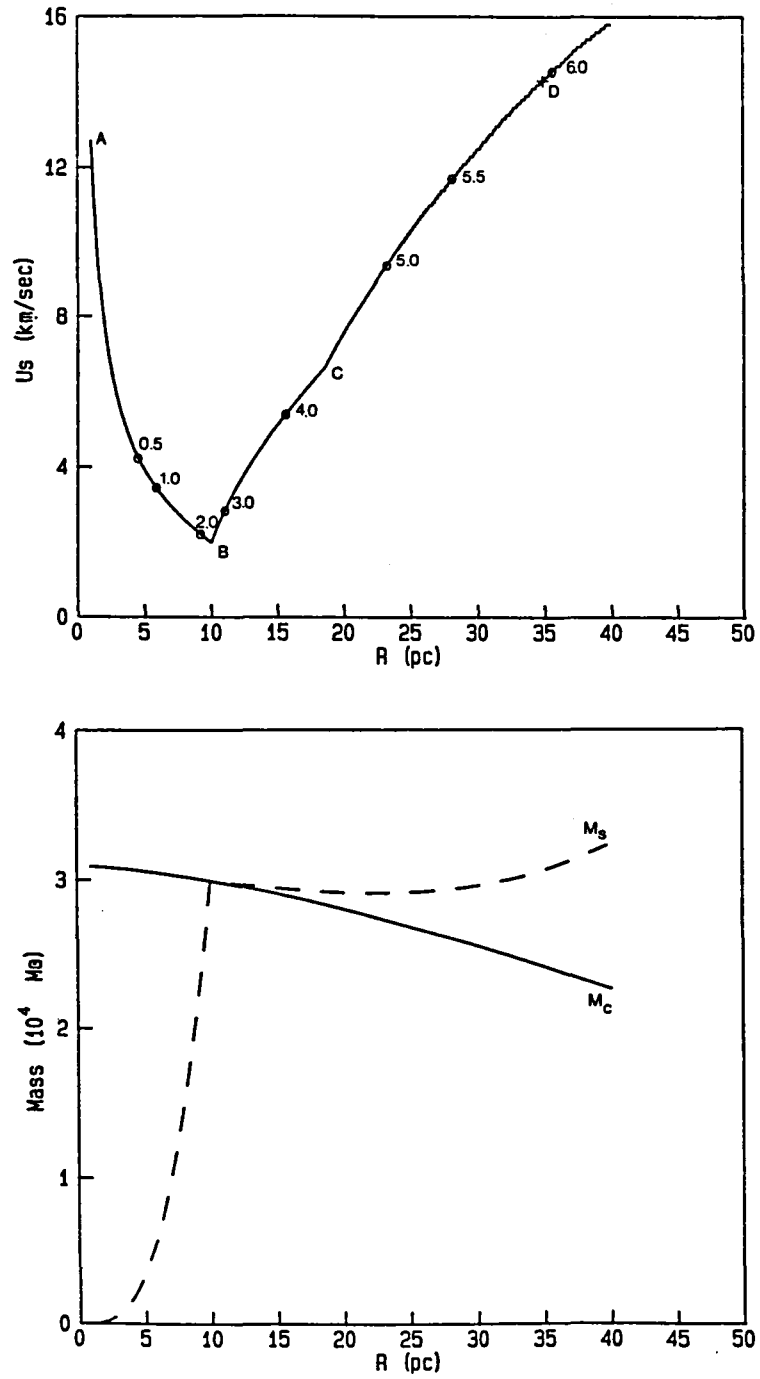
Figure APPENDIX.3

Figure APPENDIX.4

1. Report No. NASA TM-87786	2. Government Accession No.	3. Recipient's Catalog No.
4. Title and Subtitle MOLECULAR CLOUDS IN ORION AND MONOCEROS		5. Report Date June 1986
		6. Performing Organization Code 640
7. Author(s) Ronald J. Maddalena		8. Performing Organization Report No.
9. Performing Organization Name and Address NASA Goddard Institute for Space Studies 2880 Broadway New York, NY 10025		10. Work Unit No.
		11. Contract or Grant No.
		13. Type of Report and Period Covered
12. Sponsoring Agency Name and Address National Aeronautics and Space Administration Washington, DC 20546		Technical Memorandum
		14. Sponsoring Agency Code

15. Supplementary Notes

16. Abstract

About one-eighth of a well-sampled 850 deg^2 region of Orion and Monoceros shows CO emission coming from either local clouds ($d < 1$ kpc) lying as much as $25°$ from the galactic plane or from more distant objects located within a few degrees of the plane. Local giant clouds associated with Orion A and B have enhanced temperatures and densities near their western edges possibly due to compression by a high pressure region created by ~ 10 supernovae that occurred in the Orion OB association. Another giant cloud associated with Mon R2 may be related to the Orion clouds. Two filamentary clouds (one possibly 300 pc long but 10 pc wide) may represent a new class of object. An expanding ring of clouds concentric with the H II region ionized by λ Ori probably constitute fragments of the original cloud from which λ Ori formed; the gas pressure of the H II region and the rocket effect probably disrupted the original cloud.

At a distance of 3 kpc, a large (250 x 100 pc) and massive ($7-11 \times 10^5$ $M_\odot$) cloud was found with the unusual combination of low temperatures ($T_R < 2.7$ K) and wide spectral lines (~ 7 km s^{-1}). Most of the signs of star formation expected for such a massive cloud being absent, this may be a young cloud that has not yet started to form stars. The ~ 15 large clouds found in the outer galaxy ($l \sim 206° - 220°$) probably lie in two spiral arms. The distribution of outer galaxy clouds and a comparison of the properties of these clouds and those of local clouds are given.

17. Key Words (Selected by Author(s)) Molecular Clouds Cloud Structures Molecular and Atomic Hydrogen		18. Distribution Statement Unclassified - Unlimited Subject Category 90	
19. Security Classif. (of this report) Unclassified	20. Security Classif. (of this page) Unclassified	21. No. of Pages 210	22. Price* A10

End of Document